Water storage and potential hazard of moraine-dammed glacial lake in maritime glaciation region—A case study of Bienong Co

Hongyu Duan[1], Xiaojun Yao[1], Yuan Zhang[1], Huian Jin[2], ~~Yuan Zhang[1],~~ Qi Wang[3], Zhishui Du[3], Jiayu Hu[1], Bin Wang[4], Qianxun ~~Wang[4]~~ Wang[5]

5 [1] College of Geography and Environment Science, Northwest Normal University, LanZhou, 730070, China
[2] Gansu Forestry Polytechnic, Tianshui, 741020, China
[3] Northwest Engineering Corporation Limited, Power China, Xi'an 710065, China
[4] Xinjiang Transport Planning Survey and Design Institute Company Limited, Urumqi 830006, China
[45] Capital Urban Planning and Design Consulting Development Company Limited, Beijing 100038, China

10 *Correspondence to:* Xiaojun Yao (xj_yao@nwnu.edu.cn)

Abstract. The existence of glacial lakes in the Southeastern Tibetan Plateau (SETP) is a potential hazard to ~~the~~ downstream regions, as the failure of some lakes has the potential to result in disastrous glacial lake outburst flood (GLOF) events of high-magnitude. In the present study, we conducted a comprehensive investigation for Bienong Co, an end moraine-dammed glacial lake in SETP. First, the lake basin morphology was simulated and the water storage was estimated, obtaining that the maximum

15 lake depth is ~181 m and the water storage of ~102.3×10^6 m^3. Then, we assumed the ice avalanche (Scenarios A1, A2 and A3) and lateral moraine landslide (Scenarios B1, B2, B3 and C1, C2, C3) induced GLOFs process chain of Bienong Co. The volume of nine scenarios of trigger was calculated using RAMMS model and the displacement wave generation and propagation in the lake, overtopping flow and erosion on moraine dam and subsequent downstream flooding were simulated by BASEMENT model. The results show that ice avalanche scenarios produce the largest amount of material into the lake,

20 resulting in displacement wave amplitudes of up to 25.2 m (Scenario A3) near the moraine dam. And smaller volume of landslide entering the lake only result in smaller displacement waves in the lake, such as Scenario C1 has wave amplitude below 1 m near the moraine dam. Scenarios A1, A2 and A3 result in the released water from the lake of 24.1×10^6 m^3, 25.3×10^6 m^3 and 26.4×10^6 m^3, and the peak discharges at moraine dam of 4,996 m^3/s, 7,817 m^3/s and 13,078 m^3/s, respectively. These high discharges cause scour erosion of the moraine dams, resulting in breaches widths of 295.0 m, 339.4 m, 368.5 m,

25 and breach depths of 19.0 m, 19.1 m, 19.3 m, respectively. However, in landslide scenarios, only the overtopping flow generated by Scenarios B3 and C3 caused moderate erosion of the moraine dam, with breach depth of 6.5 m and 7.9 m, and breach width of 153 m and 169 m, respectively. GLOFs generated by Scenario A1, A2 and A3 can all flow through 18 settlements downstream, and will threaten more than half of the settlements. Both Scenarios B3 and C3 produced floods that flow through eight downstream settlements within 20 hours and had a relatively small impact on them. Comparisons show that

30 Bienong Co is the relative deepest glacial lake known on the Tibetan Plateau, and this study could provide a new insight of the moraine-dammed glacial lakes in the SETP and a reference for GLOFs disaster prevention to the local government.

~~, including its area evolution analysis, basin morphology simulation, water volume estimation, possible outburst triggers analysis, and one- and two-dimensional hydrodynamic simulation. The results show that the area of Bienong Co was 1.15±0.05 km² in August 2020, which has remained generally stable over the past four decades. However, it exhibits the high risk of~~

35 ~~GLOFs due to its larger area, the steep and high moraine dam, the close distance to its mother glacier, and the surrounding steep slopes. The lake basin is relatively flat at bottom and steep on both flanks, and the slope near the glacier (16.5°) is steeper than that near the moraine dam (11.3°), with a maximum lake depth of ~181.04 m and a water volume of ~1.02×10⁸ m³ in August 2020. Four scenarios of GLOFs based on different breach depths, breach widths and failure times were simulated using the hydrodynamic model of MIKE 11 and MIKE 21 to predict the potential impacts on downstream areas. An extreme~~

40 ~~magnitude GLOF would have a catastrophic impact on the downstream region, with most of the settlements, all bridges and majority of Jiazhong Highway along the flow channel being completely submerged. However, in a low magnitude GLOF,~~

~~most settlements would be safe or partially inundated. It means that most of the residents in the flow channel of Bienong Co can avoid the damage caused by a low-magnitude GLOF (smaller breach depth of dam). Although three settlements in the downstream area are at risk of being completely submerged in a low magnitude GLOF event, the flooding arrives late and people have enough time to escape. Finally, the maximum depths of glacial lakes with similar areas were compared for 16 glacial lakes with measured bathymetry data in the Himalayas and Bienong Co in SETP, according to the regional division of maritime and continental zones. The results show that glacial lakes located in maritime regions have larger depths than those in continental regions, and Bienong Co is the deepest glacial lake comparing others in the Himalayas. Therefore, a huge amount of water could be discharged by a potential GLOF event of Bienong Co, creating a serious hazard, which should be taken seriously in the future. Overall, this study of Bienong Co could provide a new understanding of the moraine-dammed glacial lakes in the SETP and a reference of GLOFs to the local government.~~

1 Introduction

Due to global warming, the accelerated retreat and thinning of glaciers has occurred in most regions compared to the last century (Zemp et al., 2019)~~.~~, resulting in ~~One result is~~ a rapid increase in the number, area, and volume of glacial lakes worldwide (Shugar et al., 2020; Wang et al., 2020). ~~This is a natural occurrence, where g~~Glacier meltwater can be~~is~~ confined and stored in certain depressions dammed by ~~, and the dam materials can be~~ moraine, ice or bedrock (Vilímek et al., 2013). ~~However, once~~ Once the dam is damaged~~, and~~ the water can be ~~is~~ suddenly and catastrophically released~~,~~ to form Glacial Lake Outburst Floods (GLOFs), which may cause ~~a~~ severe social and geomorphic impacts several dozens of kilometers and more downstream~~ can be caused~~ (Lliboutry, 1977; Richardson and Reynolds, 2000; Osti and Egashira, 2009; Carrivick and Tweed, 2016; Cook et al., 2018; Zheng et al., 2021). Moraine-dammed glacial lakes are of particular attention owing to their large volume (Fujita et al., 2013; Veh et al., 2020), weak dam composition, and exposure~~predisposition~~ to various trigger~~ing~~s, such as the ice and/or rock avalanches and heavy precipitation and intense glacier melting (Emmer and Cochachin, 2013; Nie et al., 2018), the most common sources of GLOFs (Watanbe and Rothacher, 1996; Westoby et al., 2014). The Himalayas and ~~the~~ Southeastern Tibetan Plateau (SETP)~~ region~~ are regions of ~~hotspots for the~~frequently occurrence of GLOFs caused by moraine-dammed glacial lakes (Wang, 2016). Study shows that the Himalayas, especially the southern region is likely to experience more ~~will enter a high incidence period of~~ GLOFs at the coming decades ~~due to the fluctuated pattern~~ (Veh et al., 2020).

The SETP is a broad mountainous area covering the central and eastern Nyainqêntanglha Ranges, eastern Himalayas and western Hengduan Mountains and ~~having~~ has the most complicated terrains (Ke et al., 2014). Controlling by the warm and humid Indian monsoon~~Owing to a warm and humid climate~~, a plenty of maritime glaciers have developed here (Yang et al., 2008), featured as the adequate recharge, strong ablation, low snowline distribution, high temperature, fast movement, and strong geological as well as geomorphological effect (Li et al., 1986; Qin et al., 2007; Liu et al., 2014), which have been observed with the most negative mass balances during the past decades (Kääb et al., 2012; Neckel et al., 2014; Kääb et al., 2015; Brun et al., 2017; Dehecq et al., 2019). Therefore, the combination of active glacial processes and heavy rainfall during the monsoon season makes the region prone to glacier-related natural hazards~~active glacial processes in conjunction with heavy rainfall during the monsoon season expose the region to the threat of glacial lake related hazards~~ (Wang et al., 2012b). Studies of glacial lakes in the SETP mainly focused on regional-scale assessment of glacial lake changes (Wang et al., 2011a; Song et al., 2016; Wang et al., 2017; Zhang et al., 2020; Zhang et al., 2021), identification of potentially dangerous glacial lakes (Wang et al., 2011; Liu et al., 2019; Duan et al., 2020; Qi et al., 2020), site-specific analysis of formation mechanism, development trend, risk evolution and management measures of GLOFs (Cui et al., 2003; Cheng et al., 2008, 2009; Sun et al., 2014; Liu et al., 2021; Wang et al., 2021), exploration of geological features of a single glacial lake (Yuan et al., 2012; Liu et al., 2015; Huang et al., 2016). Fewer studies applied hydrodynamic models to simulate ~~outburst flood of glacial lake~~GLOFs in the SETP. Wang et al. (2011b) evaluated the applicability of ASTER GDEM (Global Digital Elevation Model) and SRTM DEM in the

simulation of GLOF process based on HEC RAS hydrodynamic model (Brunner, 2002). Zheng et al. (2021) analyzed and reconstructed a GLOF process chain of Jinwu Co using the published empirical relationships and GIS-based r.avaflow simulation tool (Mergili et al., 2017; Pudasaini and Mergili, 2019; Mergili and Pudasaini, 2020).

As a key factor related to the peak discharge and outburst volume of a GLOF event (Evans, 1987; Huggel et al., 2002), lake storage capacity is difficult to directly obtain by means of satellite remote sensing approach. Currently, owing to the easy availability of area information from remote sensing images, the volume of glacial lakes is generally estimated using the developed empirical formulas connect glacial lake area and volume based on bathymetric data for a small number of glacial lakes (O'Connor et al., 2001; Huggel et al., 2002; Yao et al., 2014). However, the estimated volume maybe inaccurate because the unique geographical conditions of different glacial lakes (Cook and Quincey, 2015). The SETP region is an area with high incidence of GLOFs (Sun et al., 2014; Zheng et al., 2021), however, ~~GLOFs are frequent in the SETP region (Sun et al., 2014; Zheng et al., 2021) where glacial lakes are formed by strong movement of maritime glaciers. Whereas,~~ there are few publicly available bathymetric data of glacial lakes and related research works. ~~in the SETP region and p~~Previous bathymetric work~~s~~ in the ~~High Mountain Asia~~Tibetan Plateau ~~region was~~ were carried out mainly for those glacial lakes located in the Himalayas (LIGG/WECS/NEA, 1988; Geological survey of India, 1995; Yamada, 1998; Mool et al., 2001; Sakai, 2003; Yamada, 2004; ICIMOD, 2011; Sakai, 2012; Yao et al., 2012; Wang et al., 2015; Haritashya et al., 2018; Sharma et al., 2018; Li et al., 2021). This is unfavorable to fully understand the morphology and disaster prevention of glacial lakes in the SETP region. ~~Due to the distribution in harsh environments, the bathymetry measurement of glacial lakes is difficult and risky (Zhang et al., 2020).~~ In recent years, the Unmanned Surface Vessel (USV) have developed rapidly (Liu et al., 2016), which have been widely used in scenarios such as bathymetric map creation, transportation, environmental monitoring, and moraine surveys (Larrazabal and Peñas, 2016; Yan et al., 2010; Specht et al., 2019a) owing to the favorable security on personnel safety and ~~security~~ and the high flexibility in complex environments. Glacial lakes are mostly located at high altitudes and in harsh environments (Zhang et al., 2020), and USV makes the measurement of the underwater topography of glacial lakes safer, more convenient, and more accurate (Li et al., 2021).

~~Despite the wide application in the ocean (Bibuli et al., 2014; Specht et al., 2019b), the USV are rarely employed inland, particularly on glacial lakes (Li et al., 2021). However, high altitude, harsh conditions, and sophisticated instruments mean that the underwater topography survey of glacial lakes is a potential field of USV application (Li et al., 2021).~~

In this study, we aim to complete an investigation of the potential GLOF hazard of a~~n~~ ~~typical~~ end moraine-dammed glacial lake, Bienong Co (Co means lake in Tibetan) in the SETP based on field bathymetric data and remote sensing data using a multi-model combination method~~, field bathymetric data, combining hydrodynamic model~~. First, the lake basin morphology of Bienong Co is modelled. Then, multiple components of GLOF process chain, including initial mass movement from mother glacier and lateral moraine slope, displacement wave generation and propagation in the lake, overtopping flow and erosion on moraine dam and subsequent downstream flooding were simulated. This study will help the local government understand the potential hazards of Bienong Co and serve as a reference for other scholars studying glacial lakes and GLOFs in the SETP region.

~~The main tasks include to investigate the evolution of glacial lake' area and parent glacier' elevation based on remote sensing images, model the morphology and estimate the volume of Bienong Co based on field bathymetry data, assess the potential GLOF triggers of Bienong Co, and simulate potential GLOF caused hazards based on field bathymetry data and DEM data using MIKE 11 and 21 hydrodynamic models (DHI, 2007). In addition, the second purpose is to develop a relationship between the area and volume of moraine dammed glacial lakes based on bathymetric data of Bienong Co and other 16 glacial lakes in the Himalayas.~~

2 Study area

125 The study objective, Bienong Co glacial lake, is located in the upper area of Yi'ong Zangbo (Zangbo means river in Tibetan) watershed (30°05' - 31°03'N, 92°52' - 95°19'E) in the SETP (Fig. 1a). The Yi'ong Zangbo originates from the Nyainqêntanglha Mountains, extends about 286 km in length, and drains an area covering 13,533 km², which isAs a one-level tributary of the Parlung Zangbo and a two-level tributary of the Yarlung Zangbo (i.e., the Brahmaputra River), the Yi'ong Zangbo drains an area covering 13,533 km². The terrain is high in the west and low in the east with high mountains and valleys. The climate is

130 warm and humid, featuring the mean annual precipitation of 958 mm and mean annual temperature of 8.8 ℃ (Ke et al., 2013, 2014). There were 1,907.76 km² glacier coverage, 105 moraine-dammed glacial lakes with a total area of 16.87 km² in 2016 (Duan et al., 2020). Seven glacial lakes in the watershed, including Bienong Co, were considered to be have highly GLOFs potentialdangerous (Duan et al., 2020), of which, the Jinwu Co collapsed on June 26, 2020 (Zheng et al., 2021). As of 2021 there have been three recorded large GLOF events in the basin, all of which caused very significant damage to the

135 infrastructures settings in the downstream region (Sun et al., 2014; Yao et al., 2014; Zheng et al., 2021) (Fig. 1b).

Bienong Co is an end moraine-dammed lake constrained by the snout of the mother glacier (Mulang Glacier) on the south and a massive unconsolidated terminal moraine dam on the northwest (Fig. 1c). The elevation of water surface in 2021 is was 4745 m covering an with an area of 1.15 ± 0.05 km² in 2021that has experienced less significant changes. Mulang Glacier has had an area of 8.29 ± 0.22 km² and mean surface slope of ~18.28°, which has also remained largely unchanged area over the

140 last 45 years. However, the glacier ablation zone experienced a thinning process of 6.5 m/a. The flow of Bienong Co converges into Xiong Qu (Qu means river in Tibetan) which is one of the two main tributaries of the upper Yi'ong Zangbo (Fig. 1b). The flow channel from the Bienong Co to the confluence of Xiongqu and Songqu Co (another main tributary of the upper Yi'ong Zangbo) stretches ~53 km, with the river longitudinal drop ratio of 14.48‰. There are 18 settlements and 13 bridges densely distributed along the flow channel, as well as a large amount of agricultural land. In addition, the Jiazhong Highway extends

145 closely along the river (Fig. 1d).
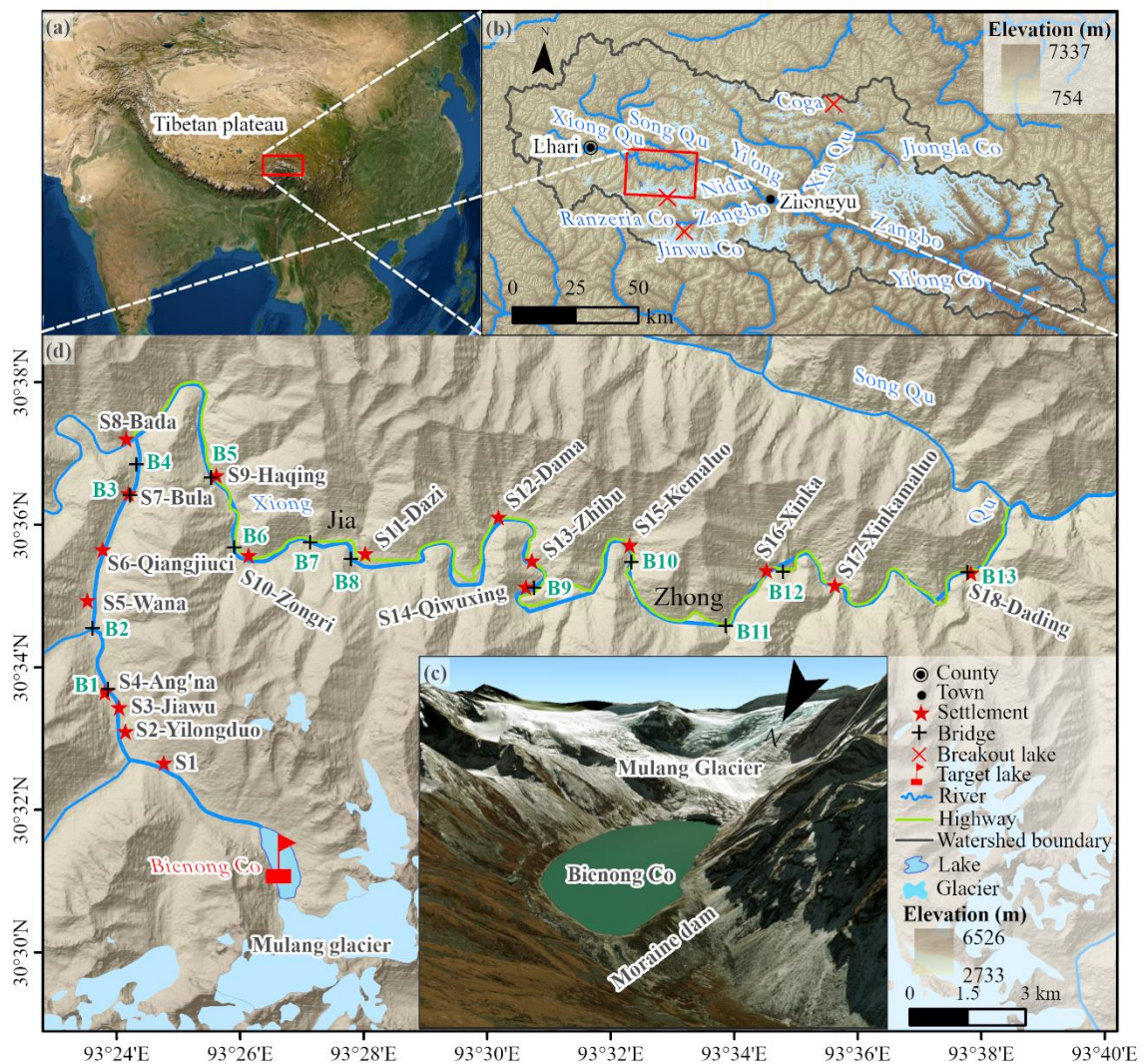
Figure 1. The overview of the study area. (a) The location of Yi'ong Zangbo watershed, (b) the location of Bienong Co, (c) the close view of Bienong Co, and (d) distribution of settlements as well as bridges within ~53 km downstream Bienong Co. Background of Fig. 1a and c is the MapWorld image, based on which, settlements, bridges and Jiazhong Highway along the flow channel were identified. Background of Fig. 1b and d is the Advanced Land Observing Satellite's (ALOS) mission Phased Array type L-band Synthetic Aperture Radar (PALSAR) Digital Elevation Model (DEM).

The area of Bienong Co has remained basically stable in the past 40 years, but it's area of 1.15 ± 0.05 km^2 in 2021 is almost twice the size of the two nearby failure glacial lakes, one is Jinwu Co (Zheng et al., 2021) and the other is Ranzeria Co, which is located just 9 km southeast of Bienong Co (Sun et al., 2014). The moraine dam of Bienong Co has an average height of 72 m, enclosing a water volume of 65.2×10^6 m^3, accounting for 64% of the total (Fig. 2e). The greater the volume of water retained in the lake, the greater the volume of water available for potential flooding (Westoby et al., 2014), and the greater the hazard caused by GLOFs. GLOFs are extremely complex phenomena, each of them is a distinctly unique event with the characteristics determined by the triggering mechanism, lake hypsometry, the geometry, composition, and structural integrity of the moraine dam, as well as the topography and geology of the flood path (Westoby et al., 2014). Studies of history GLOFs reveal that the most common cause of glacial lakes' failure in the Himalaya is mass movement (snow, ice, and/or rock) entering lakes (Richardson and Reynolds, 2000; Wang et al., 2012a; Emmer and Cochachin, 2013; Worni et al., 2014) and subsequently overtopping and eroding the moraine dam (Risio et al., 2011). Bienong Co is directly connected to Mulang Glacier whose ablation zone that is defined as the mother glacier tongue in this study has an average slope of 20° with well-developed ice crevasses (Fig. 2a and b). Lv et al., (1999) proposed that a slope of mother glacier tongue greater than 8° is conducive to the occurrence of ice avalanche. In the context of global warming, glacial meltwater can lubricate the glacier itself, increasing the

likelihood of overhanging ice sliding into the lake (Wang et al., 2015). Therefore, ice disintegration from the Mulang Glacier could be a potential trigger for GLOFs of Bienong Co. In addition, the GLOF of Jinwu Co, a moraine dammed glacial lake located about 24 km to the southeast of Bienong Co, was caused by an initial moraine landslide with slope range of 30° - 45° on the left side (Zheng et al., 2021). Bolch et al. (2011) and Rounce et al. (2016) both deemed that non-glacierized areas around a lake with a slope > 30° are potential rock fall, landslide, or other solid mass movement region. There are multi locations with lateral moraines around Bienong Co that fit into this slope range (Fig. 2c, d and e). Thus, lateral moraine landslides could also be a potential trigger for Bienong Co's GLOF.

Dam characteristics, such as dam geometry (freeboard, width to height ratio, distal face slope), dam material properties, ice-cored moraine conditions govern the stability of the dam (Huggel et al., 2004; Prakash and Wang et al., 2011a; Nagarajan, 2017). Freeboard refers to the vertical distance between the lake level and the lowest point on the dam crest, which reflects the minimum wave amplitude needed for the occurrence of the overtopping, and a higher freeboard is not conducive to the occurrence of overtopping (Emmer and Vilímek, 2014). A natural outlet with a width of ~50 m in the right of the dam (facing downstream) (Fig. 2e and f), indicating the freeboard of Bienong Co is 0 m, which signals the high potential overtopping of the lake. The moraine dam is 550 m wide and the height is variable with an average height of 72 m and the width-height ratio of 7.64 (Fig. 2e). According to the thresholds favoring GLOFs of dam width smaller than 60 m proposed by Lv et al. (1999), width-height ratio smaller than 0.2 proposed by Huggel et al. (2004), the moraine dam of Bienong Co is stable. However, freeboard of 0 m and the distal facing slope of 35° are the conditions conducive to GLOFs based on the favoring thresholds of smaller than 25 m (Mergili et al., 2011) and larger than 20° (Lv et al., 1999). The moraine dam of Bienong Co is covered with vegetation, the surface layer is a larger particle size of the stone, below the smaller particle size, the material is loose and poorly cemented, which is susceptible to destruction by water forces (Fig. 2e). The existence of ice core inside the moraine dam is unknown, but there is no ice core in Jinwu Co's breached dam. The dam crest elevation of Bienong Co is 320 m higher than that of Jinwu Co. Additionally, McKillop and Clague (2007) argued that moraines with rounded surfaces and minor superimposed ridges are considered ice-cored, whereas narrow, sharp-crested moraines with angular cross-sections are interpreted as ice-free, and the dam of Bienong Co clearly fit the latter category. In summary, we consider that the potential threats to Bienong Co are mainly from its mother glacier's ice avalanches and lateral moraine landslides.

~~The northeast-southwest oriented frontal moraine dam has the length of ~550 m, mean crest height of ~72 m, mean freeboard of ~10 m, the distal facing slope of ~35°. A natural outlet with a width of ~50 m in the right of the dam facing downstream. The dam is composed of poorly consolidated, unsorted and uncohesive sediment and the existence of ice core cannot be determined at present. The flow channel from the Bienong Co along with Xiong Qu (Qu means river in Tibetan) to converging with Song Qu stretches ~52.98 km, with the river longitudinal drop ratio of 14.48‰. There are 19 settlements and 13 bridges densely distributed along the above river channel, as well as a large amount of agricultural land. In addition, the Jiazhong Highway extends closely along the river channel (Fig. 1).~~
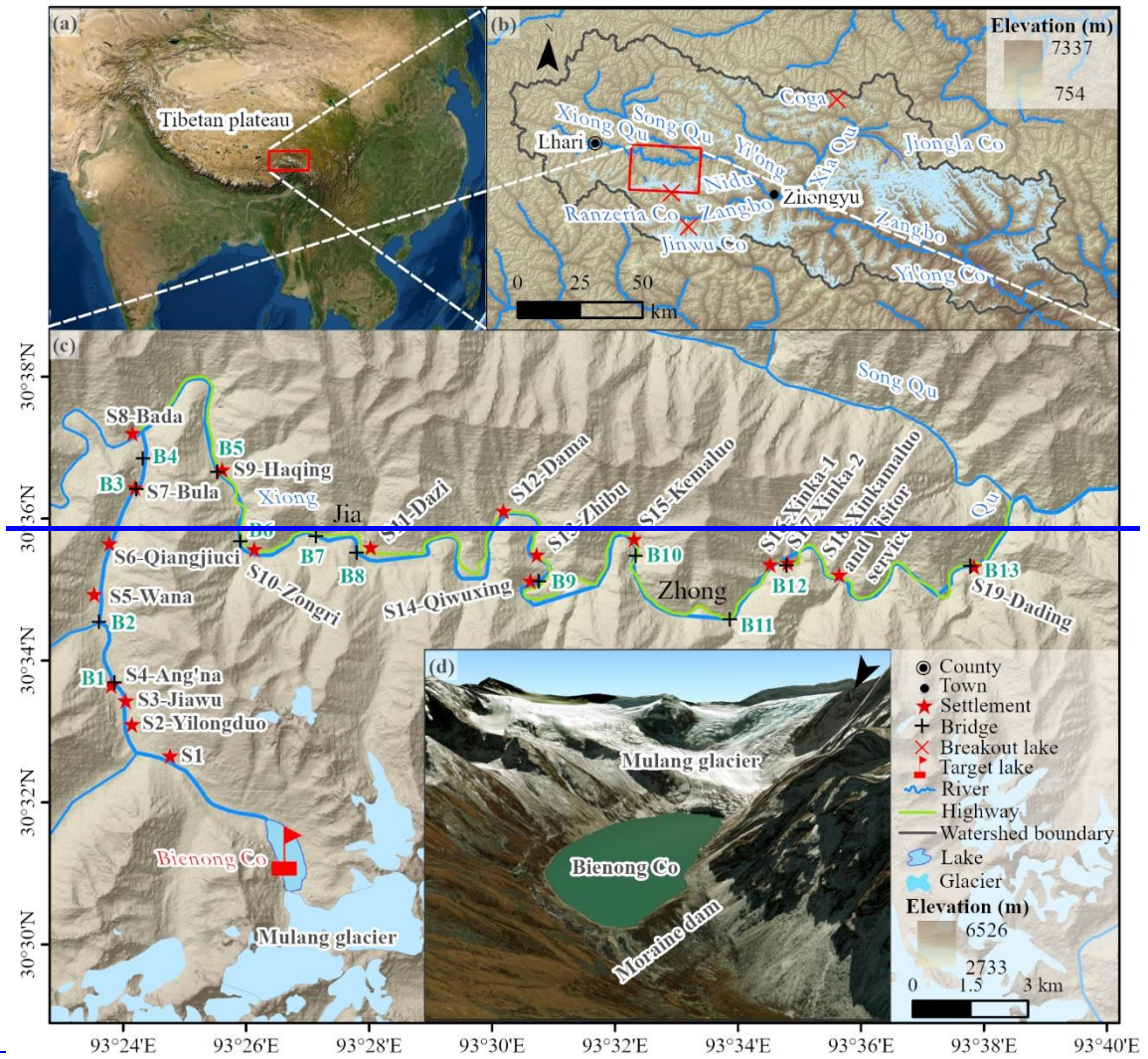
Figure 1. The overview of the study area. (a) The location of Yi'ong Zangbo watershed, (b) the location of Bienong Co, (c) distribution of settlements as well as bridges within 52.98 km downstream the Bienong Co, and (d) the close up view of Bienong Co. Bienong Co' location in High Elevation Asia and the proximity picture are from Esri ArcGIS Earth software, topography map is ALOS PALSAR DEM and the locations and the names of settlements and bridges along the flow channel are obtained from Esri ArcGIS Earth software and Zhongke Tuxin LocaSpace software.
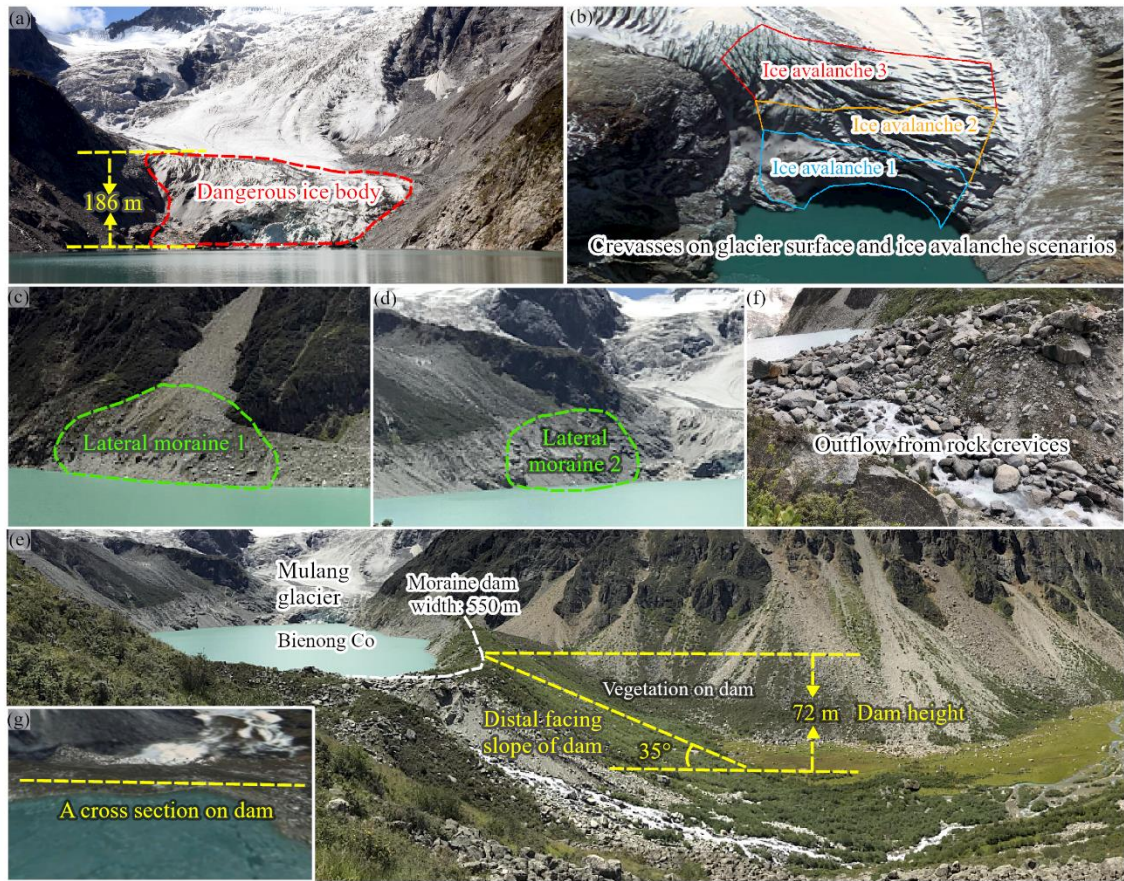
3 Methodology

3.1 Delineation of glacier and glacial lake

Due to the high spatial-temporal resolution, satellite images are primary data sources for delineating and monitoring changes in glaciers and glacial lakes (Wang et al., 2013; Zhang et al., 2015; Khadka et al., 2018; Wang et al., 2020). In this study, multi-sources of remote sensing images were used to investigate the evolution of Bienong Co and Mulang Glacier (Table 1). Since remote sensing images in STEP are heavily affected by clouds and snow, only valuable cloud-free images in late summer and autumn were selected. Images of Landsat MSS on November 10, 1976, Landsat TM on October 9, 1988 and Landsat OLI on September 8, 2021 were used to study the surface area change of Binong Co. Meanwhile, AST14DEM (Maurer et al., 2019) from 2004 to 2018 were used to analyze the surface elevation change of Mulang Glacier.

Studies show that the automatic interpretation based on spectral characteristics of ground objects has advantages in efficiency (Bhardwaj et al., 2015; Zhang et al., 2019), but the manual extraction yields more accurate results (Fujita et al., 2009; Shugar et al., 2020). Considering only one lake and glacier being investigated in this study, the manual visual interpretation method was applied to delineate Bienong Co and Mulang Glacier. While the boundary of the Mulang Glacier was manually revised based on the Second Chinese Glacier Inventory (SCGI). Then lake and glacier area were calculated based on the UTM projection and the area error was estimated using the Eq. (1) (Wang et al., 2012b):

$$\varepsilon = \frac{\lambda^2 \cdot p}{2\sqrt{\lambda^2 + \lambda^2}} = \frac{\lambda \cdot p}{2\sqrt{2}} \tag{1}$$

where *p* is the perimeter of the glacial lake and *λ* is the spatial resolution of the images used.

Table 1. Details of multi-source dataset used in this study.

Data	Date	Resolution	Application	Source
Landsat MSS	1976-11-10	60 m	Glacier and glacial lake mapping	
Landsat TM	1988-10-09	30 m	Glacier and glacial lake mapping	1
Landsat OLI	2021-09-08	30/15 m	Glacier and glacial lake mapping, River channel mapping	
World Maxar image	2017-2022	1 m	River channel mapping GLOFs simulation	2
AST14DEM dataset	2004-11-05 2005-11-17 2009-10-18 2010-10-30 2013-09-27 2013-10-13 2018-10-27	30 m	Glacier elevation measuring	3
ALOS PALSAR DEM	2006-2001	12.5 m	GLOFs simulation	3
GLC10 land use and land cover (LULC) product	2017	10 m	GLOFs simulation	4
Bathymetry data	2020-08-27	5 m	Morphology modeling of glacial lake and GLOFs simulation	5
Field photos	2020-08-27	4000×6000 dpi	Analysis of the topographic parameters of glacial lake	5
SCGI	1970-12	1:100000	Glacier mapping reference	6

1. USGS (the United States Geological Survey): https://earthexplorer.usgs.gov/
2. Esri ArcGIS Earth software: http://goto.arcgisonline.com/maps/World_Imagery
3. NASA (the National Aeronautics and Space Administration) EARTHDATA: https://earthdata.nasa.gov/
4. GLC10 LULC product: http://data.ess.tsinghua.edu.cn/fromglc10_2017v01.html
5. Field measurement.
6. Chinese National Cryosphere Desert Data Centre: http://www.ncdc.ac.cn

3.21 Bathymetry and modeling

Lake bathymetric information is one of the most important inputs in the dynamic modeling of GLOFs, which can accurately reflect the topography of the lake basin below the water surface and be used to calculate the potential flood volume released in different breach scenarios (Westoby et al., 2014). In this study, the depth data were obtained by a USV (APACHE 3) system, which consists of four main parts, i.e., the data acquisition module, the data acquisition transmission module, the positioning and navigation control module, and the power module (Li et al., 2021) (Fig. 3a and b). The USV system has a draft of 10 cm, which is smaller than the inflatable kayak used in previous studies (Haritashya et al., 2018; Sattar et al., 2019, 2021). The D230 Single-Frequency Depth Sounder mounted on the USV is designed the measure range of 0.15--300 m with the depth resolution of 1 cm and the bathymetry error of ±±1 cm+0.1%×h (water depth). The sounder can operate at 200 kHz and water temperature range of -30℃--60℃, meanwhile a real-time kinematic system enables a precise positioning for the bathymetric position with the horizontal error of ±±8 mm, the vertical error of ±±15 mm and the directional error of 0.2˚ on the 1 m

baseline. Field measurements were carried out on August 27, 2020. We designed four longitudinal routes and 13 transverse routes prior to the survey, along which the USV based measurement was conducted (Fig. 2̶3c). The maximum speed of USV can reach 8 m/s, our survey was conducted with a speed of 2 m/s for a total route of 22.58 km in the Bienong Co. Due to absence of any obstructions on the lake, such as ice or small islands, the high performance of the USV̶, and the real-time monitoring, the survey was accurately completed along the designed route. A total of 16,020 valid sounding points basically covering the entire glacial lake were measured, which well fulfilled the ~~requirement of~~ data density requirement to model the lake basin topography (Fig.2̶3c).

Bathymetric map was created within ArcGIS 1̶0̶.̶4̶Pro software using natural neighbor interpolation algorithm (Thompson et al., 2016; Haritashya et al., 2018; Watson et al., 2018). In addition, Surfer software was used to simulate the 3D morphology of the Bienong Co's lake basin. Lake capacity can be understood as the volume of water storage below a certain water level, which is the volume between a certain spatial curved surface and a certain horizontal surface (Shi et al., 1991). In this study, the volume of Bienong Co was obtained by multiplying the depth data and map resolution (5 m) as Eq. (2̶1):

$$V = \sum_{i=1}^{n} H_i \cdot \lambda \tag{2̶1}$$

where V is the volume (m³) of Bienong Co; H_i is the depth (m) at i-th pixel; n is the number of the pixels in the lake area; λ is the pixels resolution (m²) of the bathymetric map.
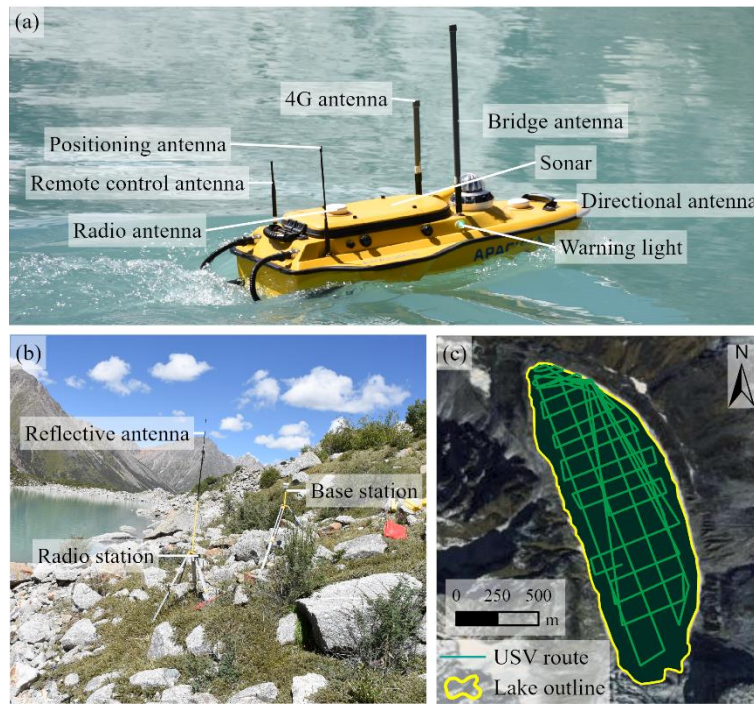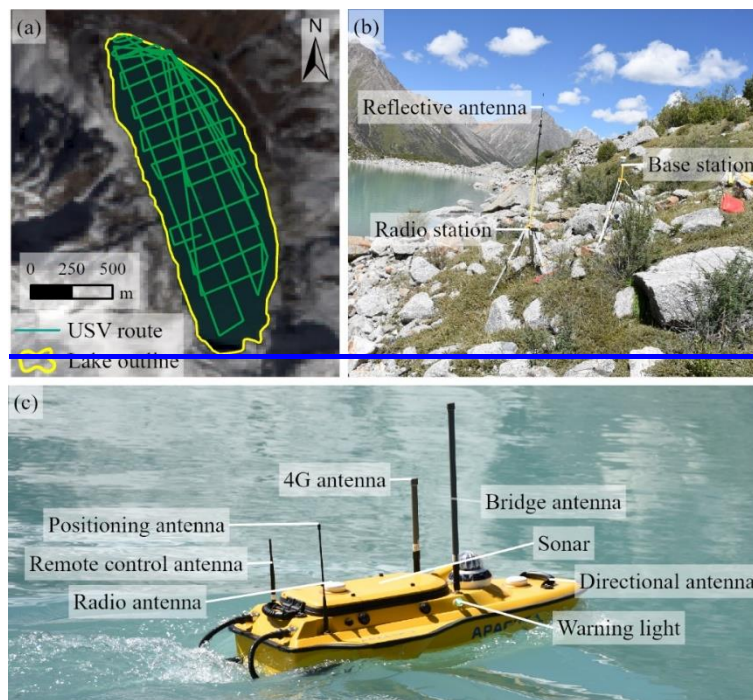
Figure 3~~2~~. The bathymetry of Bienong Co. (a) the USV sampling equipment in water, and (b) on land; (~~a~~c) ~~The~~ the sampling path of USV on Bienong Co covering the base map of ~~Landsat OLI pansharpened true color composite~~MapWorld image~~, (b) the USV sampling equipment on land, and (c) in water~~. Photos taken by Xiaojun Yao on August 27, 2020.

3.2 Potential GLOF modeling~~3.3 Simulation of the potential GLOFs~~

Emmer and Vilímek (2014) and Haeberli et al. (2001) suggested that the assessment of glacial lake hazards should be conducted based on a systematic and scientific analysis of lake types, moraine dam characteristics, eruption mechanisms, downstream processes in the river valley and possible process cascades. The methodology used in this study refers to the GLOFs process chain proposed by Worni et al. (2014), which has been employed by Somos-Valenzuela et al. (2016) and Lala et al. (2018) to study Imja Tsho in Nepal and Palcacocha and Huaraz lakes in Peru, respectively. And in this study, we aim to depict potential GLOFs induced by ice avalanches originate from the Mulang Glacier (Fig. 2a and b) and landslides from lateral moraine (Fig. 2c and d) and assess the potential inundation in the downstream region. The wave resulted from material entering Bienong Co might overtop the moraine dam and initiate an erosive breaching process, releasing considerable amounts of water and debris into the downstream flow channel (Somos-Valenzuela et al., 2016). Three model were used to simulated the GLOFs process chain, RAMMS model was used for simulation of potential mass movement (Christen et al., 2010), BASEMENT model was used to simulate the displacement wave in the lake, Heller-Hager model was used as a calibration for BASEMENT's results, and BASEMENT model was also adopted to simulate the dynamic breaching process of moraine dam, the propagation of flood wave and the inundation in downstream. In next sections, simulation methods for ice avalanches and landslides, displacement wave in lakes, overtopping flow and erosion on moraine dam, and downstream inundation were described.

3.2.1 Triggers determination and simulation

Ice avalanches are the most common GLOFs trigger in the Tibet in China (Yao et al., 204; Liu et al., 2019). Mass movements into lakes generate impulse waves that may produce overtopping flow scouring and eroding moraine dams, or disrupt the hydrostatic pressure-bearing capacity of moraine dams. Based on a survey of the environment surrounding Bienong Co, ice avalanches from Mulang Glacier and two locations of lateral moraine landslide were selected as potential triggers for GLOFs. Wang et al., (2012) defined the volume of dangerous glacier as the volume from the location of abrupt changing slope to the glacier termini or the volume of glacier snout where ice cracks are well developed. We adopted the latter, i.e., the crevasse-

developed ice body of Mulang Glacier shown in MapWorld image with a surface area of 0.19 km^2 was selected as the potentially ice avalanche source of Bienong Co (Fig. 2a). For the convenience of subsequent description, we name it Scenario A. The elevation difference between the top of the dangerous ice body and the lake surface was measured to be about 155 - 208 m based on ALOS PALSAR DEM. We divided the dangerous ice body into three parts according to elevation range to simulate subsequence processes from ice avalanches of different magnitudes (ice avalanche 1, 2 and 3 in Fig. 2b,). Scenario A1 was defined as a low-magnitude trigger, ice body at elevation below 4,844 m yields a release area of 0.05 km^2 with the maximum and average elevation differences of 99 m and 75.8 m from the lake surface. Scenario A2 was defined as a moderate-magnitude trigger, ice body at elevation below 4,889 m yields a release area of 0.11 km^2 with the maximum and average elevation differences of 144 m and 102.7 m from the lake surface. Scenario A3 was defined as an extreme-magnitude trigger, the total ice body of crevasse with an area of 0.19 km^2 was set as a release area, with the average elevation difference between glacier surface and lake surface of 131 m. In the above three cases, we assumed that the release depths of ice avalanches are the average elevation differences from the glacier surface to the lake surface, i.e., the glacier is supported by flat bedrock located at the height of the lake water table.

Lateral moraine landslide as a GLOFs trigger is not common on the Tibetan Plateau, but the GLOF of Jinwu Co in 2020 was caused by a lateral moraine landslide (Liu et al., 2021; Zheng et al., 2021), therefore it was taken as a trigger of the potential GLOF for Bienong Co. Two areas of lateral moraine within the slope range of 30° - 45° were selected as potential landslide sites, one is located on the left bank (in this study, the left and right sides are defined in a downstream-oriented manner) of Bienong Co, near the moraine dam with an area of 0.015 km^2, we named it Scenario B (Fig. 2c). Another is located on the right bank, near the mother glacier with an area of 0.024 km^2, we named it Scenario C (Fig. 2d). Two sites are at different distances from the moraine dam and we set three different release depths of 2 m (Scenario B1 and C1), 5 m (Scenario B2 and C2), and 10 m (Scenario B3 and C3) for each release area as low-, moderate- and extreme-magnitude trigger. Therefore, a total of two different types, three different locations and nine different magnitudes of materials were designed to enter the lake as potential triggers for GLOFs in this study. The above design fully considers the impact of triggers on Bienong Co under different magnitudes, and the results are used as the input for the subsequent disaster chain simulation.

In this study, ice avalanches and lateral moraine landslides of Bienong Co were modeled using the Avalanche module of Rapid Mass Movement Simulation RAMMS model (Barteltet al., 2013), which has been successfully used for simulating triggers of GLOFs (Somos-Valenzuela et al., 2016; Lala et al., 2018; and Sattar et al., 2021). RAMMS adopts the Voellmy-Salm finite volume method to solve the depth-averaged equations governing mass flow in two dimensions (Christen et al., 2010). Based on the basic inputs of DEM, the initial release area and depth, the calculation domain, and the friction parameters μ (the velocity-independent dry Coulomb) and ξ (velocity-dependent turbulent friction terms), the outputs of runout distances, flow height and flow velocity can be calculated. And time series of material entering the glacial lake can serve as the input condition for subsequent simulations. For this study case, the initial release area was determined by combining MapWorld image of the spatial resolution of 0.5 m (https://www.tianditu.gov.cn/) and ALOS PALSAR DEM with a spatial resolution of 12.5 m (https://asf.alaska.edu/data-sets/derived-data-sets/alos-palsar-rtc/alos-palsar-radiometric-terrain-correction/). Values of μ=0.12, ξ=1,000 m s^{-2}, and ρ=1,000 kg m^{-3} for ice avalanche and ρ=2,000 kg m^{-3} for landslide were used, which agree with values used in previous GLOF-producing avalanche models (Schneider et al., 2014; Somos-Valenzuela et al., 2016).

3.2.2 Hydrodynamic wave simulation

Processes following mass movement entering the lake, such as the generation and propagation of displacement wave, the overtopping flow and erosion on moraine dam, and the inundation of downstream were modeled using BASEMENT model v2.8.2 (Vetsch et al., 2017), developed by the Laboratory of Hydraulics, Glaciology and Hydrology (VAW), ETH Zurich. BASEMENT is both a hydrodynamic model and a sediment transport model, making it well suited to model much of the GLOF process chain (Worni et al., 2014). It solves 2-D shallow water equation (SWE) in combination with sediment transport

equations, primarily the Shields parameters and the Meyer-Peter and Müller (MPM) equations (Shields, 1936; Vetsch et al., 2017). The simulation of hydrodynamic waves in the lake is performed using the 2D modeling of BASEMENT based on unstructured grids. The BASEmesh plugin for QGIS (QGIS Development Team, 2016) developed by BASEMENT greatly facilitates the generation of mesh. The lake bathymetry data were produced into DEM with a spatial resolution of 5 m using ArcGIS Pro software for reflecting the lake basin topography. The triangular irregular network (TIN) within the lake area was set to a maximum area of 500 m^2 to simulate the generation and propagation of hydrodynamic waves in the lake effectively and accurately. The input boundary conditions are time series of ice avalanches and landslides generated by RAMMS model. In each time period, RAMMS calculates the total amount of sediment, and the inflow rate can be determined by calculating the difference of sediment entering the lake at the two time points. Pure rock landslides have been studied with densities ranging from 1,950 kg m^{-3} to 2,200 kg m^{-3} (Wang et al., 2017), and most ice-dominated avalanches have densities of about 1000 kg m^{-3}. In this study, the ice avalanche density was set as 1,000 kg m^{-3} and the landslide density is set to 2,000 kg m^{-3}. Since BASEMENT only accepts water as an inflow, this difference due to density is considered by expanding the landslide material entry rate by a factor of two (namely, 1,000 kg m^{-3} of water is equivalent to 1,000 kg m^{-3} of ice avalanche volume, and only 500 kg m^{-3} of landslide material), which is the usual approach used in the simulation process (Byers et al., 2018 and 2020).

It was shown that the 2D SWE used by BASEMENT model inherently leads to excessive wave attenuation. Heller-Hager model (Heller et al., 2009) is a combination of analytical and empirical equations used to simulate impulse wave generation, propagation, and run-up from the movement of material entering a lake. Although the approach relies on simplifying measurements about lake geometry, it has been used to successfully simulate multi real events and performs well in characterizing impulse waves within lakes, making it a simple but useful calibration measure for more complex hydrodynamic models (Somos-Valenzuela et al., 2016). BASEMENT simulated waves are usually considered more accurate when they are of the same order of magnitude as Heller-Hager waves; however, when they are not, the mass entry rate is varied by adjusting the inflow hydrograph and boundary width to match the amplitude of Heller-Hager empirical model near the dam of the initial wave trajectory (Lala et al., 2018). The Heller-Hager model simulates waves in two cases: (a) with longitudinal impacting slide and confined transverse wave propagation and (b) with the slide impacting across the reservoir and completely free radial wave propagation. In present study, ice avalanches belong to case (a), and landslides belongs to case (b). Compared to case (a), the impulse wave (its amplitude and energy) in case (b) decreases more rapidly because it propagates over a larger area is accompanied by wave refraction and reflection.

3.2.3 Moraine dam erosion simulation

The abnormally high lake outflow is sufficient to destroy the surface protection layer of the outlet streambed and trigger vertical dam erosion. After the initial cut, more lake water was able to flow out, followed by an increase in sediment transport rate and a gradual widening of the rift. In this study, the hydro-morphodynamic simulations of potential erosion-driven breach failures of Bienong Co was carried out by BASEMENT model, which uses the Meyer-Peter and Müller (MPM) equation to characterize sediment transport and estimates suspended and nudged mass fluxes by calculating the shear stress in the flow through the modified Shields parameter (Vetsch et al., 2017). The overtopping flow leading to erosion of the moraine dam is generated by the wave amplitude of the BASEMENT model calibrated by the Heller-Hager model. In the previous step, we adjusted the wave amplitude near the moraine dam in the BASEMENT model to be close to (difference within 1 m) that calculated by Heller-Hager model by modifying the width of the upstream boundary. ALOS PALSAR DEM is the base data for the mesh generation of moraine dam with the maximum TIN area of 200 m^2. We set a cross section along the crest of moraine dam (Fig. 2g), where the moraine dam deformation, i.e., erosion, and the overtopping as well as outflow discharges were analyzed. BASEMENT model provides both single-grain (MPM) and multi-grain (MPM-multi) algorithms to simulate material transport. The MPM-Multi model simulates hiding and armoring processes that may lead to unrealistically low levels of erosion (Vetsch

et al., 2017). The MPM model ignores these processes, however, it can lead to an overestimation of erosion. In this study, we applied the MPM-multi model to simulate the bed-load transport of moraine dam, which are composed of materials with different grain sizes. The specific grain size distribution was not measured, it was instead taken from an inventory of glacial lakes in the Indian Himalaya (Worni et al., 2013) that had performed well in recreating previous GLOFs in Nepal (Byers et al., 2020). Despite uncertainty in the actual grain size distribution, a similar GLOF modeling study in the Barun Valley (Byers et al., 2018) found little difference in simulated moraine erosion between the grain size distributions listed in Worni et al. (2013). The moraine dam of Bienong Co consists of a large grain cover with a thickness of about 0.5 m at the top and fine grain underneath, which is clearly visible on the side walls of the channel scoured by water (Fig. 2e). We set up two soil layers in BASEMENT model to represent the above situation. The largest particle size (d_{50} = 180 mm) in the upper layer with a depth of 0.5 m, while the grain size distribution of lower layer that has a depth of 71.5 m (considering the mean height of moraine dam of 72 m) is consistent with Worni et al. (2013). Finally, a correction factor of 2.0 was used in model to increase the rate of bed load transport. Values between 0.5 (low transport) and 1.7 (high transport) are generally realistic (Wong and Parker, 2006), while a value of 2.0 provides high sediment transport conditions (Somos-Valenzuela et al., 2016) to compensate the lower erosion of MPM-multi model.

3.2.4 Downstream impact analysis

The flow channel from Bienong Co to the convergence with Song Qu stretches ~53 km (Fig. 1d), along which 18 settlements, 13 bridges and Jiazhong Highway are distributed. In this study, BASEMENT model was used to simulate Hydrodynamic behavior of potential GLOFs along the flow channel, and the hazard of floods was assessed by analyzing the inundation area, flow velocity, and flood arrival time at these settlements. The 2D model for an unsteady hydraulic simulation requires input of terrain data and boundary conditions. The terrain data was represented by a 2D mesh covering the entire flow area, which was obtained from ALOS PALSAR DEM. The mesh was also generated by the BASEmesh plugin of QGIS software, and the individual cell area for main flow channel and other regions were set to 500 m^2 and 5,000 m^2 considering the accuracy requirements of the simulation and the computational efficiency of the model. Friction of the river channel to a given flow is determined by the Manning's roughness coefficient (Coon, 1998), which is dependent on the land use and land cover of the modeling river channel in the study area. In this study, the GLC10 LULC product (http://data.ess.tsinghua.edu.cn/fromglc10_2017v01.html) with a spatial resolution of 10 m was used to obtain the value of Manning's N in the flow channel. The upstream boundary is the outflow hydrograph from the moraine dam simulated by BASEMENT model. And the downstream boundary is the water level-discharge relationship of the cross-section in downstream boundary of the simulation area, it was estimated by the critical depth method (Byers et al., 2018).

3.3.1 DEM and LULC

DEM is an important data for glacier and glacial lake related research, for example the extraction of the surface elevation of glaciers and glacial lakes, the elevational parameters of dam, the cross-sections of river channel and so on. The Advanced Land Observing Satellite's (ALOS) mission Phased Array type L-band Synthetic Aperture Radar (PALSAR) yielded detailed observation of all weather from day to night and repeat pass interferometry from 2006 to 2011 (Maskey et al., 2020). The radiometrically terrain-corrected elevation product ALOS PALSAR DEM with a spatial resolution of 12.5 m was released globally in October 2014 by the Alaska Satellite Facility (https://asf.alaska.edu/data-sets/derived-data-sets/alos-palsar-rtc/alos-palsar-radiometric-terrain-correction/) (Scatter et al., 2019) and was adopted in this study, which has been successfully applied in GLOF modeling previously in the Himalayas (Dhote et al., 2019; Sattar et al., 2019; Maskey et al., 2020).

Friction of the river channel to a given flow is determined by the Manning's roughness coefficient (Coon, 1998), which is dependent on the land use and land cover of the modeling river channel in the study area. In this study, the GLC10 LULC product (http://data.ess.tsinghua.edu.cn/fromglc10_2017v01.html) with a spatial resolution of 10 m was used to obtain the

value of Manning's *N* in the flow channel.

3.3.2 Scenario scheduling

As a dangerous moraine-dammed glacial lake in SETP (Duan et al., 2020), Bienong Co may be struck by ice/snow avalanches, rock fall, landslides, heavy precipitation or earthquake and result in a GLOF event. Considering the impulse waves capable of initiating an overtopping failure of the frontal moraine caused by above factors, we assumed four scenarios based on different breach depths at the dam (Table 2). The worst scenario suffered the dam collapse from the existing outlet to the base of the moraine dam (72 m), other scenarios in which the breach height was reduced by half in turn (36 m, 18 m and 9 m). Based on the measured bathymetry of Bienong Co, the released water volume (V_w) due to different breach height can be easily achieved. And then the average breach width (W_b) and the failure time (T_f) can be calculated using empirical relationships proposed by Froehlich (1995a) (Eq. (3) and Eq. (4)), which are the mostly used empirical approach for modeling earth rock dam failures because of the high accuracy and low prediction error (Wahl, 2004).

$$\text{(3)}$$

$$\text{(4)}$$

where, V_w is the released water volume, and H_b is the breach height. All scenarios were modeled as a sine wave progressive breach model where the initial breach forms slowly and accelerates as the outflow velocity and shear stress increase through the breach (Sattar et al., 2021).

By inputting the above breach parameters to the MIKE 11 hydrodynamic model, a hydrography of breach can be obtained. Froehlich (1995b) proposed an empirical formula to estimate the peak discharge (Q_{max}) of output flow (Eq. (5)), which was used to verify results from MIKE 11 model.

$$\text{(5)}$$

Table 2. Details of breach parameters for different GLOFs scenarios, including the calculated discharge volume (m³) based on bathymetry data and the peak discharges (m³·s⁻¹) of the breach hydrograph from MIKE 11 model and empirical formula (Froehlich (1995b)).

Parameters	Scenario 1	Scenario 2	Scenario 3	Scenario 4
Breach height (H_b) (m)	72	36	18	9
Breach width (W_b) (m)	180	131	94	66
Time of failure (T_f) (h)	0.75	1.03	1.37	1.79
Discharged volume (V_w) ($\times 10^7$ m³)	6.52	3.67	1.93	0.99
Percentage of discharged volume (%)	64	36	19	10
Peak discharge (MIKE 11 model) (m³·s⁻¹)	26721	11126	3716	1294
Peak discharge (empirical formula) (m³·s⁻¹)	24630	8801	3081	1070

3.3.3 GLOFs modeling

MIKE 11 is a professional engineering software package developed by DHI Water and Environment in 1987, which has powerful capabilities for the numerical simulation of rivers and the replication and calculation of dam-breaching processes based on an implicit, finite difference computation of unsteady flows (DHI, 2007). The software has been successfully used for GLOF modeling in Himalayan basins (Jain et al., 2012; Aggarwal et al., 2013; Lohani and Jain, 2016; Thakur et al., 2016). MIKE 11 dam breach model is composed of river channels, reservoirs, dam break structures, etc., in which, the river is

represented by cross-sections at regular intervals. In this study, glacial lake was represented as a dam breach structure which includes a reservoir with water level-area relationship, and the breaching parameters of breach depth, breach width, and failure time. Then, the unsteady flow simulations were carried out based on the preset four scenarios and computational interval with dam failure mode of overtopping. Finally, the resulting outflow hydrological curves at breach were used as the upper boundary condition of the two-dimensional model MIKE 21 (DHI, 2007).

MIKE 21 Flow Model is a modeling system for 2D free-surface flows, which is applicable to the simulation of hydraulic and environmental phenomena in lakes, estuaries, bays, coastal areas and seas (DHI, 2007). MIKE 21 model was used to simulate the dynamic routing of the initial breach hydrography along the flow channel from Bienong Co to the convergence with Song Qu (Fig.1). The inputs to the two-dimensional model for an unsteady hydraulic simulation includes terrain data and boundary conditions. The terrain data was represented by a 2D mesh covering the entire flow area, which was obtained from ALOS PALSAR DEM. The unstructured mesh of MIKE 21 is an approximately equilateral triangular mesh with a cell-centered finite volume solution, which simulates the flow field in the area around the river bend and the structure over water excellently. The size of the mesh can be adjusted, namely the focal areas can be encrypted. In this study, the 2D mesh has an individual cell area of 1000 m² in main flow channel and the 10000 m² in other regions. Each cell was defined with a Manning's N value and the topographic elevation. The upstream boundary of the two-dimensional model is the outflow hydrographs at the immediately downstream of moraine dam derived from the MIKE 11 model, and the downstream boundary is the lowest elevation of the terminal of simulated flow channel. The two-dimensional dynamic modeling is solved by the depth-averaged shallow water equations. Furthermore, the significant flood wave parameters like inundation area, discharge, flow depth, flow velocity and arrival time of flood were analyzed to evaluate the potential GLOFs hazard along the flow channel, with the focused attention on the 19 settlements, 13 bridges and Jiazhong Highway.

4 Results

4.1 Evolution of Bienong Co and the mother glacier

Bienong Co is a stable glacial lake, which only experienced an expansion of about 120 m towards the Mulang Glacier from 1976 to 1988 (maybe earlier), and has remained stable since then (Fig. 3) because it has reached the ice cliff of Mulang Glacier and there is no room for expansion (Fig. 1 and Fig. 3). The same is true for the area of Mulang Glacier, which has remained largely unchanged area over the last 45 years. However, the ice thickness of the whole glacier and the glacier ablation zone has thinned, with the decreasing rate of -0.79 m/a and -6.54 m/a, showing a negative mass balance in the context of climate warming (Fig. 4).
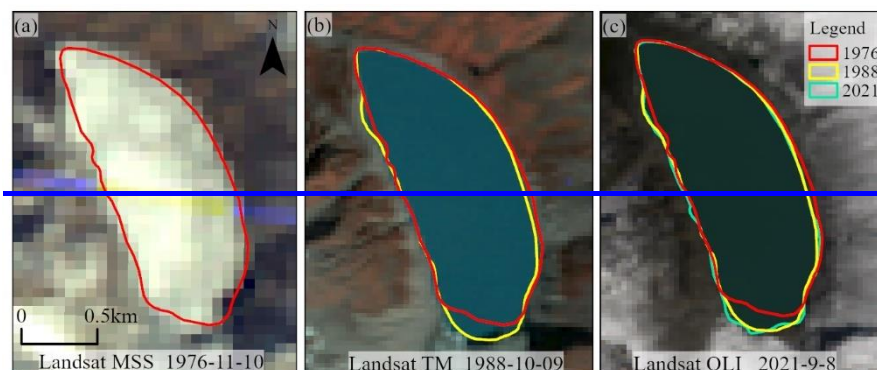
Figure 3. The evolution of Bienong Co from 1976 to 2021.
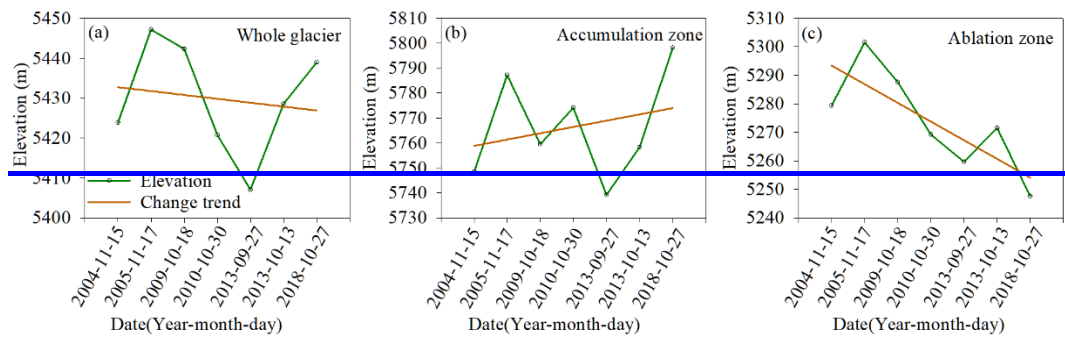
470

4.~~2~~ 1 Morphology and ~~volume~~ water storage estimation of Bienong Co

The basin morphology of Bienong Co was modeled based on the TIN grid created by the field depth data (Fig. ~~2~~3). Apparently, this lake has a relatively flat basin bottom and both deep flanks (Fig. ~~5~~4). Similar to most glacial lakes (Yao et al., 2012; Zhou et al., 2020), the slope of the lake shores near the glacier is steeper than that near the moraine dam. The water depth profile from moraine dam to mother glacier show that the depth of the lake reaches a maximum of ~~180~~ ~181 m at about 1,000 m from the moraine dam, corresponding to the slope of 11.3˚. The depth keeps stable at distance of 1,000 m to 1,500 m from the moraine dam, and the distance from the mother glacier to the deepest point of the lake is 600 m with the slope of 16.5˚. A depth profile facing the moraine dam from the left bank to the right bank shows that the left side is steeper than the right side. The glacial lake reaches its deepest point at 200 m from left shore with the slope of 43.4˚, then maintains flat to 430 m, and the distance between the bottom and right shore is 273 m with the slope of 32˚. The volume of Bienong Co, calculated using the surface elevation and the lake bed derived from the TIN grid, was about $10.\underline{2.3}\times\underline{10^7}\underline{10^6}$ m^3 in 2020, which is a generally accurate estimate of the magnitude of this moraine-dammed lake.
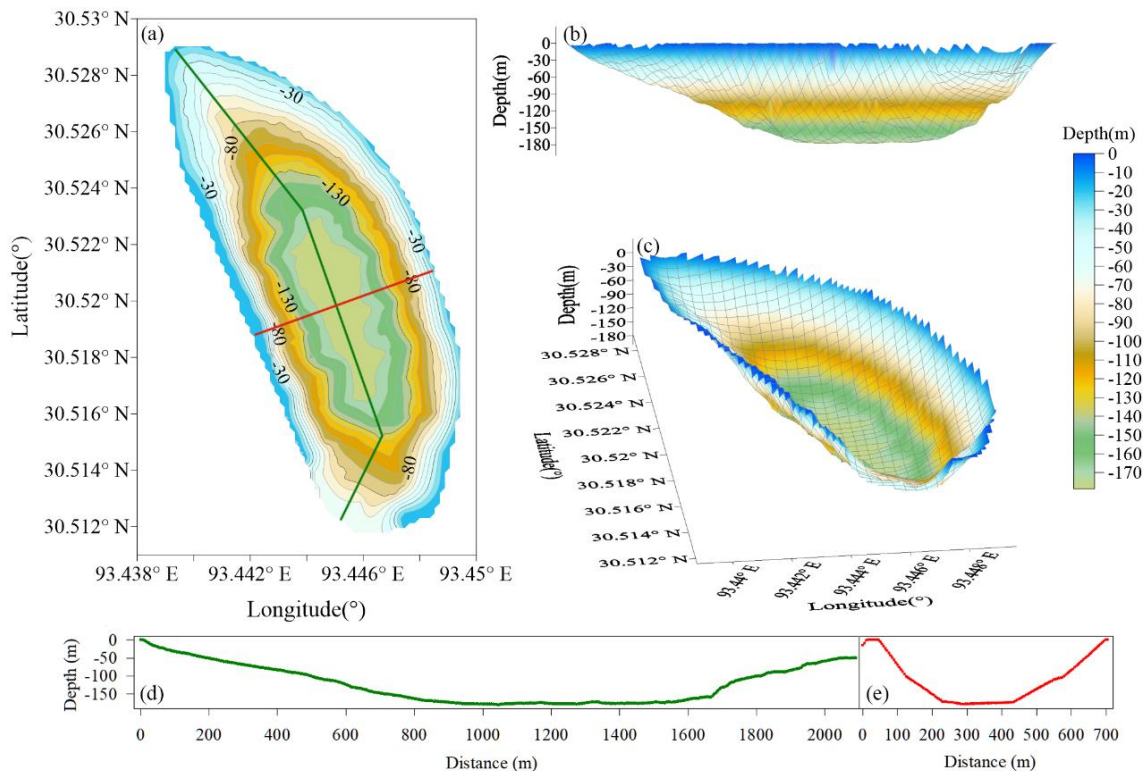
Figure ~~5~~4. Morphology modeling of Bienong Co in 2020 and the equal-scale profiles of distance and depth from the moraine dam to Mulang Glacier (green line) and from the left shore to right shore (red line).

4.~~3~~ 2 Potential GLOFs ~~simulations~~modeling

4.~~3~~2.1 Ice avalanche and lateral moraine landslide~~Moraine-breach and inter-comparison of GLOF discharge~~

As calculated by RAMMS, the volume of ice avalanches entering Bienong Co for Scenarios A1, A2, A3 are 3.8×10^6 m^3, 4.9×10^6 m^3 and 5.8×10^6 m^3 (Fig. 5a). Most of materials enter the lake within about 120 s. Based on the area of ~1.15 km^2 in 2021, above three scenarios could result in a rise of about 3.3 m, 4.2 m and 5.1 m in the lake surface. Materials volumes entering the lake by both landslides are much smaller than that of the ice avalanche (Fig. 5b and c). Scenarios B1, B2, B3 and C1, C2, C3 dump 0.03×10^6 m^3, 0.09×10^6 m^3, 0.17×10^6 m^3, and 0.06×10^6 m^3, 0.15×10^6 m^3, 0.30×10^6 m^3 of material into the lake, respectively. The time for materials entering the lake is less than in Scenario A, with Scenario B1/2/3 being completed in about 10 s and Scenario C1/2/3 in about 15 s.
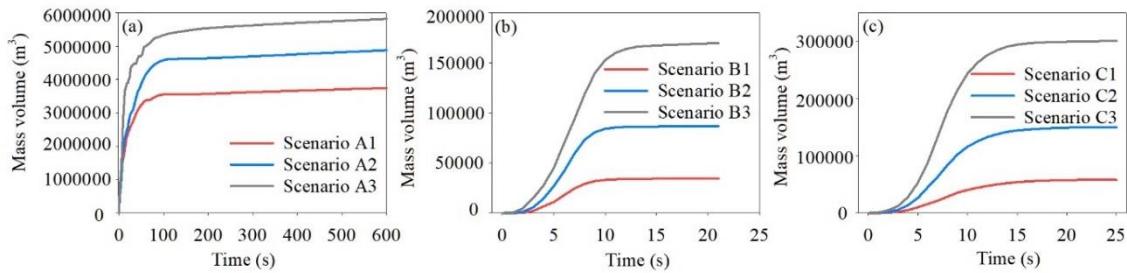
Figure 5. Volume of material entering Bienong Co for different (a) ice avalanches and (b), (c) landslide scenarios.

The impact area caused by material entering the lake differs for different scenarios. The impact zones caused by Scenarios A1, A2 and A3 are 0.27 km^2, 0.31 km^2 and 0.38 km^2, respectively, with horizontal distances of 549 m, 629 m and 752 m from the upper boundary (Fig. 6). In contrast, each of the three scenarios for Scenarios B and C result in a relatively small impact zone, with Scenario C3 being the largest of 0.14 km^2 and Scenario B1 being the smallest of 0.04 km^2. Scenarios A1, A2, and A3 produce maximum flow heights of 39.5 m, 46.2 m, and 53.5 m, and average flow heights of 12.2 m, 14.6 m, and 12.3 m in the impact area, respectively. The maximum flow height range for Scenario B1/2/3 is 6.8 - 14.6 m and the average flow height range is 1.8 - 3.5 m. The maximum and average flow height ranges for Scenario C1/2/3 are 5.7 - 29.2 m and 2.0 - 4.7 m (Fig. 6). The maximum flow velocities for Scenarios A1, A2 and A3 are 34.9 m/s, 43.1 m/s and 51.4 m/s, with the average flow velocities of 11.1 m/s, 12.3 m/s, and 16.8 m/s, respectively. The maximum and average flow velocities for Scenarios B1, B2 and B3 and C1, C2 and C3 are in the range of 21.3 - 33.6 m/s and 8.5 - 14.2 m/s, respectively (Fig. 6).
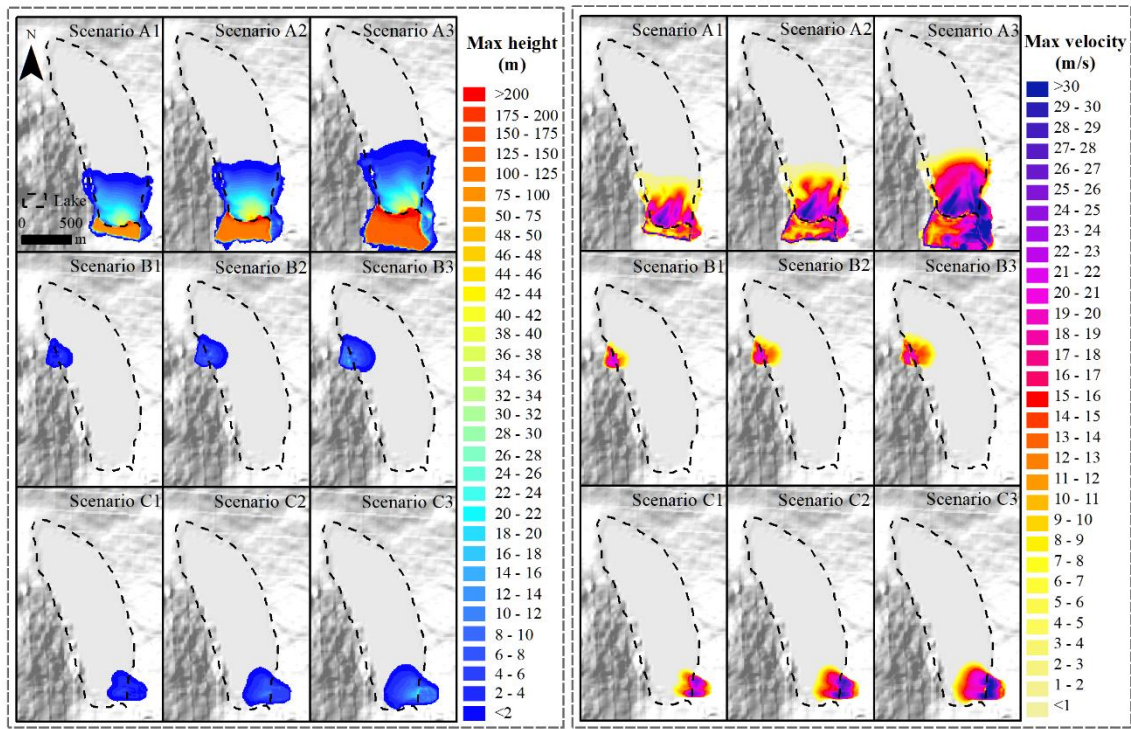
Figure 6. Maximum flow height (left) and maximum flow velocity (right) for different ice avalanches and landslides scenarios.

4.2.2 Generation and propagation of displacement wave

By counting material volumes of ice avalanches and landslides entering Bienong Co at different time periods based on RAMMS model, we derived the time series of the material entering rate as shown in Fig. 7. Compared to Scenarios A2 and A3, Scenario A1 has the highest peak flow rate of 439,952.57 m^3/s, but it decreases rapidly after reaching the peak within two seconds of the ice avalanche, i.e., the ice avalanche occurs in a moment. Scenarios A2 and A3 show obvious fluctuations in the process of ice avalanches into the lake, with sub-peaks in both scenarios that are comparable to the first peak, after which the flow rates still have strong fluctuations. The peak and sub-peak flow rate of Scenario A2 and A3 are 263,922 m^3/s, 238,086 m^3/s and 386,359 m^3/s and 373,449 m^3/s, both occurring at the 2nd and 8th seconds of the ice avalanche, respectively. This is because ice avalanches of Scenarios A2 and A3 are further away from the lake than Scenario A1, and total volumes of ice avalanches are larger than A1, so they entry into the lake undergo a more complex process. The process of landslide material entering the lake is simpler in Scenarios B and C. The peak flows increase sequentially form Scenarios B/C1, B/C2, to B/C3, with peak values of 50,849 m^3/s and 92,529 m^3/s for Scenarios B3 and C3, respectively. The peak flow for Scenario B3 is approximately 3.8 times that of B1, and it for Scenario C3 is 6.5 times that of C1, respectively. The peak flows for the six scenarios of Scenarios B and C occur in the range of 6th-8th seconds (Fig. 7).
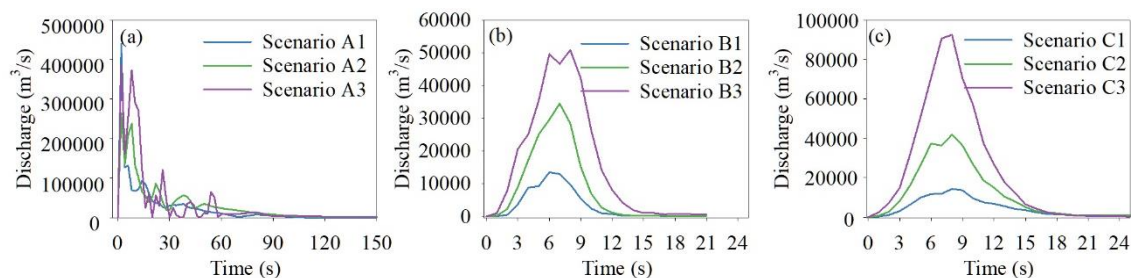
Figure 7. Time series of material entry into the lake for different ice avalanches and landslide scenarios.

The time-volume relationships of materials entering a lake have important effects on the generation and propagation of displacement waves in the lake. Ice avalanches scenarios (A1, A2 and A3) have a much greater impact on Bienong Co than two landslide scenarios (B1, B2, B3, C1, C2 and C3) because the assumed release volume of ice avalanche is much greater

than that of landslides. The wave height near the moraine dam is the result of BASEEMNT model calibrated by the Heller-Hager model. By adjusting the inflow boundary's width, we made the BASEMENT model produce wave amplitudes near the dam with a difference smaller than 1 m of those calculated by the Heller-Hager model, which is important for subsequent simulations although the maximum wave amplitude in the lake is exaggerated.

535   In Scenario A, displacement waves propagate straight from the glacier to the moraine dam and arrive the vicinity of the moraine dam at about 70 s. Scenarios A1, A2 and A3 produce the highest wave amplitudes in the lake of 35.2 m, 39.0 m and 66.4 m, respectively, and the wave amplitudes near the moraine dam of 17.1 m (72 s), 20.2 m (74 s) and 25.2 m (72 s), respectively (Fig .8). Compared with Scenario A, wave amplitudes of Scenarios B and C are much lower. In Scenario B, a landslide occurs at the left shore of Bienong Co near the moraine dam (Fig. 2c). Displacement waves first propagate to the

540   opposite shore along the perpendicular to the inflow boundary, and then they propagate to the moraine dam with the expansion. The maximum wave amplitudes in Bienong Co of Scenarios B1, B2, and B3 are 6.5 m, 14.1 m, and 18.0 m, respectively, and the wave amplitudes near the moraine dam are 1.2 m, 3.0 m, and 5.3 m, respectively (Fig. 8). The landslide in Scenario C occurs on the right bank of Bienong Co near the glacier, the same as Scenario B is that waves propagate to the opposite bank first after materials entering the lake, with the maximum wave amplitudes of 4.8 m, 9.6 m and 24.7 m for Scenarios C1, C2 and C3. Unlike Scenario B, displacement waves in Scenario C cross the entire lake reaching the moraine dam with wave

545   amplitudes of 0.6 m, 2.2 m and 4.9 m near the moraine dam, respectively (Fig. 8). Therefore, although the landslide volume of Scenario C is larger than that of Scenario B, wave amplitudes near the moraine dam are smaller than those of Scenario B.
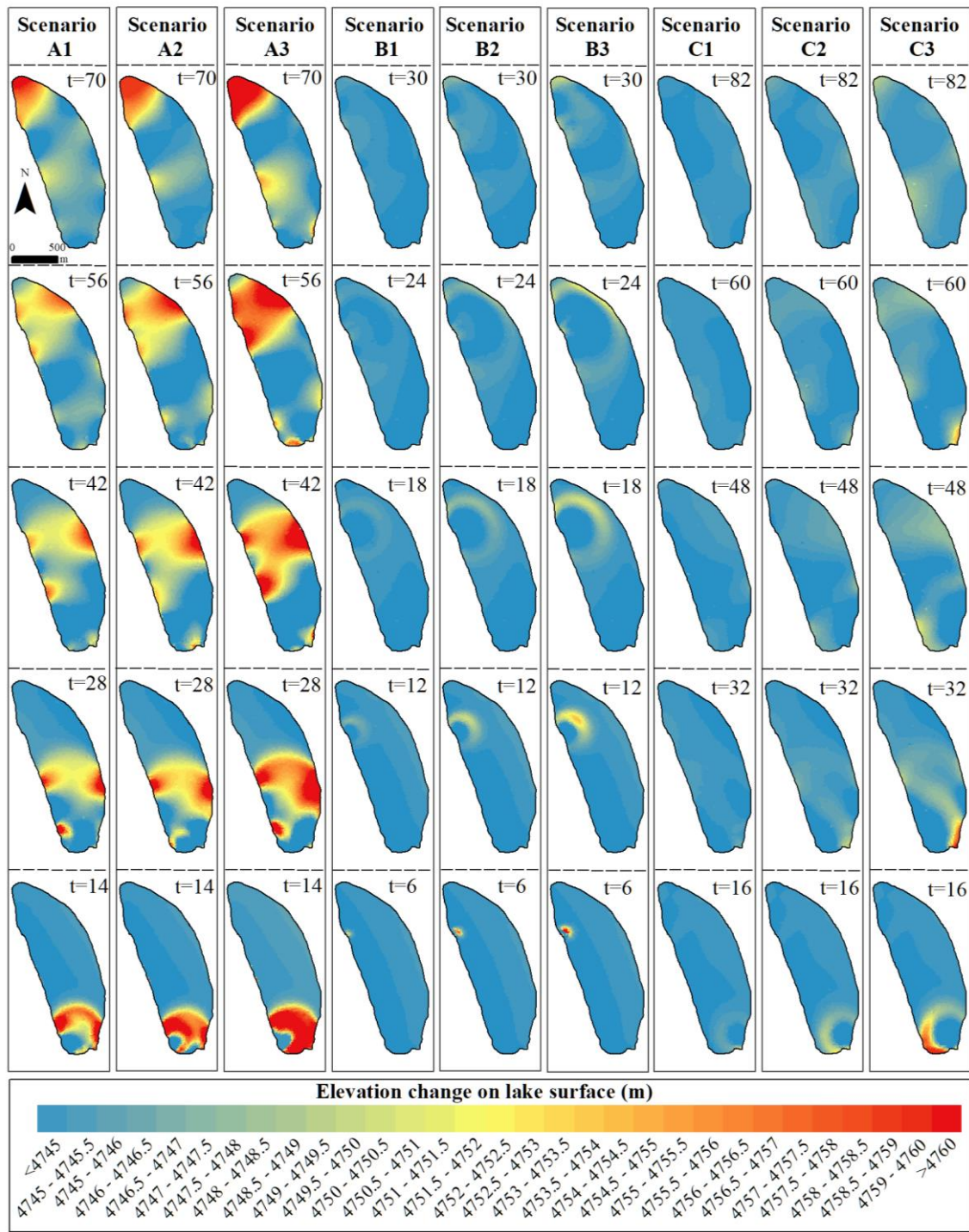
Figure 8. Propagation of displacement waves in the lake for different ice avalanches and landslide scenarios.

4.2.3 Overtopping flow and erosion on moraine dam

Since the freeboard of the moraine dam is 0 m, the occurrence of overtopping flow is inevitable in all scenarios, but there are differences in magnitude. In Scenarios A1, A2, and A3, peak discharges at breaches of moraine dam are 4,996 m^3/s, 7,817 m^3/s and 13,078 m^3/s corresponding to total released volume of 24.1×10^6 m^3, 25.3×10^6 m^3 and 26.4×10^6 m, respectively (Fig. 9). Discharges at the moraine dam stabilize after ice avalanches entering Bienong Co about 18,000 s, 10,800 s and 7,200 s, respectively. Therefore, the erosion of the moraine dam and the total volume of water lost in the lake were counted based on the above time points. Due to the huge discharge output, the moraine dam in Scenarios A1, A2, and A3 are eroded to form breaches. Due to the similar volume of released water, the depth of the breach is slightly different for Scenarios A1, A2 and A3, they are 19.0 m 19.1 m and 19.3 m, respectively (Fig. 10). While the peak discharge is much different for the three

scenarios, resulting in different breach widths of 295.0 m, 339.4 m, and 368.5 m. Scenarios B1, B2, B3 and C1, C2, C3 resulted in overtopping flows of 0.6×10^6 m³, 1×10^6 m³ and 2.6×10^6 m³, as well as 0.1×10^6 m³, 0.9×10^6 m³ and 3.4×10^6 m³, respectively, in which, only Scenarios B3 and C3 cause erosion of the moraine dam and form breach. Discharges at the breach become stable since 18,000 s following landslide material entry into the lake in Scenarios B3 and C3, with breach depths of 6.5 m and 7.9 m, respectively. And breach widths are 153 m and 169 m with the peak discharges of 504 m³/s and 733 m³/s.
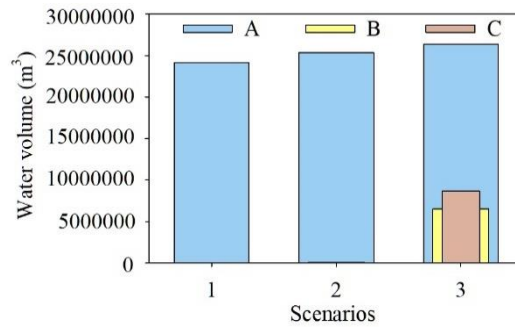
Figure 9. Discharge of water bodies in glacial lakes under different scenarios.
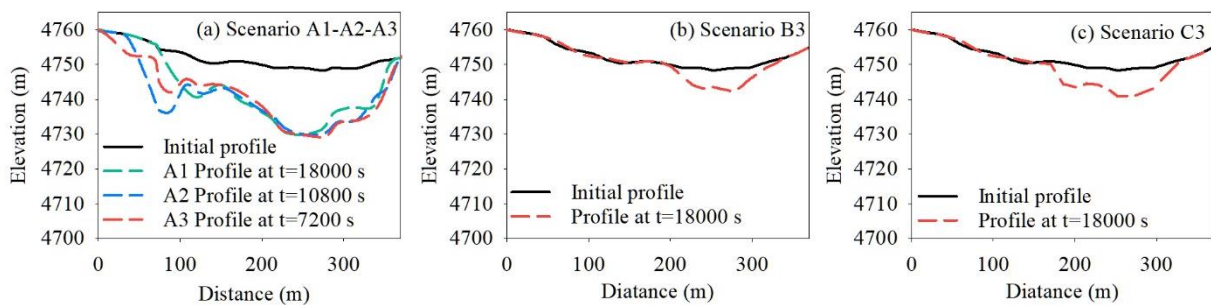
Figure 10. Erosion of moraine dams under different conditions at cross section in Fig. 2g.

4.2.4 GLOFs impact in downstream region

The hydraulic behavior of GLOFs in the flow channel that from the immediately downstream of moraine dam to the convergence with Song Qu with a distance about 53 km was simulated using BASEMENT model. Due to the lack of reliable data on small baseflows in the flow channel, they were neglected in the simulation. Considering the propagation of floods in different scenarios, we assessed the propagation of GLOF in the downstream channel within 20 hours from ice avalanche and landslide materials entry into the lake. Peak discharges at the breach outlet of Scenarios A1, A2 and A3 all occur about 600 s after the ice avalanche material enters the lake, they are 4,996 m³/s, 7,817 m³/s and 13,078 m³/s, based on which, floods all pass through 18 settlements in the downstream river in 20 hours, with the inundation areas of 7.6 km², 8.0 km² and 8.5 km² as well as average water depths of 8.4 m, 9.1 m and 10.0 m, respectively (Fig. 11). The Scenarios B1 and C1 only have a small amount of overtopping flow from the lake (peak discharges of 106 m³/s (after 40 s) and 12 m³/s (after 50 s)), and fail to generate runoff downstream of the dam. Scenarios B2 and C2 produce very limited overtopping flow with peak discharges of 177 m³/s (after 240 s) and 186 m³/s (after 480 s), and outflows remain only within approximately 1 km downstream of the dam. Peak discharges at breach outlet of Scenarios B3 and C3 are 504 m³/s (after 240 s) and 733 m³/s (after 480 s), yielding inundation areas of 1.7 km² and 2.2 km² with average water depths of 1.9 m and 2.4 m in the downstream region. Both GLOFs pass through first eight settlements, but the flood of Scenario C3 flows farther (Fig. 11). Among the nine scenarios we assumed, only Scenarios of A1, A2, A3, B3 and C3 caused GLOFs propagation in the downstream region with a far distance, in which Scenario A3 had the largest flood magnitude, and Scenario B3 had the smallest magnitude.

585
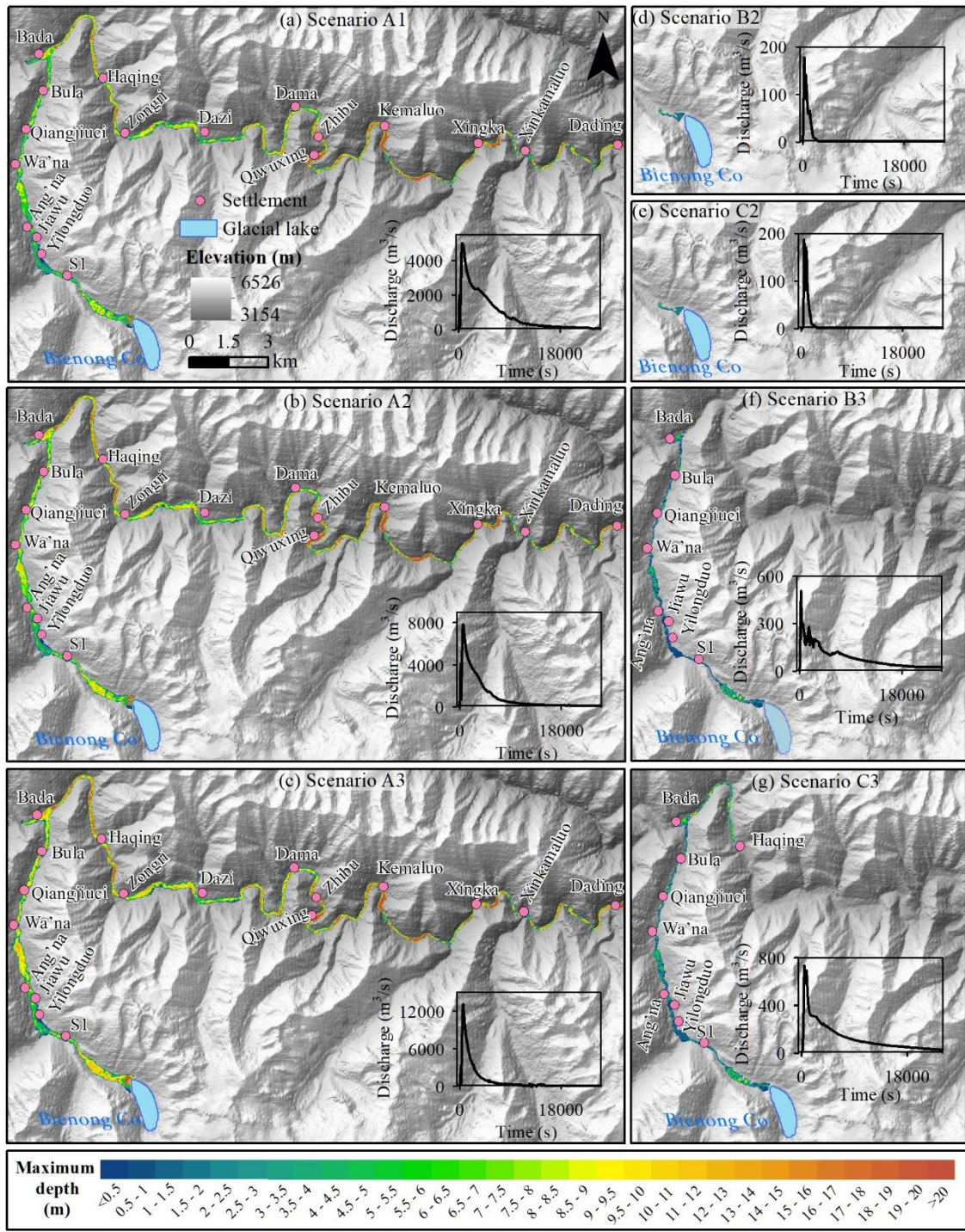
Figure 11. Propagation of flood water downstream and the time series of discharge at the breach outlet (inset) for different scenarios.

Based on the current area and dam status of Bienong Co, four hypothetical dam failure scenarios were modelled by different combinations of H_b, W_b and T_f. Without further consideration of the physics and dynamics of the breach erosion process,

590 each potential breach event yielded the different Q_{max} based on the given breach parameters (Table 2). In the extreme magnitude scenario, the breach was assumed to cut into the base of the dam with the heigh of 72 m (Fig. 6), which is rare in nature and is largely determined by the condition of the moraine dam and the triggers of the breach, but may occur, for example, under the action of a strong earthquake. In this case, the Bienong Co can drain about 6.52×10^7 m³ of V_w, accounting for 64% of the total V_w. The breach width and time of failure based on the formulas of Froehlich (1995a) are 180

595 m and 0.75 hours. Under these conditions, a sharp rise in the outflow hydrography can be caused, with the empirical formula (Froehlich, 1995b) and MIKE 11 model producing similar Q_{max} of 24,630 m³·s⁻¹ and 26,721 m³·s⁻¹, respectively, at immediately downstream of the lake (Table 2). In the high-magnitude scenario, the released V_w is 3.67×10^7 m³, accounting

for 36% of the total lake V_w (Table 2). Within 1.03 hours of the breach, the W_b reached a maximum of 131 m and the flooding peaked at 11,126 m³·s⁻¹ from MIKE 11 model, which is 8,801 m³·s⁻¹ obtained from the empirical formula and lower 24% than the former (Fig. 6). The moderate-magnitude scenario is constrained by the condition of H_b in 18 m, W_b in 94 m and T_f in 1.37 hours, resulting in a release of water volume 1.93×10⁷ m³ (19% of the total volume), and the breach peak of 3,716 m³·s⁻¹ from MIKE 11 model and 3,081 m³·s⁻¹ from empirical formula. The low-magnitude scenario (H_b: 9 m, W_b:66 m and T_f: 1.79 h) drained the V_w of 0.99×10⁷ (10% of the total V_w) with the Q_{max} of 1,294 m³·s⁻¹ based on MIKE 11 model and 1,070 m³·s⁻¹ from empirical formula. This is the most conservative situation and the one that is most likely to happen.
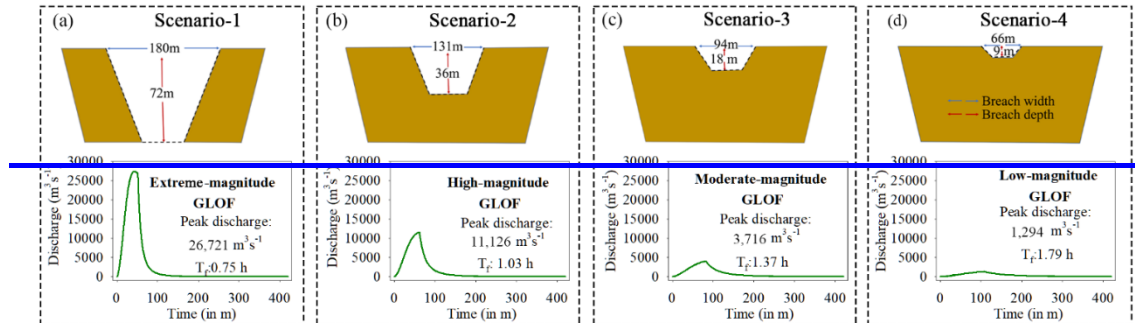
Figure 6. Schematic diagram of the breach width and breach depth (from Froehlich, 1995a) for different scenarios of GLOFs and the corresponding outflow hydrographs, (a) the Scenario-1, (b) Scenario-2, (c) Scenario-3 and (d) Scenario-4 reapectively leads to the extreme-magnitude, high-magnitude, moderate-magnitude and low-magnitude GLOFs.

4.3.2 Hydraulic characterization of GLOFs along the flow channel

The outflow hydrographs at the immediately downstream of moraine dam for four different scenarios were used as the upper boundary for the two-dimensional MIKE 21 model to simulate the hydraulic behaviors of the GLOFs from the lake to the convergence with Song Qu (Table 3, Fig.6), located at a distance of ~52.98 km downstream. Where the inundation area, Q_{max}, maximum flow depth (D_{max}) and maximum flow velocity (V_{max}) of each individual scenario were evaluated at the 19 settlements along the flow channel (Fig.1). Due to the large magnitude of the GLOF flows, any additional flow added by existing stream flows in the river channel were considered negligible.

The calculated maximum inundation areas along the given valley from Bienong Co to the ~52.98 km downstream are 13.05 km², 10.25 km², 8.32 km² and 6.64 km² for the extreme to low-magnitude scenarios, with the average D_{max} of 18.31 m, 10.75 m, 6.76 m and 4.41 m, as well as the average V_{max} of 22.44 m s⁻¹, 7.63 m s⁻¹, 4.78 m s⁻¹, 2.92 m s⁻¹, respectively (Fig.7, Fig.8 and Fig.9).

GLOFs of different magnitudes will pose different potential hazards to each settlement along the flow channel. Scenario A3 produces the most severe threat of GLOF to the downstream region. Six settlements, including Ang'na, Wa'na, Haqing, Kemaluo, Xinka and Dading, will be completely submerged by flooding. Kemaluo village, located 37.9 km downstream of Bienong Co, will experience the relatively largest maximum flow depth of 19.8 m, and the village of Ang'na, having a distance 6.0 km from Bienong Co, will experience the relatively smallest maximum flow depth of 6.1 m. Wa'na village is the most affected of all the villages by GLOF due to the most flooded houses. Eight settlements of S1, Qiangjiuci, Bula, Bada, Dama, Zhibu, Qiwuxing, Xingka and Xinkamaluo will be partial flooded. The maximum flow depth of 11.0 m in Bada village is the largest, and that of 7.2 m in both Dama and Zhibu villages is the smallest. Four settlements, Yilongduo, Jiawu, Zongri and Dazi are spared from flood, in which, Yilongduo may be slightly affected, while Dazi is the safest village owing to its far distance from river. Flooding in Scenario A2 has a relatively small impact on downstream villages compared to Scenario A3, showing the reduced extent of inundation and flow depth. Ang'na and Haqing villages have reduced flood ranges. However, villages Wa'na, Kemaluo, Xinka and Dading will still be completely flooded, but the maximum flow depth is reduced from 16.5 m, 19.8 m, 12.5 m and 17.5 m to 13.6 m, 19.3 m, 12.0 m and 16.6 m, respectively. For the nine villages partially affected

by Scenario A3, they are still affected by flooding of Scenario A2 except for Dama village, but the impact of flooding has a weaken. Scenario A1 differs from Scenario A3 in that Dama and Xingkamaluo villages have been able to be spared from flooding, while other villages have experienced significant reductions in flood extent and inundation depth. The floods of Scenarios B3 and C3 have significantly less impact in the downstream than the above three scenarios. Only Wa'na, Qiangjiuci and Bula villages will be partially affected, with the maximum flow depth of 3.1 m, 1.9 m and 2.0 m in Scenarios B3 and 4.0 m, 2.4 m and 2.7 m in Scenarios C3 (Fig. 12).

The peak discharge and velocity of GLOFs at these villages undergo a gradually decreasing process, while the arrival time of peak discharges is prolonged, favoring the evacuation of residents in the downstream area. Peak discharges in S1, Yilongduo, Jiawu and Ang'na villages are similar for each scenario, ~4,000 m^3/s of Scenario A1, ~6,000 m^3/s of Scenario A2 and ~10,000 m^3/s of Scenario A3. Wa'na, Qiangjiuci, and Bula villages have the similar peak discharges, which are ~3,800 m^3/s, ~5,000 m^3/s, and ~8,000 m^3/s for Scenarios A1, A2, and A3. Since Bula village, peak discharges of each scenario decrease significantly towards the downstream. Taking Scenario A3 as an example, at Bula village, peak discharge is 7,512 m^3/s, to Haqing village, it become smaller than 6,000 m^3/s, to Dama village, it drops below 4,000 m^3/s, to Qiwuxing village drops below 3,000 m^3/s, and at Xinka village decreases to below 1,000 m^3/s (Fig. 13). The flood flow velocity varies dramatically, with Scenarios A1, A2, and A3 corresponding to maximum velocities of 8.9 m/s, 12.2 m/s, and 14.9 m/s, respectively, at village S1. To Dading village, the maximum flow velocity of GLOFs is about 2m/s.

In the extreme magnitude GLOF, the Q_{max} reaches the nearest settlement S1, 3.18 km downstream from Bienong Co, 47 minutes after the breach occurred, which would be almost completely submerged with a V_{max} of 44.49 m s^{-1} and a D_{max} of 10.46 m (Table 3). The Q_{max} at the cross-section passing through S1 can reach up 31,091 m^3 s^{-1} (Table 3, Fig.10). The Yilongduo village is located on the right bank of the river channel 4.81 km downstream of Bienong Co, which would be completely inundated by the extreme magnitude GLOF, with the Q_{max} of up to 38,301 m^3 s^{-1}, arriving approximately 49 minutes after the event. The D_{max} and V_{max} are 6.89 m and 50.55 m s^{-1}, respectively (Table 3, Fig. 7, Fig. 8, Fig. 9 and Fig. 10). The next villages Jiawu (5.44 km: the distance from Bienong Co), Ang'na (5.98 km), Wa'na (8.52 km), Qiangjiuci (9.81 km), and Bula (11.43 km) all would be fully inundated by the extreme magnitude GLOF, with the D_{max} severe to over 10 m (Table 3 and Fig. 8). The Buda village (12.99 km) is unique in that it is not located in the flow channel but at left bank of the upper tributary of Xiong Qu before it converging with the flow channel downstream the Bienong Co (Fig.1). The super flood can cross the highland on the left bank of the flow channel, enter the upstream channel of Xiong Qu and flood Bada village with a D_{max} of 4.81 m, but the region near the mountain can spare from the flooding (Table 3, Fig. 7 and Fig. 8). Haqing village, located at the 17.8 km downstream of Bienong Co, will suffer the most severe damage with a D_{max} of 18.29 m comparing former villages due to its low elevation (Table 3 and Fig. 7). The next Zongri village and Dama village will both be partly flooded, but the Darzi village is fortunate enough to be spared from any flooding (Table 3 and Fig. 7). For the remaining seven villages, Zhibu, Qiwuxing, Kemaluo, Xinka-1, Xingka-2, Xinkamaluo and Dading, none of them were spared from being completely submerged by the extreme magnitude GLOF (Table 3 and Fig. 7). However, due to the far distance from the disaster source, they have an advantage of the later arriving of flood, thus have more time to escape. In the extreme magnitude GLOF event, almost the entire range of the Jiazhong Highway will be disturbed by flood, and all bridges along the route will be inundated and impacted.

The extreme magnitude GLOF released about 63.75% of V_w in Bienong Co, and the water body proceeds at high speed and energy in the valley, dealing a devastating blow to all man-made elements. However, this scenario rarely occurs unless an extreme earthquake causes the complete collapse of moraine dam. More common is the GLOFs caused by partial collapse of moraine dam. In the simulated high-magnitude GLOF scenario, villages of Jiawu and Zongri will be spared from flooding, and villages of Settlement-1, Yilongduo, Dama and Xinka-1 will be partially flooded. The remaining villages will still be completely flooded, but the D_{max} will be reduced by about half comparing to the extreme magnitude GLOF. In the medium magnitude GLOF, the number of villages safe from GLOF will increase to six, they are Yilongduo, Jiawu, Bada, Zongri, Dazi,

and Qiwuxing. The number of villages partially affected by flooding increased to nine, and only four villages will be fully submerged by flooding. They are Kemaluo, Xinka-2, Xinkamaluo and Dading, which all located in the downstream area of the simulated flow channel. In the low-magnitude GLOF, nine villages will avoid damage from flooding, seven villages will suffer partial influence, and only three villages at the downstream will be fully flooded, but flood will come within 4-7 hours and people can adequately avoid it. In this scenario, half of the Jiazhong Highway will be affected by flooding, but the bridges are not spared because they are located in the middle of the river, and the simulated inundation area basically covers the entire river (Fig.7). Although the simulated low-magnitude GLOF was based only on a moraine dam drop of 9 m and about 9.64% corresponding to $0.99×10^7$ m³ of the V_w in Bienong Co was released, which equal to the amount of V_w released by the 2020 GLOF at Jinwu Co that caused severe destruction of infrastructure (roads and bridges) and property losses in downstream areas (Zheng et al., 2021). Therefore, the other simulated magnitude GLOFs in this study represent the more severe scenarios that could happen. In addition, it's worth mentioning that the above GLOFs scenario has not been verified by field measured data, but is only a hypothetical state. The quality of the DEM data and the computational mechanism of the MIKE model have a strong influence on the accuracy of the simulation results. However, this study is still valuable as a reference for potential GLOFs hazards of this highly dangerous glacial lake.

Table 3 Flow hydraulics at different sites along the flow channel.

Village	Distance (km)	Scenario 1				Scenario 2				Scenario 3				Scenario 4			
		Q_{max} (m³·s⁻¹)	D_{max} (m)	V_{max} (m·s⁻¹)	$Q_{max}t$ (h)	Q_{max} (m³·s⁻¹)	D_{max} (m)	V_{max} (m·s⁻¹)	$Q_{max}t$ (h)	Q_{max} (m³·s⁻¹)	D_{max} (m)	V_{max} (m·s⁻¹)	$Q_{max}t$ (h)	Q_{max} (m³·s⁻¹)	D_{max} (m)	V_{max} (m·s⁻¹)	$Q_{max}t$ (h)
S-1	3.18	31091	10.46*	44.69	0.78	13792	4.47*	36.71	1.03	5081	2.27*	6.75	1.32	1408	NR	NR	1.82
Yilongduo	4.81	38301	6.89	50.55	0.82	12033	2.52*	3.48	1.13	5198	NR	NR	1.52	1828	NR	NR	1.95
Jiawu	5.44	39972	11.09	65.71	0.84	11643	NR	NR	1.18	4331	NR	NR	1.50	1477	NR	NR	1.85
Ang'na	5.98	37701	10.28	7.07	0.85	11670	4.22	2.50	1.12	4040	1.78*	2.76	1.45	1351	NR	NR	1.98
Wa'na	8.52	30384	14.31	9.15	0.87	11111	7.21	4.71	1.22	3833	5.81*	2.59	1.60	1262	2.99*	0.53	2.10
Qiangjiuci	9.81	27736	11.23	27.68	0.97	11843	5.71	13.16	1.28	3811	3.71*	10.02	1.67	1353	1.82*	6.81	2.23
Bala	11.43	28758	16.37	13.38	1.02	10948	8.77	8.54	1.28	3756	5.34*	6.12	1.72	1239	4.19*	3.04	2.22
Bada	12.99	2260	4.81*	0.26	1.03	886	1.05*	0.03	1.29	NR	NR	NR	NR	NR	NR	NR	NR
Haqing	17.85	23908	18.29	9.41	1.23	9947	8.48	8.37	1.55	3662	5.22*	7.11	2.03	1241	3.62*	3.95	2.68
Zongri	20.42	22992	6.19*	18.47	1.30	9751	NR	NR	1.63	3556	NR	NR	2.18	1237	NR	NR	2.87
Dazi	24.00	22409	NR	NR	1.45	9266	NR	NR	1.82	3422	NR	NR	2.38	1172	NR	NR	3.18
Dama	30.19	20463	11.63*	5.15	1.68	8545	7.93*	3.93	2.12	3260	4.42*	2.87	2.73	1119	2.69*	2.14	3.65
Zhibu	32.24	19941	18.85	12.74	1.75	8510	10.31	9.14	2.27	3192	6.73*	6.54	2.85	1106	NR	NR	3.78
Qiwuxing	33.41	18954	12.47	4.42	1.83	82210	3.64	1.52	2.27	3145	NR	NR	2.92	1092	NR	NR	3.88
Kemaluo	37.89	13849	23.36	3.49	2.20	5413	14.84	2.31	2.75	216	7.05	1.84	3.52	799	5.48	0.64	4.63
Xingka-1	43.54	11933	19.83	3.52	2.48	4802	12.06*	2.40	3.28	1915	5.72*	2.08	4.15	748	4.30*	1.26	5.42
Xingka-2	43.98	11685	16.43	6.01	2.73	4742	10.47	3.87	3.38	1867	6.70	2.16	4.18	736	3.60*	0.90	5.48
Xinkamaluo	45.89	10863	19.01	4.66	2.72	4399	11.27	2.94	3.48	1715	6.72	2.08	4.57	681	4.24	1.33	5.75
Dading	50.91	7329	15.99	5.15	3.20	3100	9.76	3.11	4.12	1157	5.84	1.95	5.15	455	3.56	1.20	6.35

Note: NR means that the flood waters did not reach here, * means that only part of the area is flooded.
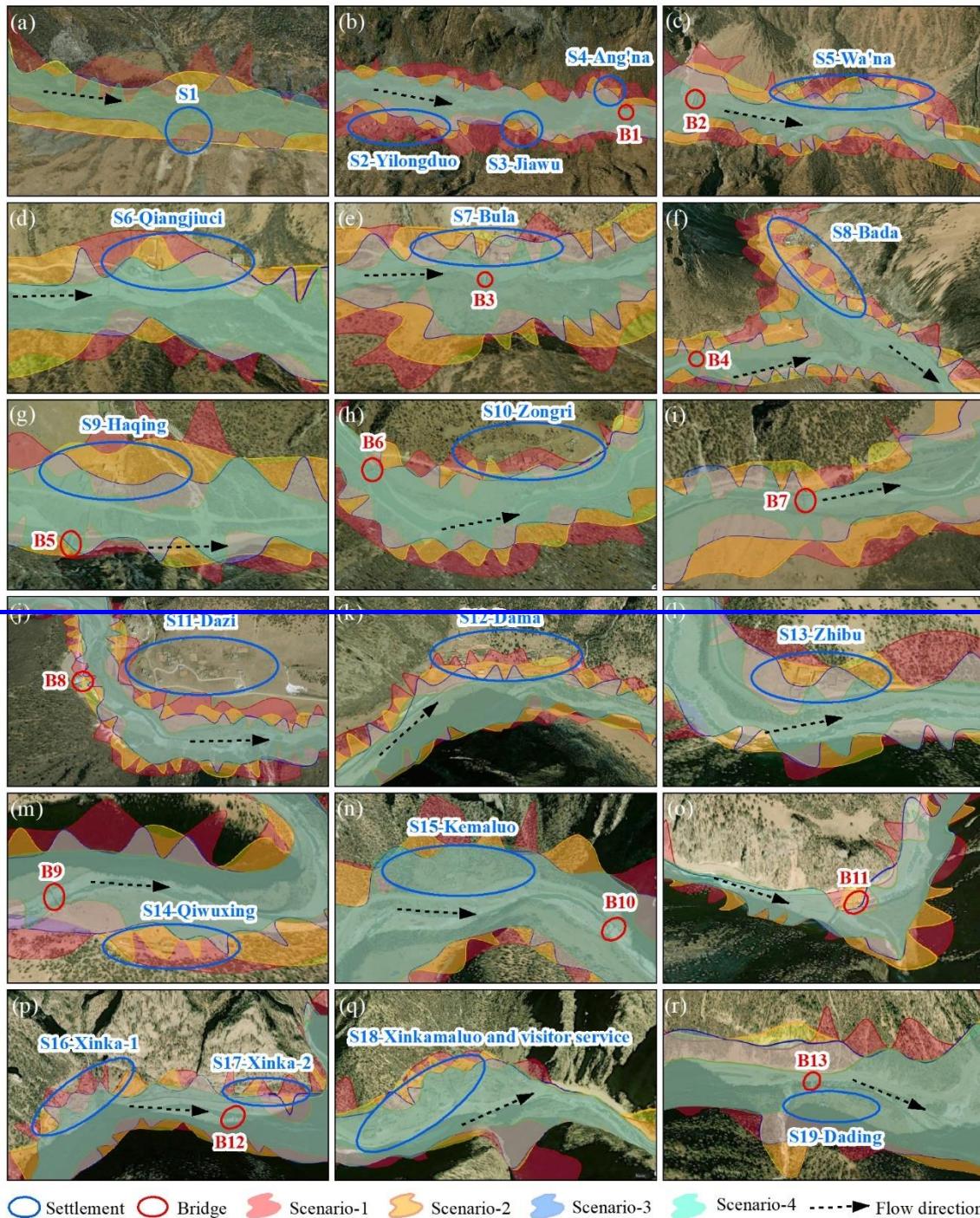
Figure 7. High-resolution images (ArcGIS Earth) showing the potential inundation extent at each downstream settlement along the flow channel (locations can see in Fig.1) for different scenarios caused GLOFs.
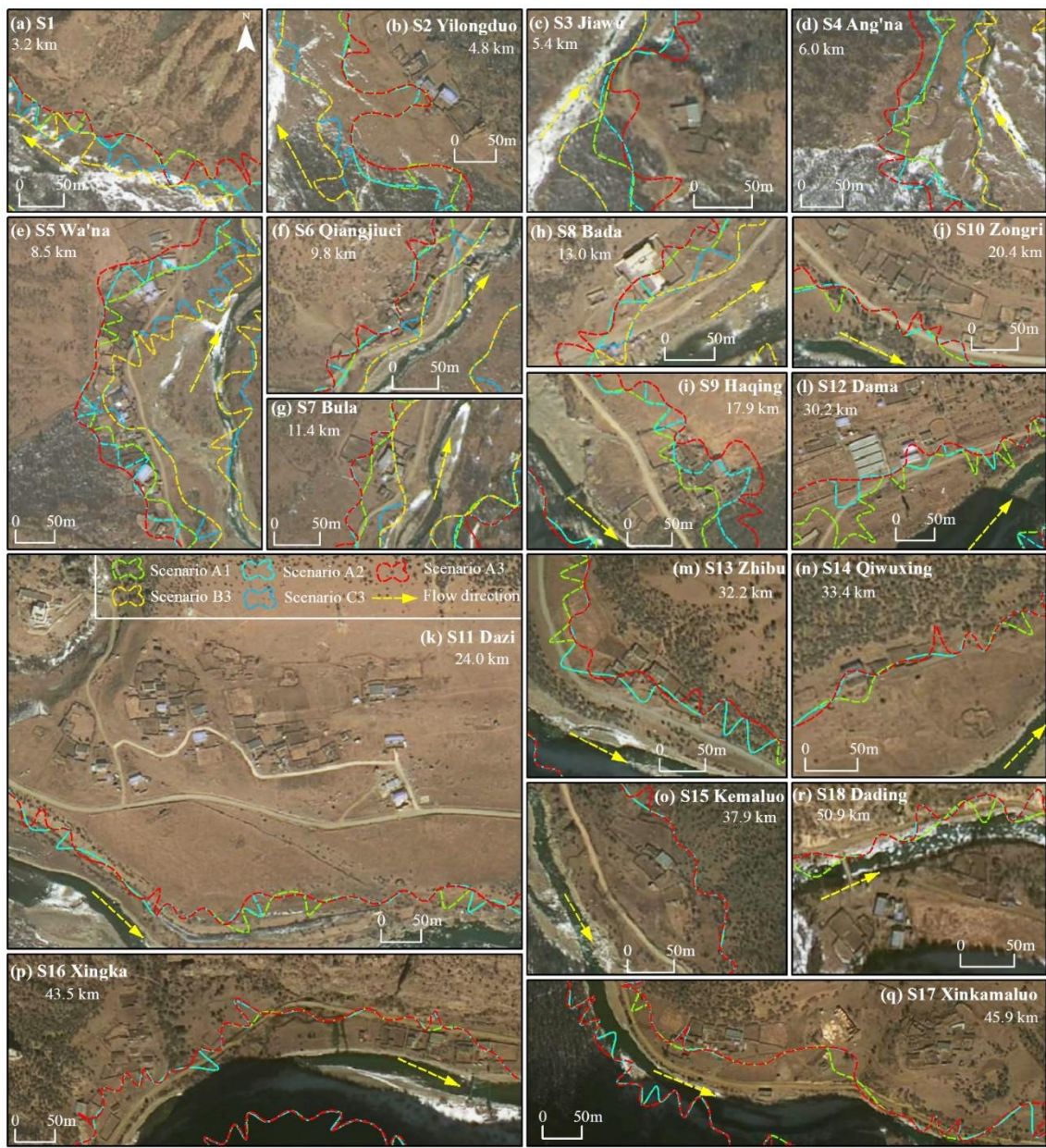
Figure 12. The potential threat of GLOFs to settlements and roads in the downstream under different ice avalanches and landslide scenarios (the background is MapWorld image).

695
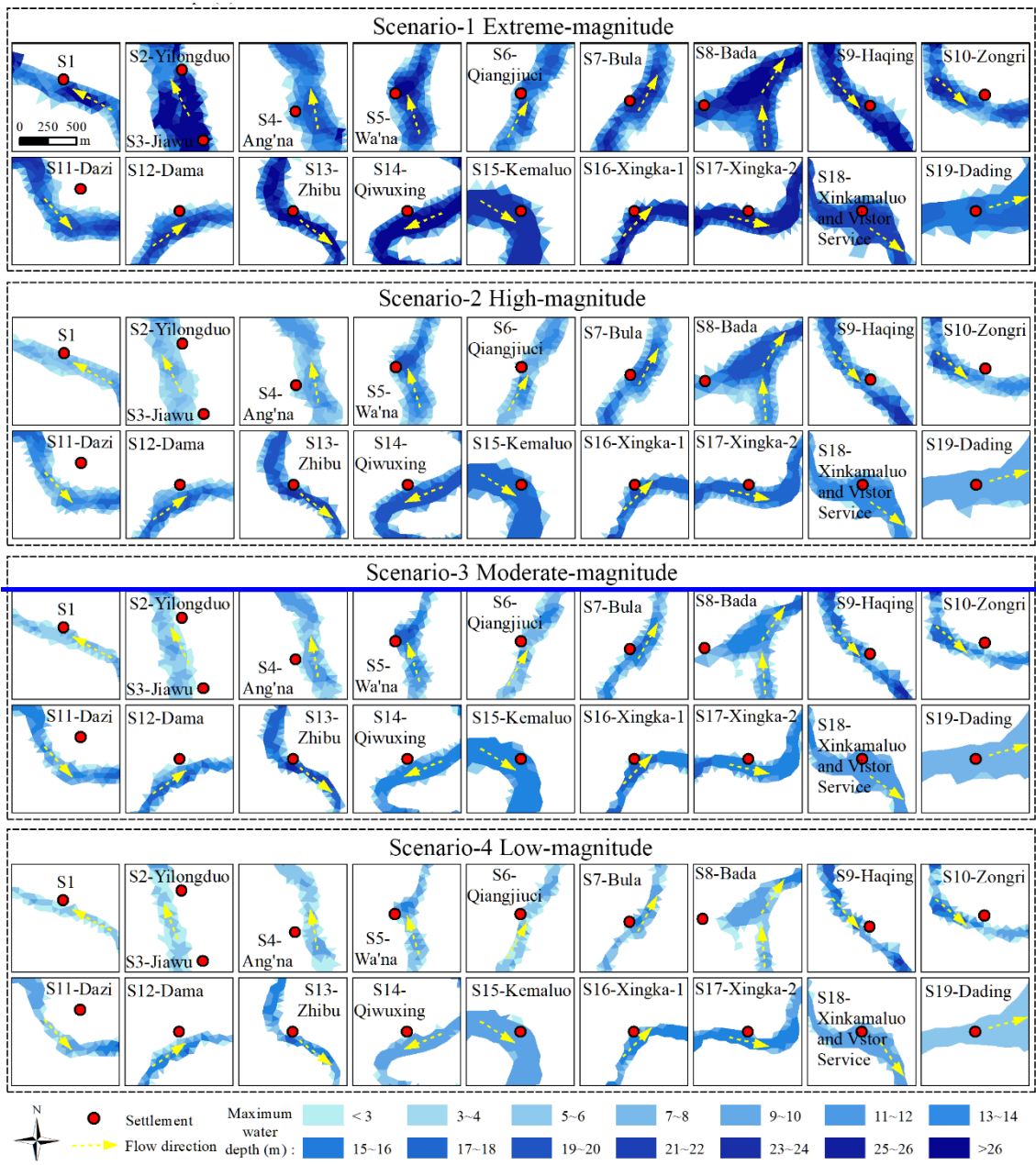
Figure 8. Spatially distributed flow depths of scenario 1, scenario 2, scenario 3, and scenario 4 at each settlement along the flow channel (locations can see in Fig.1).
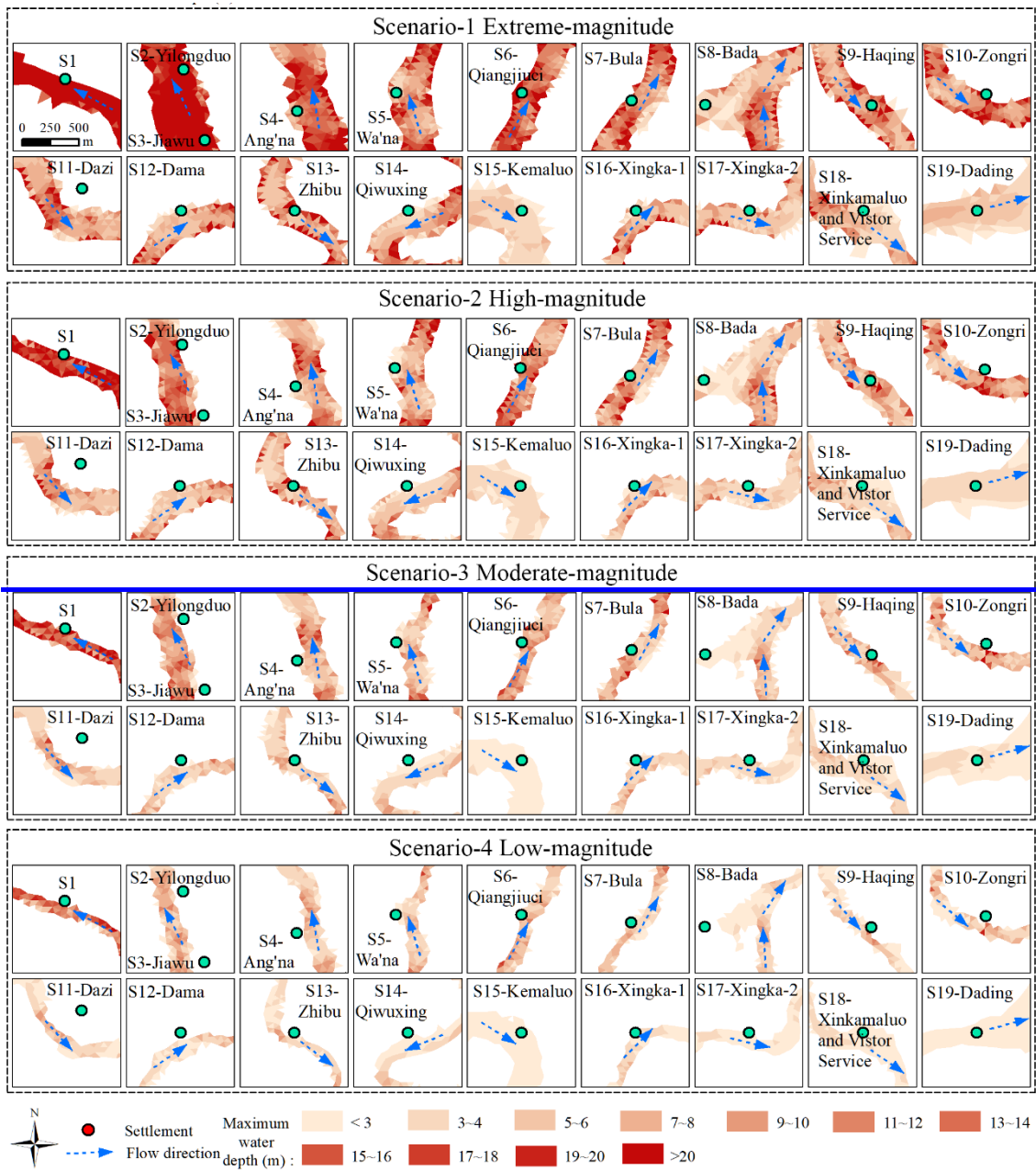
Figure 9. Spatially distributed flow velocities of scenario 1, scenario 2, scenario 3, and scenario 4 at each settlement along the flow channel (locations can see in Fig.1).

705
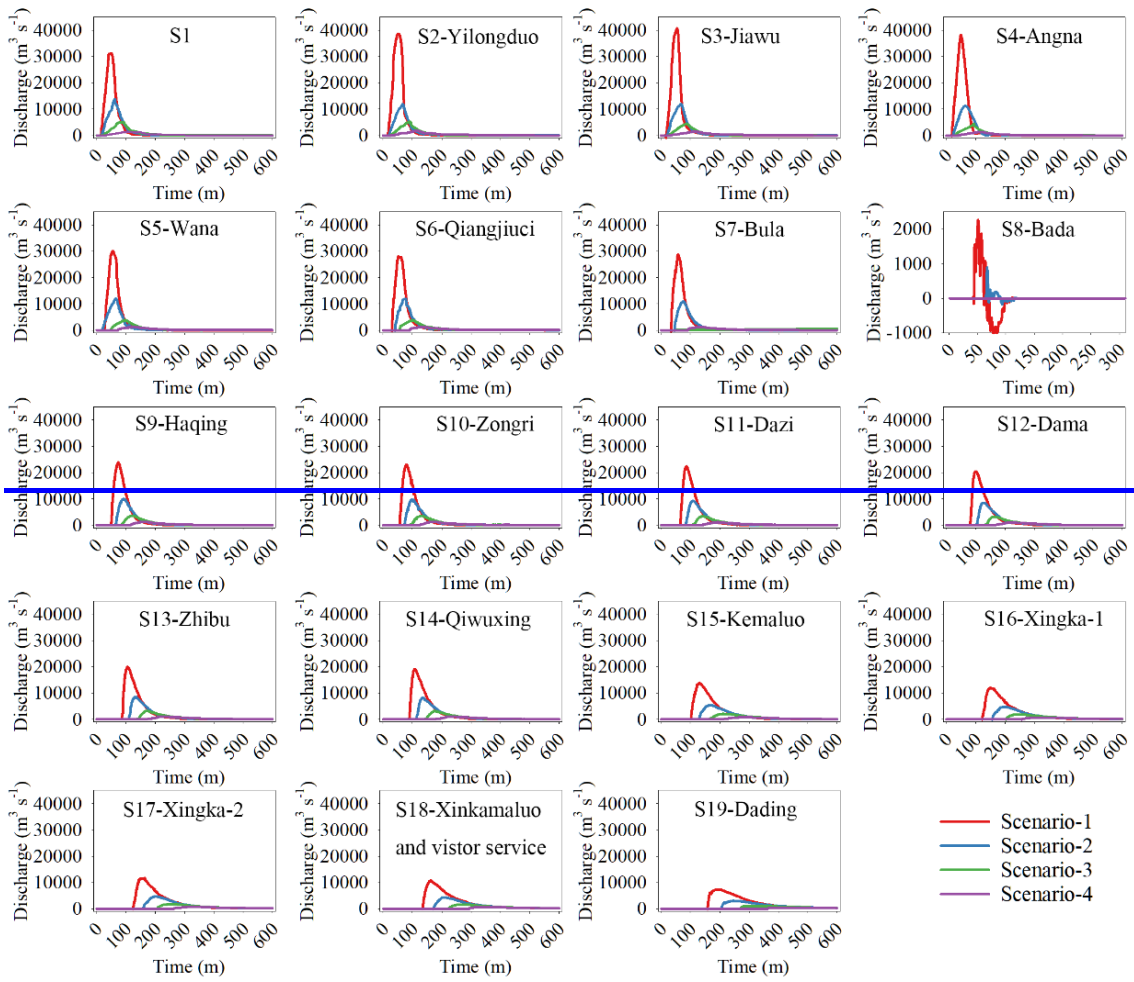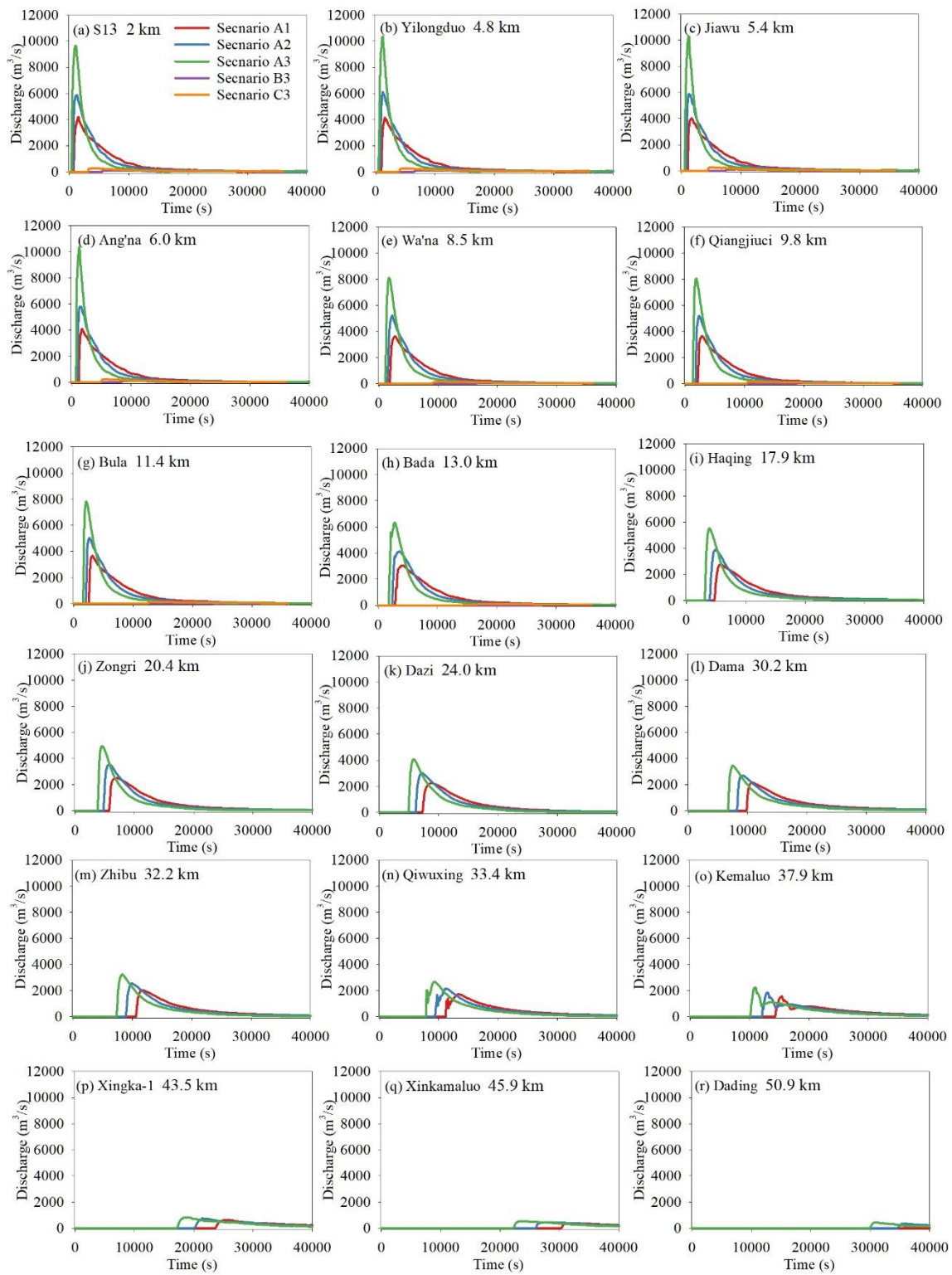
Figure 13. Time series of discharge at different settlements along the flow channel (locations in Fig. 1) of different scenarios.
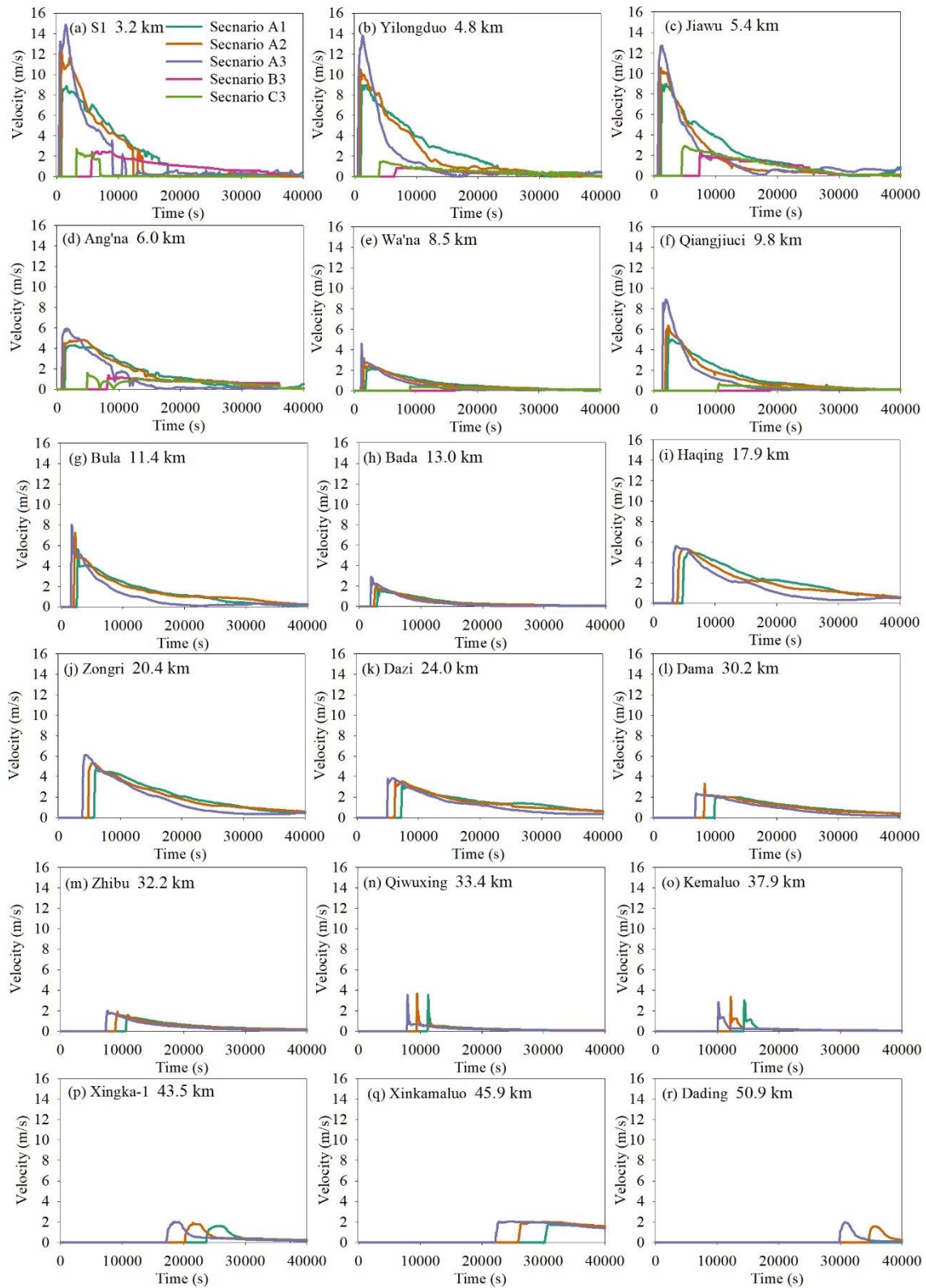
Figure 14. Time series of velocity at different settlements along the flow channel (locations in Fig.1) of different scenarios.

~~**Figure 10.** Temporal course of discharge at different settlements along the flow channel (locations can see in Fig.1) of four scenarios of GLOFs.~~

5 Discussion

5.1 Potential GLOF trigger assessment

Generally speaking, conditions required for glacial lake outburst can be divided into two aspects: the external conditions, that is, the presence of dynamic environments that promote glacial lake outbursts; the inherent conditions that the features of the glacial lake itself are conducive to the occurrence of outburst (Wang, 2016).

5.1.1 Inherent conditions

Thickness of mother glacier and the topography beneath it are critical to the further expansion of a glacial lake, and a glacial lake connected to a flat glacier tongue portion of the mother glacier has the potential for continued expansion in the future (Allen et al., 2019; Lala et al., 2018). However, Bienong Co does not have such a condition, because since the 1988 or earlier, it has reached the steep bedrock of its mother glacier, therefore, has the little space to extend due to topographic constraints (Fig. 3 and Fig. 11). Additionally, an outlet on the top of moraine dam allows for continuous drainage of the lake, which contributes to its stability (Fig. 11). And remote sensing images proves that Bienong Co has maintained the current area for a long time (Fig.3), that is to say, the current moraine dam can withstand the pressure generated by the water volume. However, the hazard of Bienong Co cannot be ignored due to its area (1.15 km²) that much larger than the three breached glacial lakes (i.e., Coga: 0.42 km² (Yao et al., 2014), Ranzeria Co: 0.58 km² (Sun et al., 2014) and Jinwu Co: 0.58 km² (Zheng et al., 2021)) in this region and other outburst triggers.

Dam characteristics, such as dam geometry (dam width to height ratio, width of crest, dam distal face slope, freeboard), dam material properties, ice-cored moraine conditions govern the stability of the dam (Huggel et al., 2004; Prakash and Wang et al., 2011a; Nagarajan, 2017). Bienong Co is constrained by the end moraine, composed of loose sand and gravel (Table 4 and Fig. 11), which has poor coagulability and stability. However, no ice body was observed from the exposed outlet section (Table 4 and Fig. 11), indicating the impossibility of a disaster caused by the collapse of the dam due to ice melting. The moraine dam is 550 m wide and the height is variable with an average height of 72 m and the width height ratio of 7.64. According to the thresholds favoring GLOFs of dam width smaller than 60 m proposed by Lv et al. (1999), width height ratio smaller than 0.2 proposed by Huggel et al. (2004), the moraine dam of Bienong Co is generally stable (Table 4 and Fig. 11). However, mean freeboard of 10 m and the distal facing slope of 35° are the conditions conducive to GLOFs based on the favoring thresholds of smaller than 25 m (Mergili et al., 2011) and larger than 20° (Lv et al., 1999) (Table 4 and Fig. 11).

Table 4 The morphometric status of Bienong Co

	Lake characteristics	Morphology		Lake characteristics	Morphology
Glacial lake	Type	Proglacial lake	**Mulang Glacier**	Area	8.29 km²
	Area	1.15±0.05 km²		Average surface slope	18.28°
	Length	2 km		Height of glacier cliff	122-186 m
	Water surface elevation	4745 m	**Moraine dam**	Type	Moraine
	Facing direction	Northwest		Width of crest	550 m
	Maximum depth	181.04 m		Mean height of crest	72 m
	Average depth	85.40 m		Width-height ratio	7.64
	Snow/avalanche site			Mean freeboard	10 m
	Outlet condition	Free flow		Distal facing slope	35°
	Contact with mother glacier	Yes		Ice core	No

Note: The area of Bienong Co and Mulang Glacier are derived from a scene of Landsat OLI image on September 18, 2021, and the elevation and slope are measured based on ALOS PALSAR DEM.
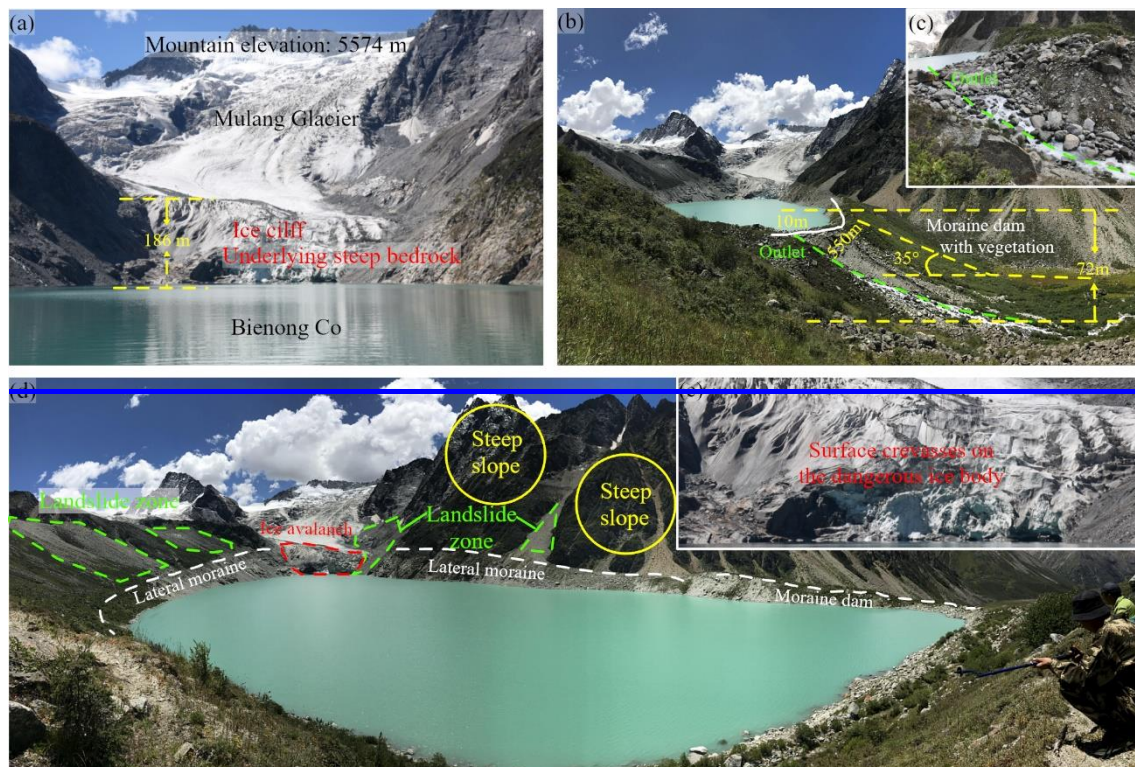
5.1.2 External conditions

Studies show that GLOFs can be triggered by several factors, mass movement such as landslides, ice avalanches and rock slides are considered to be the most important triggers in the GLOF hazard chain (Worni et al., 2014), which can cause overtopping (Risio et al., 2011). Field investigation shows that there are many granular sandy landslides around Bienong Co (Fig. 11), which is a potential trigger for disaster. The GLOF of Jinwu Co, a moraine dammed glacial lake located near the Bienong Co, was caused by an initial landslide on the left side (Zheng et al., 2021). Additionally, the steep lateral moraine and slopes that lie 45°–60° are deemed as to conducive landslides and snow avalanching (Rounce et al., 2016; Sattar et al., 2021), which exist in at least two locations around the Bienong Co. One more current concern is that the Mulang Glacier has been directly connected to the Bienong Co from the time of its area remained stable (Fig. 3), instead of separating from the mother glacier as other glacial lakes, such as Jialong Co (Li et al., 2021). The tongue of Mulang Glacier is currently steep and dangerous due to the extensive surface crevasses (Fig. 11), which makes it highly susceptible to outburst floods because of the highly exposure of the lake to ice avalanching and glacier calving. And in the context of global warming, the glacial melting water will lubricate the glacier itself, so the hanging ice is prone to slide into the lake (Wang et al., 2015), which may induce surge waves capable of overtopping terminal moraine structures. Plenty of studies documented that most of the moraine dam failure on the Tibetan Plateau were triggered by overtopping waves generated from ice avalanches (Wang et al., 2015). The elevation of the top of the hazardous ice body from the lake surface was measured to be about 122-186 m, with an area of about 0.16 km² using a boundary where the crevasse terminates and the slope changes significantly (Fig. 11). If some or all of the ice body fall into the glacial lake under extreme weather or seismic conditions, the pressure caused by its stirring waves will produce a fatal blow to the moraine dam, reducing the stability of the glacial lake dam and most likely causing the collapse of dam and the occurrence of GLOFs.

In addition to the impact of material movement on the dam, the continuous rise of water level caused by constant summer

meltwater or concentrated precipitation will also have an impact on the dynamics at the outlet of the glacial lake, increasing the scouring of the breach in extreme cases, leading to an increase in the size of the breach and triggering the occurrence of glacial lake outburst floods (Clague and Evans, 2000; Worni et al., 2012; Allen et al., 2015). The elevation difference between the glacial lake surface and the outside of the moraine dam is 80 m (Fig. 11), which creates a steep spillway that is prone to erosion of the outlet.

The potential triggers mentioned above are speculative conclusions based on already disrupted glacial lakes and current experience, and are hypothetical and probabilistic statements that will not necessarily occur. And with the current drastic changes in the external environment such as earthquakes and climate change, the above various characteristics of Bienong Co will be affected. In the future, the ground ice conditions, dam parameters and moraine dynamics of the glacial lakes should be further investigated to make more detailed simulations and early warnings of glacial lake outburst floods. Furthermore, earthquake is a non-ignorable factor, although is of the small occurrence probability, the consequences can be catastrophic once it happens. The extreme scenario of the simulated GLOF with breach down to dam bottom in this study is motivated by this assumption.

Although factors that trigger a glacial lake to produce an outburst are divided into external and internal conditions, external conditions often cause an imbalance state of the moraine-dammed glacial lake, and many GLOFs are often the result of one trigger that stimulates changes in other factors, or a combination of factors (Zheng et al., 2021). For example, the Tam Pokhari Glacial Lake in Nepal on September 3, 1998 was damaged by the resultant internal and physical properties of the dike under the combined effect of external forces such as heavy precipitation in the lake basin, earthquake, and snow/ice avalanche, and the dike was eventually breached due to a decrease in water resistance stress (Dwivedi et al., 2000; Osti et al., 2011). Whereas the Jinwu Co that occurred within this watershed in 2020 was a pre-emptive weakening of the dam due to increased flows from landslides, which may have facilitated erosion of the lake by subsequent rainfall, snowmelt, and/or smaller secondary landslide or avalanche events (Liu et al., 2021; Zheng et al., 2021).

5.2 Comparison of morphology characteristics for glacial lakes in continental and maritime glaciation regions
Accurate information of lake-bottom topography and dimensions of the associated moraine is essential to evaluate the actual mechanism of a glacial lake outburst, thereby defining the actual total volume of water that will potentially be released in a failure event, which is also one of the important inputs in the dynamic model of GLOFs (Westoby et al., 2014). However, there are very few glacial lakes with field bathymetric data. Based on the published data, bathymetric data of a total of 16 glacial lakes distributed in Himalayas including Tibet of China, India, Nepal and Bhutan were collected in this study (Table 5). Glaciers can be divided into continental type and maritime type according to the difference in physical properties (Xie and Liu, 2010), and the latter has a stronger geological and geomorphological effect than the former (Qin et al., 2007; Liu et al., 2014). In the Himalayas, glaciers on the northern aspect of the central section are of continental type, whereas those on the eastern section and the southern aspect of the central section are of maritime type (Qin et al., 2007; Liu et al., 2014). Glacial lakes are produced by glacial action, and the great difference in physical properties between continental and maritime glaciers inevitably has an impact on the lake basin's morphology. Theoretically, glacial lakes produced by maritime glaciers could have deeper basins duo to the faster movement and the induced strong geological effect (Xie and Liu, 2010). For verification, we compared the depth differences between glacial lakes of similar size in the continental and maritime glaciation zones. Longbasaba Lake is the largest glacial lake with field bathymetric data in the continental glaciation zone, having an area of ~1.22 km² and a largest depth of ~102 m in 2009 (Yao et al., 2012). In the maritime glaciation zone, Bienong Co in 2020 and Lugge Lake in 2002 had an area of ~1.15 km² and ~1.17 km², respectively, which were 5.74% and 4.10% smaller than Longbasaba Lake, however, their largest depths were 77.45% and 23.52% larger than the Longbasaba Lake. Similarly, South Lhonak Lake in 2016 and Imja Lake in 2014, with an area of 1.31 km² and 1.30 km² respectively, were 7.38% and 6.56% larger than Longbasaba Lake. And its maximum depth was 131 m and 150 m respectively, which were 28.43% and 47.06% larger than Longbasaba respectively. In addition, Abmachimai Co in the continental glaciation zone had an area of 0.56 km² in 1987, and

Lower Barun Lake in 1993 and Imja lake in 1992 in the maritime glaciation zone both had an area of 0.60 km², which was 7.14% larger than that of Abmachimai Co. Whereas the largest depth of Abmachimai Co was smaller than Lower Barun Lake's 51.29% and Imja Lake's 37.5%. As well as, the area of Qangzonk Co in the continental glaciation zone in 1987 and Thulagi lake in the maritime glaciation zone in 1995 was both 0.76 km², but the maximum depth of the former was 19.12% smaller than that of the latter. However, it's worth noting that Jialong Co and Cirenma Co, located in the continental glaciation zone, have larger depths than the glacial lakes in the continental glaciation zone of similar size, such as Lower Barun lake in 1993 and Tam Pokhari Lake (unknown date). That may because they located in the Zhangzangbo valley, where the climate is dominated by the Indian monsoon (Wang et al., 2015, Li et al., 2020) and therefore the warm and humid air currents have a greater impact on glaciers. As well as the classification of continental and maritime glacier zones is only a general range, without considering the topographic and climatic peculiarities of small areas. Overall, the comparison shows that the glacial lakes of same or similar area are deeper in the maritime glaciation zone. Notably, the subject of this study, Beinong Co, located in the SETP, has the largest average depth compared with glacial lakes in the Himalayas. The deeper glacier lake will store more water in a same area, and more volume of water will be released by a GLOF event, resulting in a more severe disaster to downstream area.

Table 5 Parameters of moraine-dammed glacial lakes having field bathymetric data.

No.	Name	Location (Lat, Lon)	Region	Survey date	Area (km²)	Mean depth (m)	Largest Depth (m)	Volume (10⁸ m³)	Mother glacier Type	Source
1	Bienong Co	30.52, 93.45	China	Aug, 2020	1.15 ± 0.05	85.40	181.04	1.02	Maritime	This study
2	Jialong Co	28.21, 85.85	China	Aug, 2020	0.59 ± 0.02	63.11	133.43	0.38	Continental	Li et al., 2021
3	Cirenma Co	28.06, 86.05	China	Sep, 2012	0.39 ± 0.4	55 ± 2	115 ± 2	0.18	Continental	Wang et al., 2015
4	Longbasaba	27.95, 88.08	China	Nov, 2009	1.22 ± 0.023	48 ± 2	102 ± 2	0.64	Continental	Yao et al., 2012
5	Abmachimai Co	28.09, 87.64	China	Apr, 1987	0.56	33.93	72	0.19	Continental	LIGG/WECS/NEA, 1988
6	Qangzonk Co	27.93, 87.88	China	Apr, 1987	0.76	28.16	68	0.21	Continental	LIGG/WECS/NEA, 1988
7	Poqu Co	28.30, 86.16	China	Apr, 1987	0.31	19.35	33.93	0.06	Continental	LIGG/WECS/NEA, 1988
8	Gelhalpu Co	27.96, 87.81	China	–	0.55	46.44	–	0.26	Continental	Sakai, 2012
9	South Lhonak	27.91, 88.20	India	Aug, 2014 & 2016	1.31 ± 0.001	50.24	131± 2.5	0.66	Maritime	Sharma et al., 2018
10	Thulagi	28.50, 84.48	Nepal	Oct, 2017	0.9	40.11	76	0.36	Maritime	Haritashya et al., 2018
				Jul, 2009	0.94	–	80	0.35		ICIMOD, 2011
				Mar, 1995	0.76	–	81	0.22		Yamada, 1998
11	Lower Barun	27.80, 87.10	Nepal	Oct, 2015	1.8	62.39	205	1.12	Maritime	Haritashya et al., 2018
				May, 1993	0.60	–	109	0.28		Yamada, 1998
12	Imja	27.90, 86.92	Nepal	Oct, 2014	1.3	60.31	150	0.78	Maritime	Haritashya et al., 2018
				May, 2009	1.01	–	97	0.36		ICIMOD, 2011
				Apr, 2002	0.90	–	91	0.355		Sakai et al., 2003
				Apr, 1992	0.60	–	99	0.28		Yamada, 1998
13	Tsho Rolpa	27.87, 86.47	Nepal	Aug-Sep, 2009	1.54	55.81	134	0.86	Maritime	ICIMOD, 2011
				Feb, 1993 & 1994	1.39	–	131	0.77		Yamada, 1998
14	Dig Tsho	27.87, 86.59	Nepal	–	0.5	20	–	0.11	Maritime	Mool et al., 2001

15	Tam Pokhari	27.74, 86.84	Nepal	–	0.47	45.21	–	0.21	Maritime	Mool et al., 2001
16	Lugge	28.09, 90.30	Buhtan	Sep-Oct, 2002	1.17	49.83	126	0.58	Maritime	Yamada, 2004
17	Raphsthren	28.10, 90.25	Buhtan	1984 & 1986	1.38	48.43	88	0.67	Maritime	Geological survey of India, 1995

5.~~3~~ 1 Water storage of Bienong Co ~~Relationship between area and volume~~

Based on the accurate bathymetric results of USV, we obtained that the maximum and depth average of Bienong Co were 181 m and 85.4 m with the water storage of 102.3×10^6 m³ in August 2020. Considering the rarity of bathymetric data but the frequent occurrence of GLOFs in the region, we try to explore more information about glacial lakes in the region by using bathymetry and water storage of Bienong Co. First, relationships with significant correlations for area-volume, area-depth and depth-volume of Bienong Co were established (Fig. 15), and the valuable information is pinned on the hope that could provide a data reference for future studies of Bienong Co and other glacial lakes in the region. Then, we compared the depth and water storage information of Bienong Co with other glacial lakes that have been measured. At present, there are few glacial lakes with measured bathymetry on the Tibetan Plateau, and they are mainly concentrated in the Himalaya of Nepal and the Poiqu basin of Tibet, China. Longbasaba is an end moraine-dammed glacial lake located at the northern slope of the Himalaya, which has an area of 1.22 ± 0.02 km² in 2009, with average and maximum depths of 48 ± 2 m and 102 ± 2 m, respectively, storing a water volume of 64×10^6 m³ (Yao et al., 2012). Although the area of Longbasaba is about 6% larger than that of Bienong Co, the water storage is only 60% of that of Bienong Co. This is an example showing that a glacial lake in the maritime glaciation zone is significantly larger in volume than a similarly sized glacial lake in the continental glaciation zone. However, due to the lack of measured bathymetric data of glacial lakes in the continental glaciation zone, no more comparisons can be made. We compared the depth and water storage of Bienong Co with other glacial lakes in the maritime glaciation zone. Comparison between and can be achieved. The area of Lugge glacial lake in Butan was about 1.17 km² in 2004, which is slightly larger than that of Bienong Co, but its average depth and maximum depth were 49.8 m and 126 m with water storage of 58×10^6 m³ (Yamada, 2004), which was smaller than the corresponding value of Bienong Co. At the time of bathymetry, both South Lhonak lake in India and Imja glacial lake in Nepal had an area of about 1.3 km², which is about 13% larger than that of Bienong Co, but both lakes have 64% and 76% of Bienong Co's water storage, respectively (Sharma et al., 2018; Haritashya et al., 2018). Areas of Raphsthren glacial lake in Buhtan and Tsho Rolpa glacial lake in Nepal were 1.4 km² and 1.5 km² when bathymetries were carried out, which are 22% and 30% larger than that of Bienong Co, but their water storage are 65% and 84% of that of Bienong Co (Geological survey of India, 1995; ICIMOD, 2011). The area of Lower Barun glacial lake in Nepal was 1.8 km², 57% larger than that of Bienong Co, but the water storage was 112×10^6 m³, only 9% larger than that of Bienong Co (Haritashya et al., 2018), showing that Bienong Co is relatively deeper and has a larger storage. This shows that the moraine glacial lakes on the south slope of the Himalayas is very different from that in SETP.

Additionally, due to the scarcity of glacial lake bathymetry data and its importance for GLOF hazard, scholars proposed relationships to estimate volumes of glacial lake through area, width and length (O'Connor et al., 2001; Huggel et al., 2002; Sakai, 2012; Wang et al., 2012a; Yao er al., 2012, Cook and Quincey, 2015; Qi et al., 2022). We estimate the water storage of Bienong Co using published equations based on glacial lakes on the Tibetan Plateau, and the results show that the eight published volume-area/width-length relationships all underestimate the volume of Bienong Co to varying degrees. It can be inferred that Bienong Co is the relative deepest glacial lake among these on the Tibetan Plateau that currently have been measured. Whether this is unique to Bienong Co or a common feature of glacial lakes in the region is not yet known, as few glacial lakes in this region has field bathymetry. Future bathymetry is necessary for more typical glacial lakes in the region.
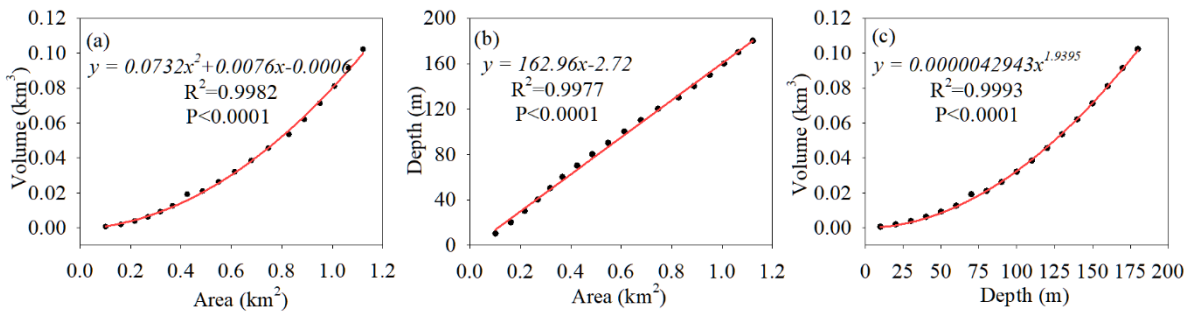
Figure 15. Fitting relationship of (a) area and volume, (b) area and depth and (c) depth and volume of Bienong Co.

Table 1 Calculated volumes of Bienong Co based on published volume-area relationships for glacial lake in Tibetan Plateau.

No	Source		Relationships	Calculated Volume	Error (%)
1	Qi et al., 2022	(1)	$V=0.04066A^{1.184}-0.003207w_{mx}/l_{mx}$	46.9×10^6 m³	-54%
2		(2)	$V=0.0126A^2+0.0056A+0.0132$	36.3×10^6 m³	-65%
3	Wang et al., 2012		$V=0.0354A^{1.3724}$	42.9×10^6 m³	-58%
4	Sakai, 2012		$V=0.04324A^{1.5307}$	53.6×10^6 m³	-48%
5	Yao et al., 2012		$V=0.0493A^{0.9304}$	56.1×10^6 m³	-45%
6	Fujita et al., 2013		$V = 0.055A^{1.25}$	65.5×10^6 m³	-36%
7	Khanal et al., 2015		$V = 0.0578A^{1.5}$	71.3×10^6 m³	-30%
8	Zhou et al., 2020		$V=0.0717 w_{mx}^2 l_{mx}$	70.3×10^6 m³	-31%

Note: Error = (Volume of empirical formulas − Bathymetrically derived volume) / Bathymetrically derived volume × 100%.

~~On the basis of the bathymetric map of USV results, the empirical relationships with significant correlations for area-volume, area-depth and depth-volume of Bienong Co were established (Fig. 12), and the valuable information is pinned on the hope that could provide a data reference for future studies of Bienong Co and other glacial lakes in the region. Due to the scarcity of glacial lake bathymetry data and its importance for GLOF hazard, several scholars have proposed the relationship between volume and area of glacial lake through available data (O'Connor et al., 2001; Huggel et al., 2002; Sakai, 2012; Wang et al., 2012a; Yao er al., 2012, Cook and Quincey, 2015). In this study, we fitted the relationship between area and volume based on a total of 24 bathymetric data for 16 glacial lakes (some lakes were measured multiple times) in the Himalayan region and Bienong Co in SETP. The results show that there is a significant correlation between area and volume with the correlation coefficient of 0.8391 at the level of significance less than 0.0001 (Fig. 13). But Bienong Co is obviously an outlier, and the correlation coefficient is lower than that by Wang et al., (2012) of 0.919. Therefore, we refitted the relationship without Bienong Co, resulting in a significant correlation with the correlation coefficient of 0.9426 higher than that by Wang et al., (2012) (Fig. 13).~~
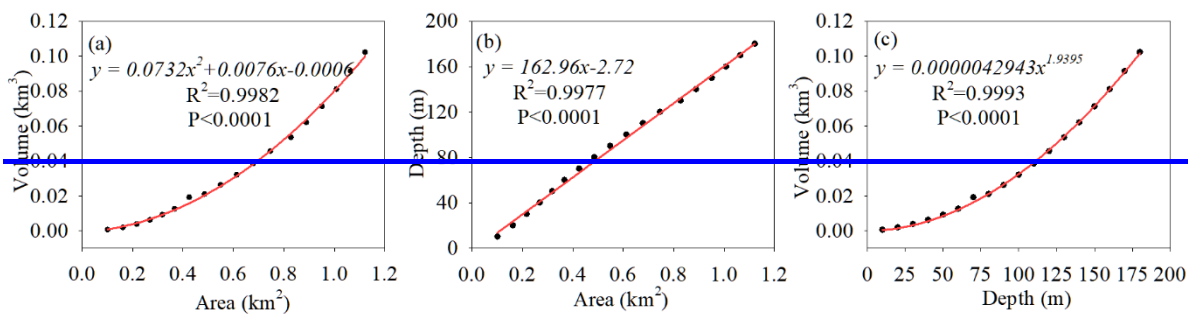
~~**Figure 12.** Nonlinear fitting of (a) area and volume, (b) area and depth and (c) depth and volume of Bienong Co.~~
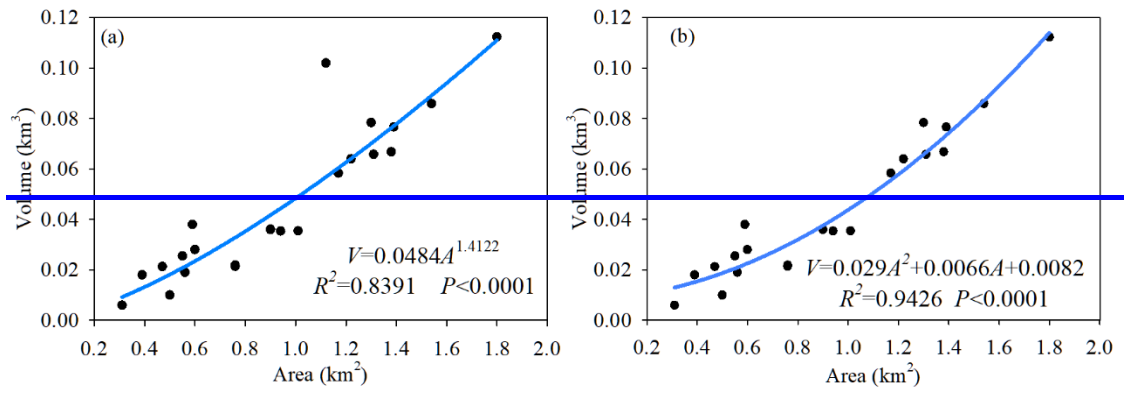
Figure 13. Relationship between area and volume of moraine-dammed glacial lakes in the Himalayas with and without Bienong Co in SETP based on available bathymetric data (in Table 5).

To compare the accuracy of our proposed area-volume relationship based on glacial lakes in the Himalayas and Bienong Co in SETP, we summarized the published area-volume relationships for glacial lakes in the global and Himalayan regions (Table 6). There are three equations extracted from just one glacial lake, three equations based on glacial lakes in the Himalaya, one equation based on glacial lakes in the Himalaya and SETP, and four equations based on other regions worldwide including the Himalaya (Table 6). Table 7 shows the comparison of measured and calculated lake volumes for moraine-dammed glacial lakes in the Himalayas and SETP (lakes in Table 5) using the relationships between area and volume in table 6, noting that only relationships based on multiple glacial lakes were selected. Overall, the calculated results based on the relationships of O'Connor et al., (2001) as well as Cook and Quincey (2015) show very exaggerated overestimation errors for most of the glacial lakes (Table 7 and Fig.14), indicating that the glacial lakes on which these equations are proposed are much deeper than those in the Himalayan region. However, Huggel et al.,'s (2002) formula, although based on glacial lakes in non-Himalayan regions, yields most of the underestimated results with small errors than that from the relationships of O'Connor et al., (2001) as well as Cook and Quincey (2015). The formulas based on all or most of the glacial lakes located in the Himalaya show relatively high calculation accuracy for the lakes in this region. In which the overall calculation accuracy of the formula proposed in this study based on the glacial lake including Bienong Co is less than that of Sakai's (2012) formula, but the formula developed without Bienong Co, namely based on glacial lakes that entirely in the Himalaya produces the highest overall calculation accuracy (Table 7 and Fig.14), showing that our formula is a reliable reference for estimating the water volume of the glacial lake in the Himalayas.

Table 6 Summary of relationships between area and volume of glacial lakes based on measured bathymetry data.

Type	Glacial lake in region	Formula (R^2:value) (A in m², V in m³)	Source
Single glacial lake	Bienong Co in SETP	$V=0.0801A^{1.9146}$ (R^2: 0.9982)	This study
	Longbasaba in Himalaya	$V=0.0493A^{0.9304}$ (R^2: 0.9903)	Yao et al., 2012
	Jialong Co in Himalaya	$V=616146.71793-20.76527A+2.6828\times10^{-4}A^2+2.17215\times10^{-10}A^3$ (R^2: 0.9999)	Li et al., 2021
Multiple glacial lakes	17 moraine-dammed glacial lakes in Himalayas and SETP	$V=0.0484A^{1.4122}$ (R^2: 0.8391)	This study (a)
	16 moraine-dammed glacial lakes in Himalayas	$V=0.029A^2+0.0066A+0.0082$ (R^2: 0.9426)	This study (b)
	Two thermokarst and 14 moraine-dammed glacial lakes in the Himalayas	$V=0.4324A^{1.5307}$ (R^2: *)	Sakai, 2012
	20 moraine-dammed glacial lakes in the Himalayas	$V=0.0354A^{1.3724}$ (R^2: 0.919)	Wang et al., 2012a
	Seven moraine-dammed glacial lakes North America	$V=3.114A+0.0001685A^2$ (R^2: *)	O'Connor et al.,

													2001			

Eight ice-dammed, one thermokarst and six moraine-dammed glacial lakes in North America, South America, Iceland and Alps Mountains — $V=0.104A^{1.42}$ (R^2: 0.91) — Huggel et al., 2002

(a) Same as above — $V=0.1217A^{1.4129}$ (R^2: 0.95) — Cook and Quincey, 2015

(b) 45 glacial lakes including supraglacial, ice-dammed and moraine-dammed glacial lakes worldwide. — $V=0.1607A^{1.3778}$ (R^2: 0.74) — Cook and Quincey, 2015

Note: R^2: * refers that the original study does not specify the value.

900 **Table 7** Comparison of measured and calculated lake volumes for moraine-dammed glacial lakes in the Himalayas and SETP (lakes in Table 5) using the relationships between area and volume in table 6.

Lake Year	Area/ km²	Meas-ured volume/ km³	This study (a)		This study (b)		Sakai, 2012		Wang et al., 2012a		O'Connor et al., 2001		Huggel et al., 2002		Cook and Quincey, 2015 (a)		Cook and Quincey, 2015 (b)	
			Volume/ km³	Error /%	Volume/ km³	Error /%	Volume/ km³	Error /%	Volume/ km³	Error /%	Volume/ km³	Error /%	Volume/ km³	Error /%	Volume/ km³	Error /%	Volume/ km³	Error /%
Bienong Co 2020	1.15	0.102	0.054	-46.92	0.059	-42.20	0.054	-47.50	0.043	-57.96	0.226	121.98	0.042	-58.83	0.148	45.36	0.195	91.01
Jialong Co 2020	0.59	0.038	0.022	-41.61	0.023	-39.54	0.019	-49.26	0.017	-54.84	0.060	59.19	0.016	-57.16	0.058	51.97	0.078	104.41
Cirenma Co 2012	0.39	0.018	0.015	-15.64	0.013	-28.87	0.010	-43.16	0.010	-45.99	0.027	49.13	0.009	-49.76	0.032	78.74	0.044	143.96
Longbasaba 2009	1.22	0.064	0.059	-7.16	0.064	0.14	0.059	-8.40	0.047	-27.33	0.255	297.80	0.046	-28.64	0.161	151.84	0.211	230.23
Abmachimai Co 1987	0.56	0.019	0.021	10.48	0.021	12.33	0.018	-6.31	0.016	-15.93	0.055	187.29	0.015	-20.44	0.054	182.33	0.072	280.47
Qangzonk Co 1987	0.76	0.021	0.030	42.70	0.033	56.43	0.028	35.28	0.024	15.67	0.100	374.72	0.023	11.06	0.083	293.25	0.110	424.30
Poqu Co 1987	0.31	0.006	0.013	117.22	0.009	54.31	0.007	19.99	0.007	18.25	0.017	185.97	0.007	8.80	0.023	287.69	0.032	433.41
Gelhalpu Co*	0.55	0.026	0.021	-20.76	0.021	-19.98	0.017	-33.40	0.016	-40.06	0.053	102.63	0.015	-43.33	0.052	101.13	0.071	171.22
South Lhonak 2016	1.31	0.066	0.067	0.93	0.071	7.38	0.065	-0.95	0.051	-22.30	0.293	344.31	0.051	-23.44	0.178	170.05	0.233	253.22
Thulagi 2017	0.9	0.036	0.038	4.53	0.042	15.86	0.037	2.22	0.031	-14.91	0.139	286.91	0.030	-17.63	0.105	191.30	0.139	286.07
Thulagi 2009	0.94	0.35	0.040	-88.56	0.044	-87.33	0.039	-88.76	0.033	-90.71	0.152	-56.62	0.032	-90.99	0.112	-68.14	0.148	-57.84
Thulagi 1995	0.76	0.22	0.030	-86.38	0.033	-85.07	0.028	-87.09	0.024	-88.96	0.100	-54.69	0.023	-89.40	0.083	-62.46	0.110	-49.95
Lower Barun 2015	1.8	0.112	0.114	1.82	0.111	-0.89	0.106	-5.07	0.079	-29.19	0.552	392.45	0.079	-29.16	0.279	149.31	0.361	222.49
Lower Barun 1993	0.60	0.28	0.023	-91.93	0.024	-91.60	0.020	-92.93	0.018	-93.73	0.063	-77.67	0.017	-94.05	0.059	-78.88	0.079	-71.61
Imja 2014	1.3	0.078	0.066	-15.65	0.070	-10.12	0.065	-17.17	0.051	-34.94	0.289	270.27	0.050	-35.92	0.176	126.04	0.231	195.74
Imja 2009	1.01	0.36	0.044	-87.65	0.049	-86.37	0.044	-87.80	0.036	-90.03	0.175	-51.38	0.035	-90.30	0.123	-65.72	0.163	-54.74
Imja 2002	0.90	0.355	0.038	-89.4	0.042	-88.25	0.037	-89.63	0.031	-91.37	0.139	-60.76	0.030	-91.65	0.105	-70.46	0.139	-60.85
Imja 1992	0.60	0.28	0.023	-91.93	0.024	-91.60	0.020	-92.93	0.018	-93.73	0.063	-77.67	0.017	-94.05	0.059	-78.88	0.079	-71.61
Tsho Rolpa 2009	1.54	0.086	0.087	1.33	0.089	3.55	0.084	-2.63	0.064	-25.55	0.404	370.24	0.064	-26.07	0.224	160.46	0.291	238.75
Tsho Rolpa 1994	1.39	0.77	0.073	-90.47	0.077	-89.99	0.072	-90.70	0.056	-92.78	0.330	-57.16	0.055	-92.86	0.194	-74.83	0.253	-67.15
Dig Tsho*	0.5	0.011	0.019	70.45	0.018	65.32	0.015	36.05	0.014	24.30	0.044	297.11	0.013	17.00	0.046	315.50	0.062	462.17
Tam Pokhari*	0.47	0.021	0.018	-15.68	0.017	-20.65	0.014	-35.17	0.013	-40.19	0.039	84.22	0.012	-43.87	0.042	99.42	0.057	170.40
Lugge 2002	1.17	0.058	0.056	-4.10	0.060	4.16	0.055	-5.20	0.044	-24.29	0.234	303.97	0.043	-25.80	0.152	161.94	0.200	243.98
Raphsthren 1986	1.3	0.067	0.066	-1.81	0.070	4.64	0.065	-3.57	0.051	-24.26	0.289	331.06	0.050	-25.40	0.176	163.15	0.231	244.30

Note: Error = (Volume of empirical formulas − Bathymetrically derived volume) / Bathymetrically derived volume × 100%.

"*" of lake/year means that the year is unclear. Formula (a) and Formula (b) are the relationships between area and volume of glacial lakes in table 5 with and without Bienong Co, respectively.
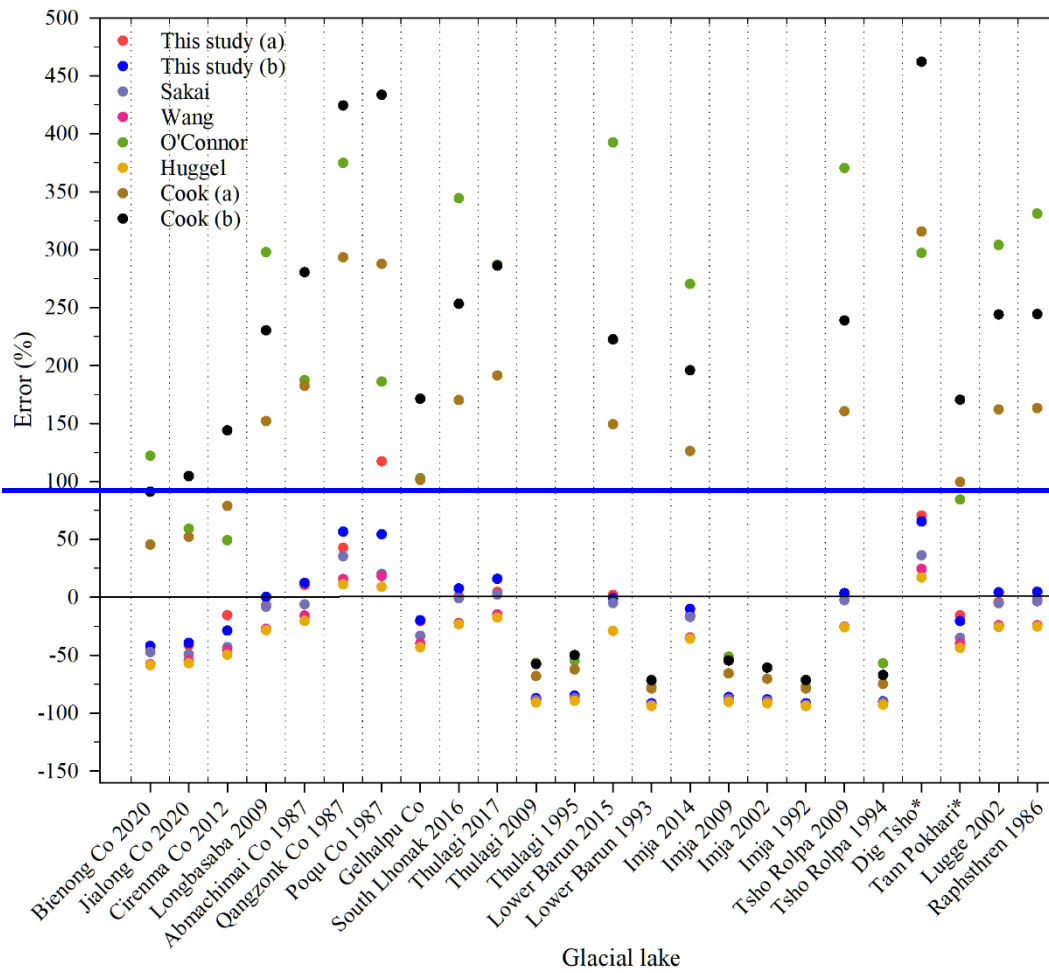
Figure 14. ~~Comparison of errors from the calculated volumes for moraine-dammed glacial lakes in the Himalayas and SETP~~ ~~(glacial lakes in Table 5) using the relationships between area and volume in table 6.~~

5.2 Limitation and uncertainties

Trigger is the beginning of the simulated GLOFs process chain in this study and we only consider ice avalanche and landslide

scenarios, instead of other factors, such as increased glacial meltwater and heavy precipitation. The magnitude, location and probability of ice avalanche and landslide are the largest sources of uncertainty in this study. Ice avalanche is the trigger for over 70% of GLOFs on the Tibetan Plateau, but there is no reliable reference of the magnitude including release area and depth of previous ice avalanche events. Ice avalanche in this study come from the mother glacier tongue where the slope is relative steep and fissures are well-developed. We simulated three different-magnitude ice avalanches, each scenario assumes that the

ice body breaks off in the vertical direction until to the lake surface, which is unrealistic and may overestimate the volume of ice avalanche. The RAMMS model can estimate the possible release volume based on the input DEM data and the release area as well as the release depth, which are 5×10^6 m^3, 13.1×10^6 m^3 and 41.3×10^6 m^3 for Scenarios A1, A2 and A3. However, simulations show that about 76%, 37% and 14% of the estimated release volume enter the lake in Scenarios A1, A2 and A3, respectively. The simulation duration is set to 600 s to ensure the integrity of the ice avalanche process, and most of the ice

avalanche is already into the lake within 100 s at the beginning. The difference between the volume of the ice avalanche entering the lake and the estimated release volume is mainly influenced by the slope between the ice body and the lake and the distance from the lake. The gentler slope and far distance from the lake of ice body in Scenarios A2 and A3 result in fewer ice avalanches entering the glacial lake, and affect the process of ice avalanche material entering the lake, e.g., Scenarios A2 and A3 have stronger fluctuations in the ice avalanche process than Scenario A1. In addition, we also consider landslide as a trigger

given the failure of Jinwu Co in 2020. Two release areas were selected by referring the slope and location of Jinwu Co's

landslide, however, the release depth has no quantified reference data and we assumed three release depths of 2 m, 5 m and 10 m for each release area to simulate the consequences resulting from as many scenarios as possible.

Secondly, the grain size distribution of moraine dam of Bienong Co was not obtained in this study, and the simulation was performed by referencing an inventory of glacial lakes in the Indian Himalaya. Although the data used have been validated to be reliably general, the grain size distribution of the moraine dam of Bienong Co itself would be more useful for an accurate simulation of moraine dam's erosion.

Finally, DEM data are the most important basic data affecting the downstream propagation of GLOFs in this study. ALOS PALSAR DEM data with a spatial resolution of 12.5 m have been widely used in studies related to cryospheric changes and disasters. In this study, the DEM was pre-processed to fill sinks, but there was still the phenomenon of flood water being piled up in some deep puddle during the simulation, i.e., there were errors in the DEM data, especially in the relatively narrow valley. We have manually smoothed several large bumps according to the elevation of the upstream and downstream. However, there are still some smaller bumps that converge the flow to a section of the flow channel, mainly in the downstream area. Therefore, the flooding situation in Qiwuxing, Kemaluo, Xingka and Dading villages might be overestimated, especially in the first two villages because they are relatively far away from the river, while the latter two villages are still very likely to be threatened by flooding due to a close distance to the river. More accurate flood hazard simulations in the future relay on more precise topographic information, such as DEM data generated using panchromatic stereo images with resolutions better than 0.8 m carried by the Gaofen-7 satellite.

6 Conclusion

As a moraine-dammed glacial lake located in the maritime glaciation region, Bienong Co has been highly regarded by local government due to its larger area and high potential ~~hazard~~ of GLOF hazard. Based on bathymetric data ~~obtained from field investigation~~, remote sensing images and DEM data, combined with multiple models of RAMMS, BASEMENT and Heller-Hager ~~remote sensing images and DEM data~~, we completed a comprehensive investigation of the potential GLOF process chain of Bienong Co, including the initial mass movement from mother glacier and lateral moraine slope, displacement wave generation and propagation in the lake, overtopping flow and erosion on moraine dam and subsequent downstream flooding. ~~we analyzed the potential hazard of Bienong Co, accurately modeled its basin morphology and estimated its water volume. Furthermore, we simulated the hydraulic behavior at breach and in the downstream flow channel based on four different scenarios of GLOFs to assess the hazard of different magnitudes.~~ The following main conclusions were drawn:

(1) According to the field bathymetric data, the lake basin morphology of Bienong Co features a relatively flat basin bottom and the steep flanks, with the slope near the glacier (16.5°) is steeper than that near the moraine dam (11.3°). The water storage of Bienong Co was ~102.3 × 10^6 m^3 in August 2020, with the maximum depth was ~181 m. The huge water storage combined with the fissure-developed mother glacier tongue, steep lateral moraine slope, steep distal facing slope of moraine dam and low freeboard make it of high GLOF potential.

(2) The volume of materials entering the lake for the three scenarios of ice avalanches (A1, A2 and A3) is much larger than the six scenarios of landslides (B1, B2, B3 and C1, C2, C3). Volumes of ice avalanches entering the lake in Scenarios A1, A2 and A3 are 3.8 × 10^6 m^3, 4.9 × 10^6 m^3 and 5.8 × 10^6 m^3, respectively. Among the six landslide scenarios, Scenario B1 releases a minimum volume of 0.03 × 10^6 m^3 and Scenario C3 releases a maximum volume of 0.30×10^6 m^3. As a result, the impact zone, maximum flow height and maximum flow velocity in the lake also present that Scenarios A1, A2 and A3 are significantly larger than the other six scenarios where Scenario B1 is the smallest and Scenario A3 is the largest. Wave amplitudes near the moraine dam in Scenarios A1, A2, and A3 are 17.1 m, 20.2 m, and 25.2 m, respectively. The overtopping flow of all three scenarios causes erosion of the dam, with little difference in breach depth (19.0 m, 19.1 m and 19.3 m) but large difference in breach width (295.0 m, 339.4 m, and 368.5 m). The volumes of water lost in the lake

of the three scenarios are 24.1 × 10^6 m^3, 25.3 × 10^6 m^3 and 26.4 × 10^6 m^3, and the flood peak flows are 4,996 m^3/s, 7,817 m^3/s and 13,078 m^3/s, respectively. Among the other six scenarios, only Scenarios B3 and C3 with larger magnitudes formed breaches on moraine dam, with breaches of 6.5 m and 7.9 m in depth and 153 m and 169 m in width, respectively.

(3) Floods all pass through 18 settlements in the downstream river in 20 hours, with the inundation areas of 7.6 km^2, 8.0 km^2 and 8.5 km^2 as well as average water depths of 8.4 m, 9.1 m and 10.0 m, respectively. The GLOFs threatened more than half of the villages in the downstream region. Scenarios B1/2 and C1/2 produce very limited overtopping flow that cannot pose a threat to the downstream region. Both Scenarios B3 and C3 produced floods that flow through eight downstream settlements within 20 hours and had a relatively small impact on them.

(4) Bienong Co is the relative deepest glacial lake among these on the Tibetan Plateau that currently have been measured and is very different from glacial lakes on the south slope of the Himalayas. In addition, it is also important to use high-precision topographic data for disaster simulation of glacial lake outburst flood lakes.

(1) Bienong Co is a very stable glacial lake that has remained essentially constant in size over the past four decades. Also maintaining its area is the mother glacier, but it has undergone significant thinning, especially in the ablation zone, which is supposed to be a response to climate warming. According to the field bathymetric data, the lake basin morphology of Bienong Co features a relatively flat basin bottom and the steep flanks, with the slope near the glacier (16.5°) is steeper than that near the moraine dam (11.3°). In August 2020, the maximum depth of Bienong Co was ~181.04 m, with the water storage capacity of ~10.2×10^7 m^3.

Four scenarios of extreme , high , medium and low magnitude of GLOFs based on different combinations of breach depth (72 m, 36 m, 18 m and 9 m), breach width (180 m, 131 m, 94 m and 66 m), and failure time (0.75 h, 1.03 h, 1.37 h and 1.79 h) produced the peak discharges of 26,721 m^{3}s^{-1}, 11,126 m^{3}s^{-1}, 3,716 m^{3}s^{-1} and 1,294 m^{3}s^{-1} by MIKE 11 model as well as 24,630 m^{3}s^{-1}, 8,801 m^{3}s^{-1}, 3,081 m^{3}s^{-1} and 1,070 m^{3}s^{-1} by empirical relationship. Extreme magnitude GLOF will have a catastrophic impact on downstream, affecting almost all man-made facilities including settlements, bridges and roads along the river channel. However, it has a small probability of occurrence, and the simulation in this paper only represents a potential possibility. In contrast, the low magnitude GLOF will produce a relatively mild influence on the downstream flow channel, with only three villages at the downstream being fully flooded. Nonetheless, the impact should not be despised, because the amount of water released in low magnitude scenario is comparable to that in the Jinwu Co' GLOF event in 2020 which caused a great damage to the downstream region.

(2) Glacial lakes in the maritime glaciation region are generally deeper than those in the continental glaciation region, therefore store more water, resulting in a more severe disaster to downstream area in the event of a GLOF. Bienong Co, a moraine dammed glacial lake located in the SETP, has the largest relative depth comparing with those located in the Himalayas. Therefore, glacial lakes in maritime glaciation region, such as in the SETP should be given more attention in the future.

Author contributions. HD contributed the conceptualization, methodology, software, formal analysis, visualization and writing of the original draft; XY contributed the conceptualization, supervision, funding acquisition, investigation of the glacial lake, as well as review and editing of the manuscript; YZ, HJ, YZ and QW contributed the investigation of the glacial lake; ZD, BW and QW contributed the model progress; JH contributed the setting up the experimental equipment and obtaining data.

Competing interests. The authors declare that they have no conflict of interest.

Financial support. This research has been supported by the National Key Research Program of China (no. 2019YFE0127700), National Natural Science Foundation of China (grant nos. 41861013 and 42071089), "Innovation Star" of Outstanding

Graduate Student Program in Gansu Province (no. 2021-CXZX-215), and Northwest Normal University's 2020 Graduate Research Grant Program (no. 2020KYZZ001012) and Outstanding PhD Student Program in Gansu Province (no. 22JR5RA139).

References

Aggarwal, A., Jain, S.K., Lohani, A.K., and Jain, N.: Glacial lake outburst flood risk assessment using combined approaches of remote sensing, GIS and dam break modelling. Geom. Nat. Hazard. Risk., 7, 18–36, https://doi.org/10.1080/19475705.2013.862573, 2013.

Allen, S., Rastner, P., Arora, M., Huggel, C., and Stoffel, M.: Lake outburst and debris flow disaster at Kedarnath, June 2013: hydrometeorological triggering and topographic predisposition, Landslides, 13, 1–13, https://doi.org/10.1007/s10346-015-0584-3, 2015.

Byers, A. C., Rounce, D. R., Shugar, D. H. A rockfall-induced glacial lake outburst flood, Upper Barun Valley, Nepal, Landslides, 533-549, https://doi.org/10.1007/s10346-018-1079-916, 2018.

Byers, A. C., Chand, M. B., Lala, J. Reconstructing the History of Glacial Lake Outburst Floods (GLOF) in the Kanchenjunga Conservation Area, East Nepal: An Interdisciplinary Approach, Sustainability, 12, 5407, https://doi.org/10.3390/su12135407, 2020.

Bibuli, M., Bruzzone, G., Caccia, M., Fumagalli, E., Saggini, E., Zereik, E., Buttaro, E., Caporale, C., and Ivaldi, R.: Unmanned surface vehicles for automatic bathymetry mapping and shores' maintenance, Oceans, Taipei, 2014, 1–7, https://doi.org/10.1109/OCEANS-TAIPEI.2014.6964440, 2014.

Bhardwaj, A., Singh, M. K., Joshi, P. K., Snehmani, Singh, S., Sam, L., Gupta, R. D., and Kumar, R.: A lake detection algorithm (LDA) using Landsat 8 data: a comparative approach in glacial environment, Int. J. Appl. Earth Obs. Geoinf., 38, 150–163, https://doi.org/ 10.1016/j.jag.2015.01.004, 2015.

Brunner, G.W.: HEC-RAS River Analysis System: User's Manual. US Army Corps of Engineers. Institute for Water Resources, Hydrologic Engineering Center, 2002.

Brun, F., Berthier, E., Wagnon, P., Kääb, A., and Treichler, D.: A spatially resolved estimate of High Mountain Asia glacier mass balances from 2000 to 2016, Nat. Geosci., 10, 668–673, https://doi.org/10.1038/ngeo2999, 2017.

Carrivick, J. L. and Tweed, F. S.: A global assessment of the societal impacts of glacier outburst floods, Global. Planet. Change., 144, 1–16, https://doi.org/10.1016/j.gloplacha.2016.07.001, 2016.

Cheng, Z., Zhu, P., Dang, C., and Liu, J.: Hazards of debris flow due to glacier lake outburst in Southeastern Tibet, Journal of Glaciology and Geocryology, 30, 954–959, https://doi.org/CNKI:SUN:BCDT.0.2008-06-006, 2008.

Cheng, Z. L., Liu, J. J., and Liu, J. K.: Debris flow induced by glacial-lake break in Southeast Tibet, Earth Science Frontiers, 16, 207–214, https://doi.org/10.2495/DEB100091, 2009.

Christen, M., Kowalski, J., Bartelt, P., RAMMS: numerical simulation of dense snow avalanches in three-dimensional terrain. Cold Reg. Sci. Technol. 63, 1–14, 2010.

Clague, J. J. and Evans, S. G.: A review of catastrophic drainage of moraine-dammed lakes in British Columbia, Quaternary. Sci. Rev., 19, 1763–1783, https://doi.org/10.1016/S0277-3791(00)00090-1, 2000.

Cook, S. J. and Quincey, D. J.: Estimating the volume of Alpine glacial lakes. Earth. Surf. Dynam., 3, 559–575, https://doi.org/10.5194/esurf-3-559-2015, 2015.

Cook, K. L., Andermann, C., Gimbert, F., Adhikari, B. R., and Hovius, N.: Glacial lake outburst floods as drivers of fluvial erosion in the Himalaya, Science, 362, 53–57, https://doi.org/10.1126/ science.aat 4981, 2018.

Coon, W. F.: Estimation of roughness coefficients for natural stream channels with vegetated banks, United States Geological Survey water-supply paper, 2441, 1998.

Cui, P., Ma, D. T., and Chen, N. S.: The initiation, motion and mitigation of debris flow caused by glacial lake outburst, Quaternary Sciences, 23, 621–628, https://doi.org/10.1016/S0955-2219(02)00073-0, 2003.

Dehecq, A., Gourmelen, N., Gardner, A. S., Brun, F., Goldberg, D., Nienow, P. W., Berthier, E., Vincent, C., Wagnon, P., and Trouvé, E.: Twenty-first century glacier slowdown driven by mass loss in High Mountain Asia, Nat. Geosci., 12, 22–27, https://doi.org/10.1038/s41561-018-0271-9, 2019.

DHI MIKE FLOOD – 1D-2D Modelling - User Manual. Denmark, Danish Hydraulic Institute, 2007.

Dhote, P. R., Aggarwal, S. P., Thakur, P. K., and Garg, V.: Flood inundation prediction for extreme flood events: a case study of Tirthan River, North West Himalaya, Himal. Geol., 40, 128–140, 2019.

Duan, H. Y., Yao, X. J., Zhang, D. H., Qi, M. M., and Liu, J.: Glacial Lake Changes and Identification of Potentially Dangerous Glacial Lakes in the Yi'ong Zangbo River Basin, Water-Sui, 12, 538, https://doi.org/10.3390/w12020538, 2020.

Dwivedi, S. K., Acharya, M., and Simard, R.: The Tam Pokhari Glacier Lake outburst flood of 3 September 1998, Journal of Nepal Geological Society, 22, 539–546, https://doi.org/10.3126/jngs.v22i0.32429, 2000.

Emmer, A. and Cochachin, A.: The causes and mechanisms of moraine-dammed lake failures in the Cordillera Blanca, North American Cordillera and Himalaya, AUC. Geogr., 48, 5–15, https://doi.org/10.14712/23361980.2014.23, 2013.

Emmer, A. and Vilímek, V. New method for assessing the susceptibility of glacial lakes to outburst floods in the Cordillera Blanca, Peru, Hydrol Earth Syst Sc, 18, 3461–3479, https://doi.org/10.5194/hess-18-3461-2014, 2014.

Evans, S. G.: The maximum discharge of outburst floods caused by the breaching of man-made and natural dams, reply. Can. Geotech. J., 24, 385–387, https://doi.org/10.1139/t87-062, 1987.

Froehlich, D. C.: Peak outflow from breached embankment dam, J. Water. Res. Plan. Man., 121, 90–97, https://doi.org/10.1061/(ASCE)0733-9496(1995)121:1(90), 1995a.

Froehlich, D. C.: Embankment Dam Breach Parameters Revisited, 887–891, American Society of Civil Engineers, 1995b.

Fujita, K., Sakai, A., Nuimura, T., Yamaguchi, S., and Sharma, R. R.: Recent changes in Imja Glacial Lake and its damming moraine in the Nepal Himalaya revealed by in situ surveys and multi-temporal ASTER imagery, Environ. Res. Lett., 4, 045205, https://doi.org/ 10.1088/1748-9326/4/4/045205, 2009.

Fujita, K., Sakai, A., Takenaka, S., Nuimura, T., Surazakov, A. B., Sawagaki, T., and Yamanokuchi, T.: Potential flood volume of Himalayan glacial lakes, Nat. Hazard. Earth. Sys., 13, 1827–1839, https://doi.org/10.5194/nhess-13-1827-2013, 2013.

Geological Survey of India: Geology environmental hazards and remedial measures of the Lunana Area, Gasa Dzongkhang, Report of 1995 Indo-Bhutan Expedition, Bhutan Unit, Geological Survey of India, Samtse, 1995.

Guo, W. Q., Liu, S. Y., Xu, J. L., Wu, L. Z., Shangguan, D. H., Yao, X. J., Wei, J. F., Bao, W. J., Yu, P. C., Liu, Q., and Jiang, Z. L.: The second Chinese glacier inventory: Data, methods and results, J. Glaciol., 61, 357-372, https://doi.org/10.3189/2015JoG14J209, 2015.

Haeberli, W., Kääb, A.,Vonder Mühll, D., Teysseire, P. Prevention of outburst floods from periglacial lakes at Grubengletscher, Valais, Swiss Alps, J. Glaciol. 47, 111–122, 2001.

Haritashya, U. K., Kargel, J. S., Shugar, D. H., Leonard, G. J., Strattman, K., Watson, C. S., Shean, D., Harrison, S., Mandli, K. T., and Regmi, D.: Evolution and controls of large glacial lakes in the Nepal Himalaya, Remote Sens-Basel, 10, 798, https://doi.org/10.3390/rs10050798, 2018.

Heller, V., Hager, W., and Minor, H. E. Landslide generated im- pulse waves in reservoirs: Basics and computation. Laboratory Of Hydraulics, Hydrology, and Glaciology, ETH Zürich, Switzerland, 172 pp, 2009.

Huang, L., Zhu, L. P., Wang, J. B., Ju, J. T., Wang, Y., Zhang, J. F., and Yang, R. M.: Glacial activity reflected in a continuous lacustrine record since the early Holocene from the proglacial Laigu Lake on the southeastern Tibetan Plateau, Palaeogeogr, Palaeocl., 456, 37–45, https://doi.org/10.1016/j.palaeo.2016.05.019, 2016.

Huggel, C., Kääb, A., Haeberli, W., Teysseire, P., and Paul, F.: Remote sensing based assessment of hazards from glacier lake outbursts: a case study in the Swiss Alps, Can. Geotech. J., 39, 316–330, https://doi.org/10.1139/t01-099, 2002.

Huggel, C., Haeberli, W., Kääb, A., Bieri, D., and Richardson, S.: An assessment procedure for glacial hazards in the Swiss Alps, Can. Geotech. J., 41, 1068–1083, https://doi.org/10.1139/t04-053, 2004.

International Centre for Integrated Mountain Development (ICIMOD): Glacial Lakes and Glacial Lake Outburst Floods in Nepal. ICIMOD, Kathmandu, 99, 2011.

1095   Jain, S.K., Lohani, A.K., Singh, R.D., Chaudhary, A., and Thakural, L.N.: Glacial lakes and glacial lakes outburst flood in a Himalayan basin using remote sensing and GIS. Nat. Hazard., 62, 887–899, https://doi.org/10.1007/s11069-012-0120-x, 2012.
Kääb, A., Berthier, E., Nuth, C., Gardelle, J., and Arnaud, Y.: Contrasting patterns of early twenty-first-century glacier mass change in the Himalayas, Nature, 488, 495–498, https://doi.org/10.1038/nature11324, 2012.

Kääb, A., Treichler, D., Nuth, C., and Berthier, E.: Brief communication: contending estimates of 2003-2008 glacier mass
1100   balance over the Pamir-Karakoram-Himalaya, The Cryosphere, 9, 557–564, https://doi.org/10.5194/tc-9-557-2015, 2015.

Ke, C. Q., Kou, C., Ludwig, R., and Qin, X.: Glacier velocity measurements in the eastern Yigong Zangbo basin, Tibet, China, J. Glaciol., 59, 1060–1068, https://doi.org/10.3189/2013jog12j234, 2013.

Ke, C. Q., Han, Y. F., and Kou, C.: Glacier Change in the Yigong Zangbu Basin, Tibet, China (1988 to 2010), Dragon 3 Mid Term Results, November 2014, http://articles.adsabs.harvard.edu/pdf/2014ESASP.724E.16K, 2014.

1105   Khadka, N., Zhang, G., and Thakuri, S.: Glacial lakes in the Nepal Himalaya: inventory and decadal dynamics (1977-2017), Remote Sens-Basel, 10, 1-19, https://doi.org/ 10.3390/rs10121913, 2018.

Lala, J. M., Rounce, D. R., and Mckinney, D. C.: Modeling the glacial lake outburst flood process chain in the Nepal Himalaya: Reassessing Imja Tsho's hazard, Hydro. Earth. Syst. Sc., 22, 3721–3737, https://doi.org/10.5194/hess-2017-683, 2018.

Larrazabal, J. M. and Peñas, M. S.: Intelligent rudder control of an unmanned surface vessel, Expert. Syst. Appl., 55, 106–117,
1110   https://doi.org/10.1016/j.eswa.2016.01.057, 2016.

Li, J.J., Zhen, B. X., and Yang, X. J.: Glaciers in Tibet. Science Press, Beijing, 1986.

Li, D., Shangguan D. H., Wang, X.Y., Ding, Y. J., Su, P. C., Liu, R. L., and Wang, M. X.: Expansion and hazard risk assessment of glacial lake Jialong Co in the central Himalayas by using an unmanned surface vessel and remote sensing, Sci. Total. Environ., 784, 147249, https://doi.org/10.1016/j.scitotenv.2021.147249, 2021.

1115   LIGG/WECS/NEA: Report on First Expedition to Glaciers and Glacier Lakes in the Pumqu (Arun) and Poiqu (Bhote-Sun Koshi) River Basins, Xizang (Tibet), China. Sino-Nepalese Joint Investigation of Glacier Lake Outburst Flood in Himalayas in 1987, 192, 1988.

Liu, J., Yao, X. J., Gao, Y. P., Qi, M. M., Duan, H. Y., and Zhang, D. H.: Glacial lake variation and hazards assessment of glacial lakes outburst in the Parlung Zangbo River Basin, Journal of Lake Sciences, 31, 1132–1143,
1120   https://doi.org/10.18307/2019.0420, 2019.

Liu, J. K., Zhou, L. X., Zhang, J. J., and Zhao, W. Y.: Characteristics of Jiwencuo GLOF, Lhari county, Tibet. Geological Review, 67: 17–18. https://doi.org/10.16509/j.georeview.2021.s1.007, 2021.

Liu S.Y., Pu J. C., and Deng, X. F.: Glaciers and Glacier Landscapes in China. Shanghai Popular Science Press, Shanghai 38–41, 2014.

1125   Liu, W. M., Lai, Z. P., Hu, K. H., Ge, Y. G, Cui, P., Zhang, X. G., and Liu, F.: Age and extent of a giant glacial-dammed lake at Yarlung Tsangpo gorge in the Tibetan Plateau, Geomorphology, 246, 370–376, https://doi.org/10.1016/j.geomorph.2015.06.034, 2015.

Liu, Z. X., Zhang, Y. M., Yu, X., and Yuan, C.: Unmanned surface vehicles: an overview of developments and challenges, Annu. Rev. Control., 41, 71–39, https://doi.org/10.1016/j. arcontrol.2016.04.018, 2016.

1130   Liu, J. k., Zhang, J. J., Gao, Bo., Li, Y. L., Li, M. Y., Wujin, D. J., Zhou, L. X. An overview of glacial lake outburst flood in Tibet, China. Journal of Glaciology and Geocryology, 41, 1335–1347, https://doi.org/10.7522/j.issn.1000-0240.2019.0073, 2019.

Lliboutry, L.: Glaciological problems set by the control of dangerous lakes in Cordillera Blanca, Peru. II. Movement of a

covered glacier embedded within a rock glacier, J. Glaciol., 18, 255–274, https://doi.org/10.3189/S0022143000021341, 1977.

1135 Lohani, A.K. and Jain, S.K.: Analysis of Glacier Lake Outburst Floods. Bharatiya Vaigyanik Evam Audyogik Anusandhan Patrika (BVAAP) 24, 55–59, 2016.

Lv, R. R., Tang, X. B., and Li, D. J.: Glacial lake outburst mudslide in Tibet, Chengdu University of Science and Technology Press, Chengdu, 69–105, 1999.

Maurer, J. M., Schaefer, J. M., Rupper, S., and Corley, A.: Acceleration of ice loss across the Himalayas over the past 40 years,
1140 Sci. Adv., 5, eaav7266, https://doi.org/10.1126/sciadv.aav7266, 2019.

Maskey, S., Kayastha, R. B., and Kayastha, R.: Glacial Lakes Outburst Floods (GLOFs) Modelling of Thulagi and Lower Barun Glacial Lakes of Nepalese Himalaya, Progress in Disaster Science, 7, 100106, https://doi.org/10.1016/j.pdisas.2020.100106, 2020.

Mckillop, R. J. and Clague, J. Statistical, remote sensing-based approach for estimating the probability of catastrophic drainage
1145 from moraine-dammed lakes in southwestern British Columbia, Global Planet Change, 56, 153–171, https://doi.org/10.1016/J.GLOPLACHA.2006.07.004, 2007.

Mergili, M. and Schneider, J. F.: Regional-scale analysis of lake outburst hazards in the southwestern Pamir, Tajikistan, based on remote sensing and GIS, Nat. Hazard. Earth. Sys., 11, 1447–1462, https://doi.org/10.5194/nhess-11-1447-2011, 2011.

Mergili, M., Fischer, J. T., Krenn, J., and Pudasaini, S. P.: r.avaflow v1, an advanced open-source computational framework
1150 for the propagation and interaction of two-phase mass flows, Geosci. Model Dev., 10, 553–569, https://doi.org/10.5194/gmd-10-553-2017, 2017.

Mergili, M. and Pudasaini, S. P.: r.avaflow–The open source mass flow simulation model, available at: https://www.avaflow.org/, last access: 30 October 2020.

Mir, R. A., Jain, S. K., Lohani, A. K., and Saraf, A. K.: Glacier recession and glacial lake outburst flood studies in Zanskar
1155 basin, western Himalaya, J. Hydrol., 564, 376-396, https://doi.org/10.1016/j.jhydrol.2018.05.031, 2018.

Mool, P.K., Bajracharya, S.R., and Joshi, S.P.: Inventory of Glaciers, Glacial Lakes and Glacial Lake Outburst Floods, Monitoring and Early Warning Systems in the Hindu Kush- Himalayan Region: Nepal, ICIMOD & UNEP RRC-AP, 363, 2001.

Neckel, N., Kropáček, J., Bolch, T., and Hochschild, V.: Glacier mass changes on the Tibetan Plateau 2003–2009 derived from ICESat laser altimetry measurements, Environ. Res. Lett., 9, 468–475, https://doi.org/10.1088/1748-9326/9/1/014009, 2013.

1160 Nie, Y., Liu, Q., Wang, J. D., Zhang, Y. L., Sheng, Y. W., and Liu, S. Y.: An inventory of historical glacial lake outburst floods in the Himalayas based on remote sensing observations and geo-morphological analysis, Geomorphology, 308, 91–106, https://doi.org/10.1016/j. geomorph.2018.02.002, 2018.

O'Connor, J. E., Hardison, J. H., and Costa, J. E.: Debris flows from failures of neoglacial-age moraine dams in the Three Sisters and Mount Jefferson wilderness areas, Oregon, United States Geological Survey Professional Paper, 1606, 11–40,
1165 https://doi.org/10.1007/BF01211117, 2001.

Osti, R. and Egashira, S.: Hydrodynamic characteristics of the Tam Pokhari glacial lake outburst flood in the Mt. Everest region, Nepal, Hydrol. Process., 23, 2943–2955, https://doi.org/10.1002/hyp.7405, 2009.

Osti, R., Bhattarai, T. N., and Miyake, K.: Causes of catastrophic failure of Tam Pokhari moraine dam in the Mt. Everest region, Nat. Hazards, 58, 1209–1223, https://doi.org/10.1007/s11069-011-9723-x, 2011.

1170 Prakash, C. and Nagarajan, R.: Outburst susceptibility assessment of moraine-dammed lakes in Western Himalaya using an analytic hierarchy process, Earth. Surf. Proc. Land., 42, 2306–2321, https://doi.org/10.1002/esp.4185, 2017.

Pudasaini, S. P. and Mergili, M.: A Multi-Phase MassFlow Model, J. Geophys. Res.-Earth, 124, 2920–2942, https://doi.org/10.1029/2019jf005204, 2019.

Qi, M. M., Liu, S. Y., Yao, X. J., R, Grünwald., and Liu, J.: Lake inventory and potentially dangerous glacial lakes in the Nyang
1175 Qu Basin of China between 1970 and 2016, J. Mt. Sci-Engl, 17, 851–870, https://doi.org/10.1007/s11629-019-5675-5, 2020.

Qin D. H., Dong, W. J., and Luo, Y.: Climate and Environment Change in China. China Meteorologiacal Press, Beijing, 116-

121, 2012.

Richardson, S. D. and Reynolds, J. M.: An overview of glacial hazards in the Himalayas, Quatern. Int., 65, 31–47, https://doi.org/10.1016/S1040-6182(99)00035-X, 2000.

Risio, M., Girolamo, P. D., and Beltrami, G. M.: Forecasting landslide generated Tsunamis: a review, the Tsunami threat-research and technology, 81–106, https://doi.org/10.5772/13767, 2011.

Rounce, D. R., McKinney, D. C., Lala, J. M., Byers, A. C., and Watson, C. S.: A new remote hazard and risk assessment framework for glacial lakes in the Nepal Himalaya, Hydrol. Earth. Syst. Sc., 20, 3455–3475, https://doi.org/10.5194/hess-20-3455-2016, 2016.

Sakai, A., Yamada, T., and Fujita, K.: Volume Change of Imja Glacial Lake in the Nepal Himalayas. International Symposium on Disaster Mitigation & Basin Wide Water Management, Niigata, 2003, 556–561. 2003.

Sakai, A.: Glacial lakes in the Himalayas: a review on formation and expansion processes, Global Environmental Research, 16, 23–30, 2012.

Sattar, A., Goswami, A., and Kulkarni, A. V.: Hydrodynamic moraine-breach modeling and outburst flood routing–a hazard assessment of the South Lhonak lake, Sikkim, Sci. Total. Environ., 668, 362–378, https://doi.org/10.1016/j.scitotenv.2019.02.388, 2019.

Sattar, A., Haritashya, U. K., Kargel, J. S., Leonard, G. J., and Chase, D. V.: Modeling Lake Outburst and Downstream Hazard Assessment of the Lower Barun Glacial Lake, Nepal Himalaya, J. Hydrol., 598, 126208, https://doi.org/10.1016/j.jhydrol.2021.126208, 2021.

Schneider, D., Huggel, C., Cochachin, A., Guillén, S., García, J. Mapping hazards from glacier lake outburst floods based on modelling of process cascades at Lake 513, Carhuaz, Peru. Adv. Geosci, 35, 145–155, https://doi.org/10.5194/adgeo-35-145-2014, 2014.

Sharma, R. K., Pradhan, P., Sharma, N. P., and Shrestha, D. G.: Remote sensing and in situ-based assessment of rapidly growing South Lhonak glacial lake in eastern Himalaya, India, Nat. Hazards., 93, 393, https://doi.org/10.1007/s11069-018-3348-2, 2018.

Shi, W. L., Yang, C. T., You, G. X., and Jin, M. X.: The measurement of reserve of glacier block lake on the upper stream of Yerqiang river and the calculation of its maximum flood, Arid Land Geography., 14, 31–35, 1991.

Shugar, D., Burr, A., Haritashya, U. K., Kargel, J. S., Watson, C. S., Kennedy, M. C., Bevington, A. R., Betts, R. A., Harrison, S., and Strattman, K.: Rapid worldwide growth of glacial lakes since 1990, Nat. Clim. Change., 10, 939–945, https://doi.org/10.1038/s41558-020-0855-4, 2020.

Song, C., Sheng, Y., Ke, L., Nie, Y., and Wang, J.: Glacial lake evolution in the southeastern Tibetan Plateau and the cause of rapid expansion of proglacial lakes linked to glacial-hydrogeomorphic processes, J. Hydrol., 540, 504–514, https://doi.org/10.1016/j.jhydrol.2016.06.054, 2016.

Somos-Valenzuela, M.A., Chisolm, R.E., Rivas, D.S., Portocarrero, C., McKinney, D.C. Modeling glacial lake outburst flood process chain: the case of Lake Palcacocha and Huaraz, Peru. Hydrol Earth Syst Sc, 20, 2519–2543, https://doi.org/10.5194/hess-2015-512.

Specht, M., Specht, C., Lasota, H., and Cywiński, P.: Assessment of the steering precision of a hydrographic unmanned surface vessel (USV) along sounding profiles using a low-cost multi-global navigation satellite system (GNSS) receiver supported autopilot, Sensors-Basel, 19, 3939, https://doi.org/10.3390/s19183939, 2019a.

Specht, M., Specht, C., Lasota, H., and Cywiński, P.: The use of unmanned surface vessels in bathymetric measurements of waterbodies with highly dynamic seafloor relief, 19th International Multidisciplinary Scientific Geo Conference SGEM, Sofia, 28 June 2019, 375–382, https://doi.org/10.5593/sgem2019/2.2/S09.046, 2019b.

Sun, M. P., Liu, S. Y., Yao, X. J., and Li, L.: The cause and potential hazard of glacial lake outburst flood occurred on July 5, 2013 in Jiali County, Tibet, Journal of Glaciology and Geocryology, 36, 158–165, https://doi.org/158-165,10.7522/j.issn.1000-

0240.2014.0020, 2014.

Thakur, P.K., Aggarwal, S., Aggarwal, S.P., and Jain, S.K.: One-dimensional hydro-dynamic modeling of GLOF and impact on hydropower projects in Dhauliganga Riverusing remote sensing and GIS applications. Nat. Hazard., 83, 1057–1075, https://doi.org/10.1007/s11069-016-2363-4, 2016.

Thompson, S., Benn, D. I., Mertes, J., and Luckman, A.: Stagnation and mass loss on a himalayan debris-covered glacier: Processes, patterns and rates, J. Glaciol., 62, 467–485, https://doi.org/10.1017/jog.2016.37, 2016.

Veh, G., Korup, O., Specht, S. V., Roessner, S., and Walz, A.: Unchanged frequency of moraine-dammed glacial lake outburst floods in the Himalaya, Nat. Clim. Change., 9, 379–383, https://doi.org/10.1038/s41558-019-0437-5, 2019.

Vetsch, D., Siviglia, A., Ehrbar, D., Facchini, M., Kammerer, S., Koch, A., Peter, S., Vonwiller, L., Gerber, M., Volz, C., Farshi, D., Mueller, R., Rousselot, P., Veprek, R., and Faeh, R.: System Manuals ofBASEMENT, Version 2.7. Laboratory of Hydraulics, Glaciology and Hydrology (VAW), ETH Zurich, available at: http://www.basement.ethz.ch, last access: 3 October 2022.

Vilímek, V., Emmer, A., Huggel, C., Schaub, Y., and Würmli, S.: Database of glacial lake outburst floods (GLOFs)–IPL project no. 179, Landslides, 11, 161–165, https://doi.org/10.1007/s10346-013-0448-7, 2013.

Wahl, T. L.: Uncertainty of Predictions of Embankment Dam Breach Parameters, J. Hydraul. Eng., 130, 389–397, https://doi.org/10.1061/(ASCE)0733-9429(2004)130:5(389), 2004.

Wang, S. J., Yang, Y., Gong, W., Che, Y., Ma, X., and Xie, J.: Reason analysis of the Jiwenco glacial lake outburst flood (GLOF) and potential hazard on the Qinghai-Tibetan Plateau, Remote Sens-Basel, 13, 3114, https://doi.org/10.3390/rs13163114, 2021.

Wang, W. C., Yao, T. D., Gao, Y., Yang, X. X., and Kattel, D. B.: A first-order method to identify potentially dangerous glacial lakes in a region of the southeastern Tibetan Plateau, Mt. Res. Dev., 31, 122–130, https://doi.org/10.1659/MRD-JOURNAL-D-10-00059.1, 2011a.

Wang, W. C., Yang, X. X., and Yao, T. D.: Evaluation of ASTER GDEM and SRTM and their suitability in hydraulic modelling of a glacial lake outburst flood in southeast Tibet, Hydrol. Process., 26, 213–225, https://doi.org/10.1002/hyp.8127, 2011b.

Wang, W. C., Yao, T. D., Yang, W., Joswiak, D., and Zhu, M. L.: Methods for assessing regional glacial lake variation and hazard in the southeastern Tibetan Plateau: a case study from the Boshula mountain range, China, Environ. Earth. Sci., 67, 1441–1450, https://doi.org/ 10.1007/s12665-012-1589-z, 2012.

Wang, W. C., Gao, Y., Anacona, P. I., Lei, Y. B., Xiang, Y., Zhang G. Q., Li, S. H., and Lu, A. X.: Integrated hazard assessment of Cirenmaco glacial lake in Zhangzangbo valley, Central Himalayas, Geomorphology, 306, 292–305, https://doi.org/10.1016/j.geomorph.2015.08.013, 2015.

Wang, X., Liu, S. Y., Ding, Y. J., Guo, W. Q., Jiang, Z. L., Lin, J., and Han, Y.: An approach for estimating the breach probabilities of moraine-dammed lakes in the chinese himalayas using remote-sensing data. Nat. Hazard. Earth. Sys., , 12, 3109-3122, https://doi.org/10.5194/nhess-12-3109-2012, 2012a.

Wang, X., Liu, S. Y., Guo, W. Q., Yao, X. J., Jiang, Z. L., and Han, Y. S: Using Remote Sensing Data to Quantify Changes in Glacial Lakes in the Chinese Himalaya, Mt. Res. Dev., 32, 203–212, https://doi.org/10.1659/MRD-JOURNAL-D-11-00044.1, 2012b.

Wang, X., Ding, Y. J., Liu, S. Y., Jiang, L., Wu, K., Jiang, Z. L., and Guo, W. Q.: Changes of glacial lakes and implications in Tian Shan, central Asia, based on remote sensing data from 1990 to 2010, Environ. Res. Lett., 8, 575–591, https://doi.org/10.1088/1748-9326/8/4/044052, 2013.

Wang X. Methodology and application of moraine lake outburst hazard evaluation in the Chinese Himalayas, Science Press, Beijing, 2016.

Wang, X., Chai, K. G., Liu, S. Y., Wei, J. F., Jiang, Z. L., and Liu, Q. H.: Changes of glaciers and glacial lakes implying corridor-barrier effects and climate change in the Hengduan Shan, southeastern Tibetan Plateau, J. Glaciology., 63, 535–542, https://doi.org/10.1017/jog.2017.14, 2017.

Wang, X., Guo, X. Y., Yang, C. D., Liu, Q. H., Wei, J. F., Zhang, Y., Liu, S. Y., Zhang, Y. L., Jiang, Z. L., and Tang, Z. G.:

Glacial Lake inventory of high-mountain Asia in 1990 and 2018 derived from Landsat images, Earth. Syst. Sci. Data., 12, 2169–2182, https://doi.org/10.5194/essd-2019-212, 2020.

Watanbe, T. and Rothacher, D.: The 1994 Lugge Tsho glacial lake outburst flood, Bhutan Himalaya, Mt. Res. Dev., 16, 77–81, h https://doi.org/10.2307/3673897, 1996.

Watson, C. S., Quincey, D. J., Carrivick, J. L., Smith, M. W., Rowan, A. V., and Richardson, R.: Heterogeneous water storage and thermal regime of supraglacial ponds on debris covered glaciers, Earth. Surf. Proc. Land., 43, 229–241, https://doi.org/10.1002/esp.4236, 2018.

Westoby, M. J., Glasser, N. F., Brasington, J., Hambrey, M. J., Quincey, D. J., and Reynolds, J. M.: Modelling outburst floods from moraine-dammed glacial lakes, Earth-Sci. Rev., 134, 137–159, https://doi.org/10.1016/j.earscirev.2014.03.0092014, 2014.

Worni, R., Stoffel, M., Huggel, C., Volz, C., Casteller, A., and Luckman, B.: Analysis and dynamic modeling of a moraine failure and glacier lake outburst flood at Ventisquero Negro, Patagonian Andes (Argentina), J. Hydrol., 444–445, 134–145, https://doi.org/10.1016/j.jhydrol.2012.04.013, 2012.

Worni, R., Huggel, C., Clague, J. J., Schaub, Y., and Stoffel, M.: Coupling glacial lake impact, dam breach, and flood processes: A modeling perspective, Geomorphology, 224, 161–176, https://doi.org/10.1016/j.geomorph.2014.06.031, 2014.

Wong, M. and Parker, G. Reanalysis and correction of bed-load relation of meyer-peter and mã¼ller using their own database. Journal of Hydraulic Engineering, 132, 1159–1168, https://doi.org/10.1111/j.1600-0587.1978.tb00950.x, 2006.

Xie, Z. C., and Liu, C. H: Introduction to Glaciology. Shanghai Science Popular Press, Shanghai, 425–426, 2010.

Yan, R. J., Pang, S., Sun, H. B., and Pang, Y. J.: Development and missions of unmanned surface vehicle, J. Mar. Sci. Appl., 9(4), 451–457, https://doi.org/10.1007/s11804-010-1033-2, 2010.

Yang, W., Yao, T. D., Xu, B. Q., Wu, G. J., Ma, L. L., and Xin, X. D.: Quick ice mass loss and abrupt retreat of the maritime glaciers in the Kangri Karpo Mountains, southeast Tibetan Plateau, Chin. Sci. Bull., 53, 2547–2551, https://doi.org/10.1007/s11434-008-0288-3, 2008.

Yamada, T.: Glacier lake and its outburst flood in the Nepal Himalaya. Data Center for Glacier Research, Japanese Society of Snow and Ice, 1, 96, 1998.

Yamada, T. N., Naito, S., Kohshima, H., Fushimi, F., Nakazawa, T., Segawa, J., Uetake, R., Suzuki, N., Sato, Karma, I. K., Chhetri, L., Gyenden, H., Yabuki, and Chikita, K.: Outline of 2002: research activity on glaciers and glacier lakes in Lunana region, Bhutan Himalayas. Bull. Glaciol. Res., 21: 79–90, 2004.

Yao, X. J., Liu, S. Y., Sun, M. P., Wei, J. F., and Guo, W. Q.: Volume calculation and analysis of the changes in moraine-dammed lakes in the north Himalaya: a case study of Longbasaba lake, J. Glaciol, 58, 753–760, https://doi.org/10.3189/2012JoG11J048, 2012.

Yao, X. J., Liu, S. Y., Sun, M. P., and Zhang, X. J.: Study on the Glacial Lake Outburst Flood Events in Tibet since the 20th Century, Journal of Natural Resources, 8, 1377–1390, https://doi.org/10.11849/zrzyxb.2014.08.010, 2014.

Yuan, G. and Zeng, Q.: Glacier-dammed Lake in Southeastern Tibetan Plateau during the Last Glacial Maximum, J. Geol. Soc. India., 79, 295–301, https://doi.org/10.1007/s12594-012-0041-z, 2012.

Zemp, M., Huss, M., Thibert, E., Eckert, N., McNabb, R., Huber, J., Barandun, M., Machguth, H., Nussbaumer, S. U., Gartner-Roer, I., Thomson, L., Paul, F., Maussion, F., Kutuzov, S., and Cogley, J. G.: Global glacier mass changes and their contributions to sea-level rise from 1961 to 2016, Nature, 568, 382–386, https://doi.org/10.1038/s41586-019-1071-0, 2019.

Zhang, B., Liu, G. X., Zhang, R., Fu, Y., and Li, Z. L.: Monitoring dynamic evolution of the glacial lakes by using time series of Sentinel-1A SAR images, Remote Sens-Basel, 13, 1313, https://doi.org/10.3390/rs13071313, 2021.

Zhang, G. Q., Yao, T. D., Xie, H. J., Wang, W. C., and Yang, W.: An inventory of glacial lakes in the Third Pole region and their changes in response to global warming, Global. Planet. Change., 131, 148–157, https://doi.org/10.1016/j.gloplacha.2015.05.013, 2015.

~~Zhang, G. Q, Bolch, T., Allen, S., Linsbauer, A., Chen, W. F, Wang, W. C.: Glacial lake evolution and glacier-lake interactions in the Poiqu River basin, central Himalaya, 1964-2017. J. Glaciol., 65, 347–365. https://doi.org/10.1017/jog.2019.13, 2019.~~

Zhang, M. M., Chen, F., Tian, B. S., Liang, D., and Yang, A. Q.: High-frequency glacial lake mapping using time series of Sentinel-1A/1B SAR imagery: An assessment for southeastern Tibetan Plateau, Nat. Hazard. Earth. Sys., 1–18, https://doi.org/10.5194/nhess-2019-219, 2020.

Zhang, Y., Yao, X. J., Duan, H. Y., and Wang, Q.: Simulation of Glacial Lake Outburst Flood in Southeastern Qinghai-Tibet Plateau—A Case Study of JiwenCo Glacial Lake, Fronter in Earth Science, Frontiers in Earth Science, 10: 1–13. https://doi: 10.3389/feart.2022.819526, 2022.

Zheng, G. X., Mergili, M., Emmer, A., Allen, S., and Stoffel, M.: The 2020 glacial lake outburst flood at Jinwuco, Tibet: causes, impacts, and implications for hazard and risk assessment, The Cryosphere, 15, 3159–3180, https://doi.org/10.5194/tc-2020-379, 2021.

Zhou, L. X., Liu, J. K., Li, Y. L.: Calculation method of mathematical model of the moraine dammed lake storage capacity. Science Technology and Engineering, 2020, 20: 9804–9809.